Microscopic Theory of Terahertz Spectroscopy on Semiconductor Nanostructures

Dissertation
zur
Erlangung des Doktorgrades
der Naturwissenschaften
(Dr. rer. nat.)

dem Fachbereich Physik
der Philipps-Universität Marburg
vorgelegt

von
Andrea C. Klettke

aus Marburg

Marburg (Lahn), 2013

Vom Fachbereich Physik der Philipps-Universität Marburg
als Dissertation angenommen am 15.04.2013

Erstgutachter: Prof. Dr. S. W. Koch
Zweitgutachter: PD Dr. S. Chatterjee

Tag der mündlichen Prüfung: 19.04.2013

Zusammenfassung

In den letzten zwanzig Jahren wurden Mikrochips und elektronische Bauelemente für Computer und Multimedia nicht nur immer schneller und leistungsfähiger, sondern auch bedeutend kleiner. Ein moderner Mikrochip besteht typischerweise aus Halbleitermaterial mit Strukturen im Bereich von mehreren zehn Nanometern [1]. In diesen Größenordnungen gewinnen quantenmechanische Effekte zunehmend an Bedeutung.

In sehr kleinen Schichten oder Streifen sind Ladungsträger wie Elektronen und Löcher in ihren Bewegungen auf zwei oder weniger Dimensionen eingeschränkt. Dies führt zu dramatischen Änderungen der Materialeigenschaften [2]: Quantenfilme, in denen die Ladungsträger in quasi zwei Dimensionen eingeschränkt sind, Quantendrähte (quasieindimensional) und Quantenpunkte (nulldimensional) erlauben die Erforschung einer Vielzahl von neuen und spannenden physikalischen Effekten [3]. Es ist eine wichtige Aufgabe der heutigen Forschung, die Physik dieser niedrigdimensionalen Systeme zu verstehen, um die Computersysteme der Zukunft zu entwickeln.

Bei sehr niedrigen Temperaturen verhalten sich Halbleiter wie Isolatoren: Im Bändermodell bezeichnet man das oberste vollständig mit Elektronen gefüllte Band als Valenzband. Es wird vom nächsthöheren, leeren Band (Leitungsband) energetisch durch die Bandlücke getrennt. Die Bandlücke ist mehrere Elektronenvolt groß, was der Photonenenergie von optischem oder nahinfrarotem Licht entspricht. (Der Einfachheit halber sprechen wir in dieser Arbeit nur von *optischem Licht* anstelle von *optischem oder nahinfrarotem Licht*.) Bei höheren Temperaturen sind thermische Fluktuationen stark genug, um Elektronen in das Leitungsband anzuheben. Das führt dazu, dass die Halbleiter sich dann wie Metalle verhalten [4]. Bei niedrigen Temperaturen führt optisches Licht zu einer großen Bandbreite an Vielteilchenanregungen [2, 5–7], angefangen von Polarisationen zwischen Elektronen im Leitungsband und Löchern im Valenzband (sogenannten *kohärente Exzitonen*), die sich schließlich in inkohärente Exzitonen, Biexzitonen und andere Vielteilchenanregungen umwandeln [2, 8–13]. Die Tatsache, dass sich höhere Korrelationen erst aus niedrigeren Korrelationen ausbilden, ist der Ausgangspunkt für die Cluster-Entwicklung [7, 14]. In der Terminologie der Cluster-Entwicklung kann man viele grundlegende Anregungen wie kohärente Exzitonen bereits als *Singlets* beschreiben und den Einfluss der höheren Korrelationen und Streueffekten phänomenologisch behandeln.

In vielerlei Hinsicht ähneln kohärente Exitonenen dem Wasserstoffatom: Es gibt beispielsweise diskrete Energiezustände unterhalb des Leitungsbandes durch die Coulombwechselwirkung zwischen den verschieden geladenen Ladungsträgern in Valenz- und Leitungsband. Die Energiezustände lassen sich mit Quantenzahlen wie für das Wasserstoffproblem beschreiben, lediglich die Übergangsenergien sind um den Faktor 1000 herunterskaliert: Anstelle von mehreren Elektronenvolt (eV) wie im Wasserstoffatom liegen die Übergangsenergien im Bereich von mehreren Millielektronenvolt und somit im Terahertzbereich. Der große Erfolg der Spektroskopie von atomaren Systemen legt nahe, Exzitonen mit Terahertzlicht zu spektroskopieren und zu überprüfen, welche Effekte aus der Atomphysik auch in der Festkörperphysik zu finden sind. Die Entwicklung von Terahertzlasern und Detektoren ermöglichte in den letzten zehn Jahren vermehrt

die Spektroskopie von Exzitonen [8, 15–23]. Terahertzlicht hat den großen Vorteil, dass die Energie eines Terahertzphotons sehr viel kleiner als die Bandlücke ist und damit nur sehr schwer Polarisationen erzeugen kann. Daher durchquert Terahertzlicht unangeregte Halbleiter ohne zu wechselwirken. Andererseits ist Terahertzlicht resonant zu Anregungen innerhalb des Exzitons. Der Impuls eines Terahertzphotons reicht allerdings nicht aus, um Polarisation entlang des parabolischen Energiebandes anzuregen; dafür sind zusätzliche Mechanismen wie die Coulombwechselwirkung oder Phononen nötig. Ein einfachzyklischer Terahertzpuls hat die zeitliche Länge von etwa einer Pikosekunde und ist damit kürzer als die Zerfallszeit der optischen Polarisation von GaAs (mehreren Pikosekunden). All dies macht Terahertzspektroskopie zum idealen Mittel, um Anregungen in Halbleitern zu studieren, insbesondere auch kohärete Exitonen [24–29]. Studien mit gleichzeitiger optischer und Terahertz-Anregung wurden bereits an verschiedensten Systemen durchgeführt, z.B. am Elektron–Loch-Gas, an der Photolumineszenz von Magnetoexzitonen, an exzitonischer Rabiaufspaltung sowie bei der Anregung von höheren Harmonischen [19, 30–33]. Die Kopplung zwischen den vielen exzitonischen Energiezuständen führt dazu, dass das System im Allgemeinen zu kompliziert für Zweiniveaunäherungen ist. Es wurde bereits in früheren Arbeiten gezeigt, dass mikroskopische Rechnungen notwendig sind, wenn man die Dynamik der intraexzitonischen Übergänge verstehen möchte [19].

Im Rahmen dieser Doktorarbeit konzentrieren wir uns auf die Analyse von zwei Arten von Experimenten: In Kapitel 3 wird Terahertzspektroskopie an Quantenfilmen beschrieben, bei denen die Wechselwirkung des Terahertzlichts mit anderen Materialien als dem Quantenfilm vernachlässigt werden kann. Kapitel 4 behandelt Quantenfilme, die mit einer Kavität wechselwirken. Beide Themen sind aufgrund der Ähnlichkeiten von Exzitonen mit atomaren Systemen von grundsätzlichem Interesse. Ein sehr fundamentaler Effekt, der beide Themen verbindet, ist der AC-Stark-Effekt [2]: Er beschreibt das Aufspalten von Spektrallinien durch die Anwesenheit eines elektrischen Feldes. In Atomen wird dies Rabiaufspaltung genannt [34].

Die Rabiaufspaltung des 1s-Exzitonenzustandes durch Terahertzlicht wird in Kapitel 3 besprochen, während in Kapitel 4 der 1s-Exzitonenzustand bereits durch die Wechselwirkung mit der Kavität aufgespalten ist (*Vakuum-Rabiaufspaltung* [35, 36]) Im Einzelnen behandelt Abschnitt 3.1 die Frage, wie kohärente Exzitonen mit spektral breitem Terahertzlicht interagieren. Durch unsere Analyse zeigen wir, dass die Exzitonen ionisiert werden, ähnlich der Ionisation von Atomen: Die Polarisation wird durch die Wechselwirkung in Zustände mit hohen Energien und Orbitalnummern transferiert. Unsere Studie kann daher analog zur Ionisation oberhalb der Grenzschwelle in atomaren Systemen gesehen werden [37]. Die Ergebnisse sind in Veröffentlichung I beschrieben. Sie waren überraschend, da kurz zuvor ein ähnliches Experiment mit einem Zweiniveaumodell erklärt wurde. Dort wurde ein spektral schmaler Terahertzpuls verwendet [30]. Um die Lücke zwischen beiden unterschiedlichen Systemen (Ionisation und Zweiniveaumodell) zu schließen, wurde eine gemeinsame Studie durchgeführt. Dabei wird die Anregung mit dem spektral-schmalen Puls mit einer mikroskopischen Theorie untersucht. Die Ergebnisse (Veröffentlichung IV) werden in Abschnitt 3.2 beschrieben. Wir konnten zeigen, dass das Auftreten von *anticrossing* zwischen den beiden Rabiresonanzen

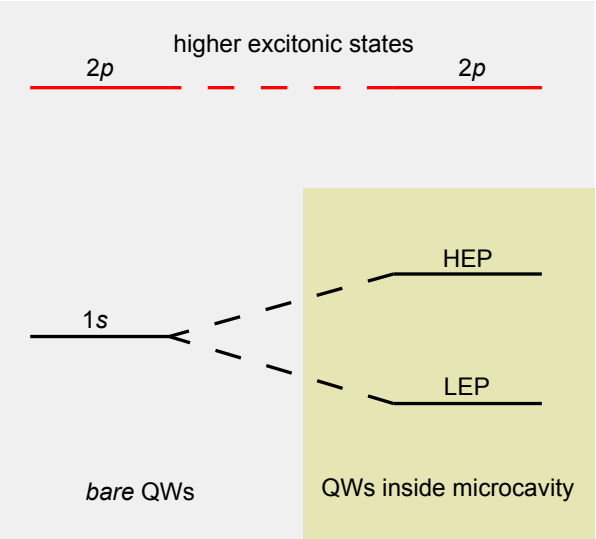

Figure 0.1: Energieniveaus (ohne THz-Einfluss) in Kapitel 3 und 4: Für die Terahertzspektroskopie an Quantenfilmen sind $1s$ und $2p$ die wichtigsten Zustände. Bei Quantenfilmen in einer resonanten Kavität spaltet der $1s$-Zustand in zwei Exziton-Polariton-Resonanzen auf. In beiden Szenarien kann der Einfluss der höheren exzitonischen Zustände nicht vernachlässigt werden.

wie in [30] nicht ausreicht, um die Gültigkeit einer Zweiniveaunäherung zu beweisen, auch wenn *anticrossing* bereits für Zweiniveausysteme auftritt [2]. Einige Systemeigenschaften wie die Rabifrequenz werden allerdings recht gut vorhergesagt, wenn wir unsere Analyse auf die beiden wichtigsten Niveaus beschränken, nämlich die exzitonischen $1s$- und $2p$-Niveaus. Dennoch kann diese Zweiniveaunäherung die genaue Position der Resonanzen in den Spektren und die Dynamik der Polarisationen nicht korrekt vorhersagen. Zusätzlich zu diesen beiden Studien ist eine weitere Studie in Arbeit, bei der mit dem spektral breitem Terahertzpuls Anregungen in Germanium untersucht werden. Die Details werden nicht in dieser Doktorarbeit gezeigt; wir fanden heraus, dass das System prinzipiell sehr ähnlich zu GaAs-Quantenfilmen ist. Unsere Untersuchungen zeigen, dass die Pulsform des Terahertzvektorpotentials entscheidend ist für den Terahertzeinfluss auf das System und nicht das Profil des elektrischen Feldes, obwohl jenes im Experiment die Messgröße ist.

In Kapitel 4 wird Terahertzspektroskopie an Exziton-Polaritonen beschrieben. Diese entstehen, wenn Quantenfilme an eine Kavität koppeln. Die $1s$-Exzitonenresonanz spaltet auf in tiefere und höhere Exziton-Polaritonen (*lower- and higher exciton polariton, LEP and HEP* - siehe Abbildung 0.1). Mit Halbleiterkavitäten kann man viele interessante Effekte beobachten wie bspw. *cavity quantum electrodynamics (cavity QED)* [38–43] oder Bose–Einstein-Kondensation von Exziton-Polaritonen [44–47]. Die Übergangsenergien von Exziton-Polaritonen zu höheren exzitonische Zuständen liegen im Terahertzbereich. Dies warf die Frage auf, wie Exziton-Polaritonen als Mischzustände aus Licht und Materie auf Terahertzlicht reagieren: Dominiert der Lichtanteil die Wechsel-

wirkung (optisches Licht interagiert nicht direkt mit Terahertzlicht), der exzitonische Anteil (also die 1s-artige Polarisation) oder tragen beide Anteile zu einer Wechselwirkung bei? In Zusammenarbeit mit der experimentellen Gruppe um Yun-Shik Lee (Oregon State University, USA) wurde gezeigt, dass die beiden Exziton-Polaritonen gemeinsam mit dem exzitonischen 2p-Zustand ein Λ-System bilden, ähnlich wie bei Systemen aus der Atomphysik [48]. Die Ergebnisse sind in Veröffentlichung II publiziert und werden in Abschnitt 4.1 zusammengefasst.

Die Wechselwirkung der exzitonischen Polarisation mit den Eigenmoden der Kavität kann mit der Wechselwirkung zweier harmonischer Oszillatoren verglichen werden. Nicht nur die Eigenfrequenzen spalten sich auf; zusätzlich oszilliert auch die Energie zwischen beiden Systemen, dem elektrischen Feld und der Polarisation. Durch die Verbindung von Terahertzspektroskopie mit einer theoretischen Analyse können wir diese Schwebung (*beating*) direkt beobachten. Genaueres dazu in Abschnitt 4.3 und in Veröffentlichung V. Die Gleichungen, mit denen wir die Experimente modellieren, sind die Maxwell-Halbleiter-Bloch-Gleichungen [2, 49] erweitert für zusätzliche Terahertzfelder [7]. Ein Überblick über die Gleichungen wird in Kapitel 2 gegeben. Sie bieten eine mikroskopische Beschreibung und sind daher geeignet, die Ursachen der spektralen Änderungen in den zugrundeliegenden Prozessen zu ergründen. Besonders beeindruckend ist, dass wir dadurch quasi mit den gleichen Gleichungen und dem gleichen Computerprogramm völlig unterschiedliche experimentelle Situationen simulieren können, wie Strukturen mit vielen Quantenfilmen oder Vakuum-Rabiaufspaltung in Kavitäten. Dieser Ansatz ist aufgrund der großen Flexibilität sehr vielversprechend bei der Analyse weiterer Experimente.

Denn die im Rahmen dieser Doktorarbeit behandelten Themen sind keineswegs abgeschlossen. Die Eigenschaften von exzitonischen Systemen werden weiterhin mit Hochdruck untersucht, befeuert durch die Möglichkeiten, qualitativ immer hochwertigere Materialien herzustellen und besser zu messen. Die Untersuchung von Exzitonen mit Terahertzspektroskopie wird weiterhin genutzt, um kohährente und inkohärente Exzitonen besser zu verstehen, beispielsweise, wie ihr Streuverhalten von Magnetfeldern beeinflusst wird [50]. Die Kontrolle des exzitonischen 1s–2p-Übergangs ist ein möglicher Weg, um Qubits für Quantencomputer zu entwickeln [51].

Das genaue Verständnis und die Kontrolle von Exzitonen sind auch von grundlegender Wichtigkeit, um kompliziertere Systeme mit Quantenfilmen zu verstehen. Das wird in Kapitel 4 klarer, in dem der exzitonische 1s-Zustand mit den Eigenmoden einer Kavität gekoppelt ist. Das Verständnis dieses komplizierteren Systems fußt auf unserer Fähigkeit, die kohärenten Exzitonen zu modellieren. Weitere Arbeiten an ähnlichen Systemen sind in Planung, bspw. an solchen mit sehr großer Rabiaufspaltung wie in [52]. Terahertzspektroskopie an Exziton-Polaritonen und das hierdurch entdeckte Λ-System sind der Ausgangspunkt für weitere Forschung. Wir glauben, dass das Λ-System robust genug ist, um Phänomene aus der Atomphysik wiederzufinden, wie Stimulated Raman Adiabatic passage (STIRAP) [53], elektromagnetisch induzierte Transparenz (EIT) [54] oder langsames Licht [55]. Weitere Studien in dieser Richtung sind bereits in Arbeit [56]. Doch dies waren nur einige wenige mögliche Anwendungen aus der Sicht der Grundlagenforschung. Die nächsten Jahre werden zeigen, wieviel mehr wir noch von Terahertzspektroskopie an Halbleiternanostrukturen erwarten können.

Danksagung

Mein größter Dank gilt Professor Stephan Koch und Professor Mackillo Kira für das spannende Thema und die engagierte und motivierende Betreuung. Die stets hilfreichen Diskussionen und Ratschläge halfen mir, alle großen und kleinen Herausforderungen des Forschungsalltags zu meistern, ohne den Blick auf das große Ganze zu verlieren.

Bei PD Sangam Chatterjee bedanke ich mich für die guten Kooperationen, die vielen lehrreichen Diskussionen und die Bereitschaft, das Zweitgutachten zu verfassen. Ebenso bedanke ich mich bei Benjamin Ewers und Niko Köster für die gute Zusammenarbeit und die vielen Treffen, bei denen wir gegenseitig von den verschiedenen Blickwinkeln von Experiment und Theorie profitieren konnten.

Bei Professor Yun-Shik Lee bedanke ich mich für unsere spannenden gemeinsamen Projekte im Bereich der Polaritonen.

Für die gemeinsamen Studien und fruchtbaren Diskussionen bedanke ich mich bei Professor Manfred Helm und Martin Teich.

Ein besonderer Dank gilt Hanno Steiner, dessen Doktorarbeit und Programmcode meinen direkten Einstieg in die physikalischen Analysen ermöglichten.
Die tolle Atmosphäre und Diskussionsfreude in unserer Arbeitsgruppe mir war zu allen Zeiten eine große Unterstützung. Besonders gilt mein Dank Benjamin Breddermann, Christoph Böttge, Daniel Golde, Martin Mootz, Johanna Grönqvist, Fredrik Jansson, Lukas Schneebeli, Phillip Springer, Tineke Warncke, Ada Bäumner, Alex Bronn, Christian Berger, Ulrich Huttner und Jakob Geipel für die unzähligen fachlichen Diskussionen und gemeinsamen Kochabende.
Bei Professor Peter Thomas bedanke ich mich für die Organisation der Wanderungen und die gemeinsame Aquarienpflege.
Mein Dank gilt Professor Wolfgang Bestgen für die vielen guten und stets motivierenden Ratschläge.

Mein herzlichster Dank gilt meiner Familie für die durchgehende Unterstützung während meiner Doktorarbeit. J'adresse mes plus grands remerciements à ma famille, en Allemagne et en France.

Pour Matthieu

Author's Contributions

Publications

Papers

(I) B. Ewers, N. S. Köster, R. Woscholski, M. Koch, S. Chatterjee, G. Khitrova, H. M. Gibbs, A. C. Klettke, M. Kira, and S. W. Koch, *Ionization of coherent excitons by strong terahertz fields*, Phys. Rev. B **85**, 075307 (2012).

(II) J. L. Tomaino, A. D. Jameson, Y.-S. Lee, G. Khitrova, H. M. Gibbs, A. C. Klettke, M. Kira, and S. W. Koch, *Terahertz Excitation of a Coherent Λ-Type Three-Level System of Exciton-Polariton Modes in a Quantum-Well Microcavity*, Phys. Rev. Lett. **108**, 267402 (2012).

(III) A. C. Klettke, M. Kira, S. W. Koch, J. L. Tomaino, A. D. Jameson, Y.-S. Lee, G. Khitrova, and H. M. Gibbs, *Terahertz excitations of lambda systems in a semiconductor microcavity*, accepted at phys. stat. sol. (c), Proceedings of the International Workshop NOEKS-11

(IV) M. Teich, M. Wagner, D. Stehr, H. Schneider, M. Helm, G. Khitrova, H. M. Gibbs, A. C. Klettke, S. Chatterjee, M. Kira, and S. W. Koch, *Systematic investigation of THz-induced excitonic Rabi splitting*, submitted to Physical Review B

Papers in Preparation

(V) A. D. Jameson, J. L. Tomaino, Y.-S. Lee, G. Khitrova, H. M. Gibbs, A. C. Klettke, M. Kira, and S. W. Koch, *Terahertz Spectroscopy of Light-Polarization Beating inside a Microcavity*, in preparation

(VI) N. S. Köster, B. Ewers, R. Woscholski, M. Koch, S. Chatterjee, A. C. Klettke, M. Kira, and S. W. Koch, *Rabi splitting in Germanium Quantum Wells*, in preparation

Posters and Talks

(i) A. C. Klettke, J. T. Steiner, M. Kira, S. W. Koch, and Y.-S. Lee, Talk: *THz studies of strong coupling microcavity systems*, DPG Spring Meeting, Dresden (March 13-18, 2011).

(ii) A. C. Klettke, J. T. Steiner, M. Kira, S. W. Koch, S. Chatterjee, B. Ewers, N. S. Köster, and Y.-S. Lee, Poster: *Microscopic Theory for Strong-Field THz Spectroscopy*, THz Science and Technology - The Castle Meeting, Marburg (July 03-06, 2011).

(iii) A. C. Klettke, J. T. Steiner, M. Kira, S. W. Koch, S. Chatterjee, B. Ewers, N. S. Köster, and Y.-S. Lee, Talk: *Terahertz interaction with optically excited semiconductors*, Materialforschungstag Mittelhessen, Marburg (July 10, 2012).

(iv) A. C. Klettke, J. T. Steiner, M. Kira, S. W. Koch, S. Chatterjee, B. Ewers, N. S. Köster, and Y.-S. Lee, Poster: *Microscopic Theory for Strong-Field THz Spectroscopy*, Interdisciplinary Summer School Get Ahead With Optics, Tunisia (September 02-12, 2012).

(v) A. C. Klettke, J. T. Steiner, M. Kira, S. W. Koch, J. L. Tomaino, A. D. Jameson, Y.-S. Lee, G. Khitrova, and H. M. Gibbs, Talk: *Terahertz-induced optical transitions in semiconductor microcavities*, 11th International Workshop on Nonlinear Optics and Excitation Kinetics in Semiconductors, Stuttgart (September 23-27, 2012).

Original Contributions

In the projects presented within this Thesis, I simulated and analyzed experiments with simultaneous optical and terahertz (THz) excitation of semiconductor nanostructures.

My main own contribution is the numerical simulations and based on them the analysis of experimental and theoretical data. I also participated in the preparations for the publications. My numerical simulations are based on equations which were already used in former studies; I also received the basic of the programming code from Johannes T. Steiner, including a basic transfer-matrix method for the propagation of terahertz and optical light. I optimized the numerics of the program and extended the Fortran code for each of the theoretical situations (e.g., the microcavity).

We discussed the preliminary results of all projects in many internal meetings, where we also planned the basic strategy of the simulations. All numerical simulations and data analysis were performed by myself.

In the first part of my Thesis, I analyze three experiments with multiple-quantum well systems. All three studies were made in a collaboration where the experiments were done in the group of Sangam Chatterjee (Philipps-Universität Marburg), one in addition with the group of Manfred Helm at the Helmholtz-Zentrum Dresden Rossendorf. The first project is about excitonic Rabi splitting with a single-cycle THz pulse. With our theoretical simulation, we found that the spectrally-broad THz pulse *ionizes* the exciton: The polarization is transferred via multi-photon absorption into higher excitonic states. The principle behavior of the THz interaction with excitons was already expected from former studies, but not yet seen in such good experimental conditions. Our results are published in Paper I.

We made a similar study in cooperation with the group of Manfred Helm from the Helmholtz-Zentrum Dresden Rossendorf. The main difference to the previous study is the spectrally very narrow terahertz pulse, generated by a free-electron laser. This makes it possible to follow the transition from an effective two-level system to the exciton ionization mentioned above. The results are described in Paper IV. We also studied a sample with germanium quantum wells with a similar THz pulse as for Paper I . We could reproduce the experimental results with our theory, showing that the THz-induced changes follow the THz vector potential and not the electric field of the THz pulse, even

though the THz electric field is the parameter measured in the experiment. The results are in preparation for publication in Paper VI.

The second type of experiments described within this Thesis is terahertz spectroscopy on exciton polaritons. Unlike for excitons, the coupling of exciton polaritons with THz excitation was not studied before. The splitting of exciton and cavity resonances into two normal-mode peaks is a strong-coupling phenomenon. Hence, the system is very sensible to small changes and disorder effects in the material, making the numerical simulation demanding. In cooperation with the group of Yun-Shik Lee (Oregon State University, USA), we found that lower- and higher-exciton polariton build, together with the excitonic $2p$ state, a unique Λ system. More details can be found in Paper II. We performed with the parameters of the Λ system an additional numerical study focussed on the role of the excitonic $2p$ state: We compare the Λ-system transitions with the $1s$–$2p$ transition in a system without microcavity. As a results, we see that the general behavior is similar to the $1s$–$2p$ transition studied in bare quantum wells. The coupling to the continuum is important in both systems. The results are published in Paper III. These results are very promising for further studies, for example, I started simulating situations with several terahertz pulses in order to study Stimulated Raman Adiabatic Passage (STIRAP) with our Λ system.

Another interesting phenomenon we study with THz spectroscopy is the temporal evolution of exciton polaritons. The experimental results (again from the group of Yun-Shik Lee) show oscillations in the differential reflectivity spectrum when sweeping the arrival time of the THz pulse as compared to the optical light. Our analysis of the experimental finding proved that they originate from cavity beating: Inside the microcavity, energy is transferred back and forth between optical field and polarization. As the THz pulse only couples to exciton polaritons if polarization is present, the THz influence depends on the phase of the polarization at the THz arrival time and thus leads to the oscillations mentioned. The results are in preparation for publication in Paper V.

I presented parts of my projects in a talk at the DPG Spring Meeting (2011) [i], as posters at the *Terahertz Science and Technology* conference (Marburg, 2012) [ii] and at the *Get Ahead With Optics* Summer School (Tunisia, 2012) [iii], and in talks at the Materialforschungstag (Marburg, 2012) [iv] and the NOEKS workshop (Stuttgart, 2012) [v].

Contents

1 Introduction

In the last twenty years, microchips and electronic devices for computers and multimedia hardware became not only faster and more powerful, but also significantly smaller. A modern microchip is typically made of semiconductor material patterned in length scales of tens of nanometers [1]. At length scales near to 10 nm, quantum mechanical effects start to play a role. In very thin layers, stripes, or dots, charge carriers like electrons and holes are quasi-confined to two or less dimensions which changes the material properties significantly [2]: Quantum wells (QWs) where the carries are confined to two dimensions (quasi 2D), quantum wires (quasi 1D) and quantum dots (0D) give rise to a wide range of new effects and exciting physics [3]. It is an important task of today's research to understand the fundamental physics in these low-dimensional semiconductor nanostructures in order to design the hardware of the future.

At very low temperatures, semiconductors are insulators: In terms of the energy band model, electrons are inside a filled valence band, separated from the empty next-higher energy band, the conduction band, by an energetic band gap. The band gap is in the order of few electron volts, equal to the photon energy of optical or near-infrared light. This means that electrons can be lifted from the valence band into the conduction band by optical or near-infrared light. (For simplicity, we speak in this Thesis only of *optical light* instead of *optical or near-infrared light*.) At higher temperatures, when thermal fluctuations are large enough to lift electrons into the conduction band, the semiconductor behaves more like a metal [4]. At low temperatures, optical light creates in semiconductors a whole bunch of many-body excitations [2, 5–7], starting from polarization between electrons in the conduction band and holes in the valence band (so-called coherent excitons) which eventually transform within a few picoseconds into incoherent excitons, biexcitons, and other many-body excitations [2, 8–13]. The fact that the higher-order correlations build up from—and temporarily after—lower-order correlations is the starting point of the Cluster-expansion approach [7, 14]. Speaking in terms of the Cluster expansion, many fundamental effects concerning coherent excitons can already be described with singlets; in some cases, higher-order terms like scattering contributions can be treated with phenomenological models.

In many ways, coherent excitons have hydrogen-like features: They appear, e.g., as discrete energy levels spectrally below the conduction band due to the attractive Coulomb interaction between the oppositely charged carriers in valence and conduction band. There are even similar quantum numbers as for the hydrogen system, only with transition energies scaled down by a factor of 1000. Instead of the several eV of the hydrogen atom, we have transition energies of few milli-electron volts (meV), i.e., in the terahertz range. These analogies motivate spectroscopy on excitons and the search for condensed-matter equivalences of coherent atomic effects. The development of THz lasers and de-

tectors suiting the intraexcitonic transitions during the last decade stimulated the THz spectroscopy on excitons [8, 15–23]. Exciton spectroscopy with THz light has the great advantage that the THz photon energy is much smaller than the band gap and highly off-resonant to the creation of excitonic polarization. Consequently, it passes through the unexcited semiconductor. Instead, it is resonant with intraexcitonic transitions. As the momentum carried by a THz photon is not sufficient to transfer polarization along the parabolic energy band, additional interaction processes like the Coulomb and phonon interaction are needed to allow THz-induced intraexcitonic transitions. A single-cycle THz pulse has a duration of around 1 picosecond (ps), shorter than the decay time of optical polarization in GaAs of several picoseconds. All this makes THz light an ideal tool to study semiconductor excitation and in particular coherent excitons [24–29]. Studies using both optical and THz light were already made on electron–hole gas, high-harmonic generation, photoluminescence quenching of magnetoexcitons and excitonic Rabi splitting [19, 30–33]. The coupling between the many excitonic levels make the systems in general too complicated for few-level models. It was shown that fully microscopic calculations are needed to understand the dynamics of the intraexcitonic transitions [19].

In this Thesis, we focus on the analysis of two types of experiments: Chapter 3 discusses THz spectroscopy on *bare* QWs (meaning that the interaction with material around the QWs is neglectable), while Chapter 4 is devoted to the spectroscopy on QWs interacting with the light modes inside a microcavity. Both topics are also interesting from a fundamental point of view because of the similarities of excitons with atomic systems described earlier. A very basic effect connecting both topics of this Thesis is the AC Stark effect [2]: It describes the splitting of spectral lines in the presence of an electric field. In atoms, the line splitting due to the resonant excitation of a transition between two atomic states is called Rabi splitting [34]. The Rabi splitting of the 1s-exciton peak due to THz light is discussed in Chapter 3, while Chapter 4 describes THz spectroscopy on a system where the 1s-exciton peak is already split due to the interaction with a microcavity (vacuum Rabi splitting [35, 36]). In particular, in Section 3.1, we study coherent excitons in $Ga_{0.97}In_{0.03}As$ QWs interacting with a spectrally broad THz pulse. As a result of the analysis, we observe exciton ionization, a situation similar to the ionization in atoms: The polarization is pushed into states with high energy and orbital numbers. Our study can be interpreted as analogous to the above-threshold ionization scenario in atomic systems [37]. The results are presented in Paper I. This was a surprising result as recently, a similar experiment with a spectrally-narrow THz pulse was explained using a two-level model [30]. To close the gap between these two different regimes of ionization and two-level system, we have launched a joint study with spectrally-narrow THz light and a microscopic analysis. The results are published in Paper IV and discussed in Section 3.2. We found out that the observation of anticrossing like in [30] is not enough to prove the suitability of a two-level model, even if the anticrossing is already predicted from two-level calculations [2]. Some system properties like the Rabi frequency were well predicted when we restricted our theoretical analysis to the two most important states, the excitonic 1s and 2p states. However, this two-level approximation fails to determine correctly, e.g., the peak position in the spectra and the polarization dynamics. In addition to these two studies, another study with broad THz excitation on germanium

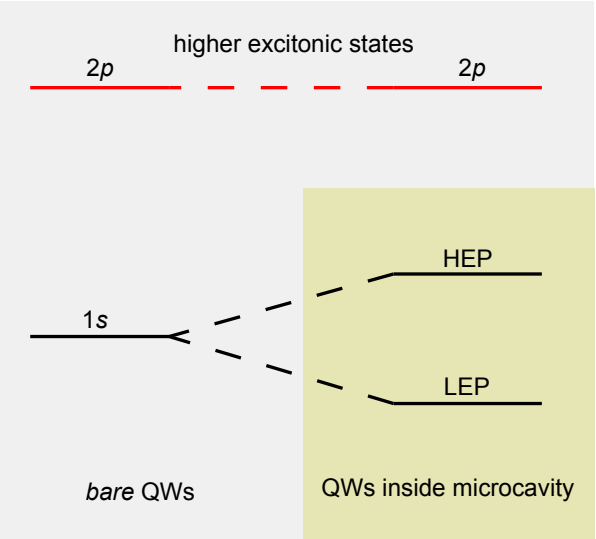

Figure 1.1: Main excitonic energy levels (without THz influence) in Chapter 3 and Chapter 4: For THz spectroscopy on bare QWs, the 1s and the 2p states are the most important excitonic states. For QWs inside a 1s resonant microcavity, the 1s energy level splits into lower and higher exciton polariton (LEP and HEP). Both cases have in common that contributions of higher excitonic states cannot be neglected.

quantum wells is in preparation at the moment, but not presented within this Thesis. We found out that the germanium system is very similar to the GaAs multiple quantum-well systems. Using strong THz fields shows that the temporal profile of the THz vector potential is crucial for the THz influence on the system and not the electric field of the THz pulse, even if it is the measured value in the experiment. This is in agreement with theoretical equations and the results of our theoretical study.

Chapter 4 describes THz spectroscopy on excitons inside a microcavity where the 1s exciton energy level is split into lower- and higher-exciton polariton (see Fig. 1.1). Semiconductor microcavities are used to study interesting effects like cavity quantum electrondynamics (cavity QED) [38–43] or Bose–Einstein condensation (BEC) of exciton polaritons [44–47]. The transition energies from the exciton polaritons into higher excitonic states still lie in the THz range, so the question arose whether exciton polaritons as mixed light–matter states behave more like light (optical light does not directly interact with THz light) or like excitons with shifted energy levels, so to say: how *excitonic* are exciton-polaritons? A collaboration with the group of Yun-Shik Lee (Oregon State University) unveiled that the two exciton-polaritons together with the excitonic 2p state constitute a Λ system, with similarities with Λ systems found in atomic physics [48]. The results are published in Paper II and summarized in Section 4.1. In addition, vacuum Rabi splitting also has similarities with the coupling of two harmonic oscillators: Not only the eigenenergies split, but the energy also oscillates forth and back between the electric field and the polarization [36, 57]. Using THz spectroscopy in connection with

our theory allows us to directly observe the beating of the energy between the optical polarization inside the quantum wells and the electric field inside the cavity. More details can be found in Section 4.3 and in Paper V.

The equations which we used to model the experimental situations are the Maxwell-semiconductor Bloch equations [2, 49] extended to additional THz fields [7]. They are fully microscopic, which makes it possible to gain more knowledge of the underlying processes causing experimentally observed spectral changes. Furthermore, it allows basically the same implementation of the physics to model completely different experimental situations such as multi-quantum well structures or normal-mode coupling in microcavities. An overview of the physical equations is given in Chapter 2. Finally, a summary and a short outlook are presented in Chapter 5.

2 Theoretical approach

In this Chapter, I briefly introduce the theoretical basics and equations. My investigations are based on established theories: The Maxwell-semiconductor Bloch equations (MSBE) [2, 49] describe the interaction between optical light and semiconductor crystals self-consistently. The experiments discussed in the later Chapters involve semiconductor quantum well (QW) structures interacting with both optical and THz light, therefore we use the MSBE extended for additional THz fields [7, 58]. Since those basic theoretical concepts have already been discussed [18–20, 33], I will focus only on the main equations and not on their derivations.

The scheme of the numerical calculations is depicted in Fig. 2.1: Optical light (green box, top) and THz light (red box, bottom) propagate into the sample (cyan box, middle). The incoming THz light is represented by its vector potential A_{inc}, while the incoming optical light is denoted by its electric field E_{inc}. The sample is either a multiple quantum-well structure (Chapter 3) or a microcavity enclosing quantum wells (Chapter 4). Inside the sample, reflection and transmission of the fields are determined using a standard Transfer Matrix Method [36]: The optical and THz fields propagating in the different directions are denoted by $E^{\pm}$ and $A^{\pm}$, respectively. In the experimental situations studied within this Thesis, optical and THz light are off-resonant from other matter excitations except those of the quantum well material. The semiconductor Bloch equations determine how the polarization in the material is influenced by the optical and THz fields, and Maxwell's equation describes the back coupling of the polarization onto the fields. In particular, the optical field couples only to optical polarization, while the THz field redistributes existing polarization. As the optical spectra are determined by the optical polarization [7], the optical spectrum is changed when THz transforms optical polarization into (optically) dark polarization.

Within this Chapter, I will review in Section 2.1 the concept of coherent excitons and in Sections 2.2 the semiconductor Bloch equation for additional THz fields. Section 2.3 is devoted to the Wannier Equation, which allows us to project our results into the exciton basis and Section 2.4 the back coupling of the polarization onto the fields. More details can be found in [7]. A nice overview especially for the parts used in this Thesis is given in [58].

2.1 Coherent excitons

Coherent excitons are polarizations $p_{\mathbf{k}}$ induced by optical light between electrons in the conduction band and holes in the valence band of a semiconductor, as shown schematically in Fig. 2.2. This situation of two carriers of opposite charge interacting via Coulomb

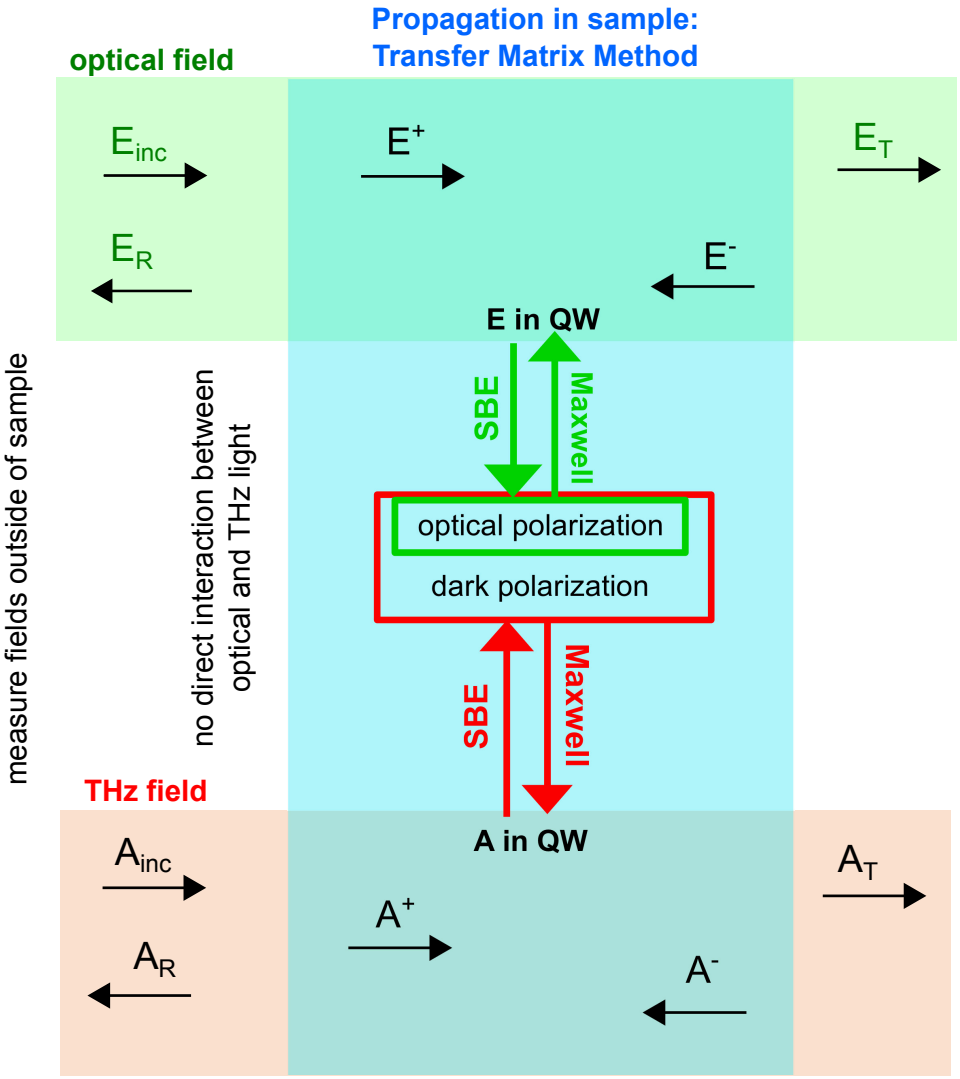

Figure 2.1: Calculation scheme: The optical field E and the vector potential of the THz light A enter the sample and propagate back and forth due to changes of the refractive index inside the sample ($E^{\pm}$ and $A^{\pm}$), determined via a Transfer Matrix Method. The interaction of the light with the QWs is described by the Maxwell-semiconductor Bloch equations, where optical light couples only with the optical polarization. Fields transmitted through the sample or reflected back from it ($A_{\mathrm{T/R}}$ and $E_{\mathrm{T/R}}$) are used for comparison with experimental transmission or reflection measurements.

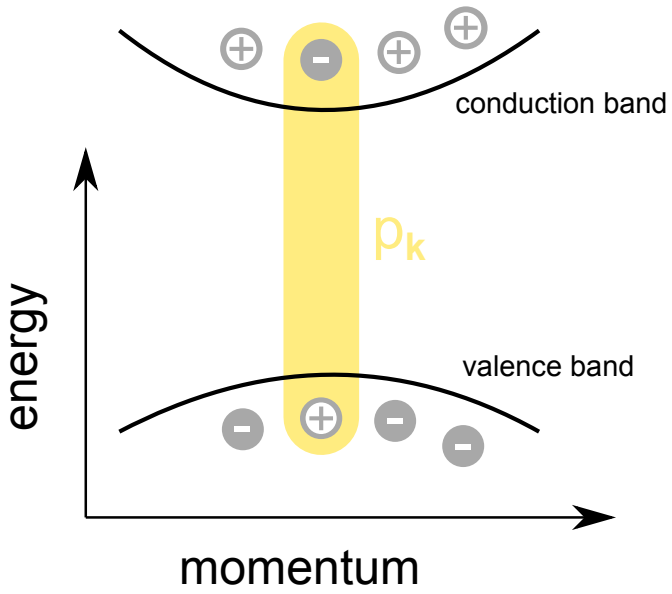

Figure 2.2: Schematic picture: An excitonic polarization $p_{\mathbf{k}}$ is a superposition state between an electron (filled circles) in the mostly empty conduction band and a hole (empty circles) in the (mostly filled) valence band.

interaction is mathematically very similar to the hydrogen problem, including the occurrence of distinct eigenvalues (eigenenergies) and eigenfunctions (electron wave functions). Likewise, the excitonic eigenvalues are denoted by quantum numbers like for the hydrogen problem. In particular, its principal quantum number is linked to the energy, while the magnetic quantum number refers to the angular momentum. We use these quantum numbers from the hydrogen atom to describe the polarization dynamics and selection rules for transitions with a commonly used vocabulary. The polarization in exciton basis p_λ is linked to the polarization $p_{\mathbf{k}}$ via the left- and right-handed excitonic wave functions $\phi^{\mathrm{L/R}}$ [7]:

$$p_\lambda = \sum_{\mathbf{k}} \phi^{\mathrm{L}}_\lambda(\mathbf{k})\ p_{\mathbf{k}}, \qquad p_{\mathbf{k}} = \sum_{\lambda} \phi^{\mathrm{R}}_\lambda(\mathbf{k})\, p_\lambda. \tag{2.1}$$

The similarities between excitonic polarization (coherent excitons) and the hydrogen problem rise the question which effects known from atomic physics (e.g. Rabi splitting [34] or the Mollow triplet [59]) exist also in coherent excitons systems.

2.2 Semiconductor Bloch equation for additional terahertz fields

The semiconductor Bloch equations (SBE) for additional THz fields follow from the Cluster-expansion approach [7, 14, 60]. In the experiments discussed within this Thesis, the relevant time scales are a few picoseconds which is the decay time of the polarization (depending on the material system). Coherent light is very close to *classical light*, this is

why a semiclassical description of the electromagnetic fields is often sufficient. Moreover, it allows us to use the singlet approximation from the Cluster expansion and treat the scattering contributions phenomenologically.

We discuss here experiment with weak optical light is weak, exciting only low carrier densities. This allows us to use constant densities and to rewrite the equation for the polarization dynamics into the exciton basis. Extended for additional THz fields [14, 58], it reads

$$\begin{aligned} i\hbar\frac{\partial}{\partial t}p_\lambda = &\left(E_\lambda + \frac{|e|^2}{2\mu}A_{\mathrm{THz}}^2\right)p_\lambda - \sum_\nu J_{\lambda,\nu}\; A_{\mathrm{THz}}\; p_\nu \\ &+ d_{\mathrm{c,v}}\sqrt{S}\;\phi_\lambda^{\mathrm{R}}\left(\mathbf{r}=0\right)E_{\mathrm{opt}} - i\Gamma_\lambda, \end{aligned} \tag{2.2}$$

where $\lambda = (n, m)$ refers to the excitonic states consisting of principal quantum number n and azimuthal quantum number m, denoting the shape of the orbit. The optical field E_{opt} is the source term for the creation (and annihilation) of polarization. The excitonic wave functions $\phi_\lambda^{\mathrm{R}}$ are centered around $\mathbf{r} = \mathbf{0}$. Note that only s-like wave functions are non-zero at $\mathbf{r} = \mathbf{0}$, hence, optical light couples only to s-like polarization. (Physically, this originates from the selection rules for the p-like heavy-hole valence band and the s-like conduction band at the Γ point.) The light–matter coupling is scaled by the dipole-matrix element $d_{\mathrm{c,v}}$ between conduction and valence band. $\sqrt{S}$ denotes the quantization length. The THz field appears via its vector potential A_{THz}. As mentioned in the introduction, it passes through the unexcited semiconductor, as it does not contribute in the absence of polarization (for $p_\lambda = 0$). The THz influence is twofold: The ponderomotive current $\frac{|e|^2}{2\mu}A_{\mathrm{THz}}^2$ renormalizes the kinetic energy E_λ but does not drive transitions, i.e., the quantum numbers are not changed. Due to this, it is sometimes neglected [61]. However, this is not possible in all conditions ([33] and Section 3.1.6). The constants e and μ are the electron charge and the reduced mass of the electron–hole pair [33, 62], respectively. The THz vector potential couples also to the excitonic current matrix element $J_{\lambda,\nu}$ and redistributes the polarization p_λ into p_ν, according to the overlap of the wave functions:

$$J_{\lambda,\nu} = \sum_{\mathbf{k}} \phi_\lambda^{\mathrm{L}}\left(\mathbf{k}\right) j\left(\mathbf{k}\right) \phi_\nu^{\mathrm{R}}\left(\mathbf{k}\right). \tag{2.3}$$

Here, $\mathbf{k}$ is the (2-dimensional) momentum inside the quantum well, $\phi^{\mathrm{L/R}}$ the right/left handed excitonic wave function (see [7] and Section 2.3) and j is the current-matrix element. The wave functions are—apart from the scaling—close to those of the hydrogen problem and thus lead to similar selection rules. In particular, THz can only induce transitions from $\lambda = (n, m)$ to $\nu = (n', m\pm1)$, i.e., it only allows transitions into neighbouring orbitals like s-to$p$ transitions and vice versa. The decay due to scattering and higher-order correlations can be treated microscopically by the diffusive scattering model [7]. In the experiments analyzed within this Thesis, it is sufficient to use a phenomenological treatment with a dephasing constant $\Gamma_\lambda = \gamma_\lambda\, p_\lambda$. The typical values for γ_λ in my studies are in the range between 0.2 meV (yielding a dephasing time of 3.3 ps), and 2.2 meV (300 fs). The exact values used for the analysis are given in the parameter list. Typically,

as a first approximation one uses a constant $\gamma_\lambda \equiv \gamma$; as a second approximation, one takes into account that the 1s state decays much slower than the other excitonic states, as shown in microscopic calculations for GaAs [7].

In practice, the SBE (Eq. (2.2)) is solved via the standard 4th-order Runge Kutta algorithm which enables us to study the time-dependent polarization dynamics $p_\lambda(t)$. Therefore, we supply the SBE with the optical and THz field at each time step and each quantum well position. The excitonic eigenenergies E_λ, the wave functions $\phi_\lambda^{\mathrm{L/R}}$ and, by means of the wave functions, the current matrix element $J_{\lambda,\nu}$ are extracted from the Wannier equation.

2.3 Wannier equation

As discussed earlier, we use the SBE in exciton basis, i.e., with excitonic wave functions ϕ, eigenenergies E_λ and excitonic quantum numbers λ. The excitonic wave functions are obtained from the Wannier equation [7]:

$$\epsilon_{\mathbf{k}}\phi_\lambda^{\mathrm{R}}(\mathbf{k}) - \left(1 - f_{\mathbf{k}}^{\mathrm{e}} - f_{\mathbf{k}}^{\mathrm{h}}\right)\sum_{\mathbf{k}'} V_{\mathbf{k}-\mathbf{k}'}\phi_\lambda^{\mathrm{R}}(\mathbf{k}') = E_\lambda\phi_\lambda^{\mathrm{R}}(\mathbf{k}) \tag{2.4}$$

The Wannier equation is the homogeneous solution of the SBE (in momentum basis) [2]. For low densities of electrons and holes $f_{\mathbf{k}}^{\mathrm{e/h}}$, the equation is mathematically identical to the well-known hydrogen problem [7]. The appearance of the phase-filling factor $\left(1 - f_{\mathbf{k}}^{\mathrm{e}} - f_{\mathbf{k}}^{\mathrm{h}}\right)$ leads to the occurrence of the left- and right-handed eigenfunctions $\phi^{\mathrm{L/R}}$, unlike in the hydrogen problem. $\epsilon_{\mathbf{k}}$ is the renormalized kinetic energy of an electron–hole pair, which consists of the kinetic energies of the carriers, and which is renormalized due to the Coulomb interaction $V_{\mathbf{k}-\mathbf{k}'}$ between electrons and holes. Solving the equation numerically provides us with the excitonic eigenenergies E_λ and the left- and right-handed eigenfunctions $\phi_\lambda^{\mathrm{L/R}}$. Note that the optical light does not appear in the Wannier equation, the renormalization of the eigenenergies induced by the fields (Stark effect) are not taken into account by the Wannier equation. The weak fields used in the experiments allow us to follow in the exciton basis how the THz field redistributes the polarizations.

2.4 Maxwell's wave equation

The previous Sections describes with the SBE the influence of optical and THz fields on the polarization (Section 2.2) and how we project the results in terms of excitonic components (Section 2.3). In Equation (2.2), the changes in the polarization due to optical and THz fields were given. For a self-consistent treatment, one needs to simultaneously take into account the influence of the polarization on the optical and THz fields. This is especially crucial for the optical field in our experimental situations, as it is the way we monitor changes in the optical spectrum and even more when we simulate the interaction of optical light with a microcavity, where energy is transferred back and forth between

optical field and polarization. For light propagating in z direction, the back coupling according to Maxwell's equation reads

$$\left[\frac{\partial^2}{\partial z^2} - \frac{n^2(z)}{c^2}\frac{\partial^2}{\partial t^2}\right] E_{\text{opt}}(z,t) = \mu_0 \delta(z - z_{\text{QW}}) \frac{\partial^2 P}{\partial t^2} \tag{2.5}$$

The refractive-index profile of the sample is given by $n(z)$. The source term for changes in the optical field is the macroscopic polarization P, which is the sum of the optical polarizations. The speed of light and the vacuum permeability are denoted by c and μ_0, respectively. The Dirac delta function $\delta(z - z_{\text{QW}})$ describes that the back coupling is only taking place when the optical light is at the QW position z_{QW}. Within this Thesis, the back coupling on the THz field is not taken into account, as the influence of the changes in the THz field on the polarization is neglecteble. However, for future projects like STIRAP on the excitonic Λ system, it will be needed to incooperate them into the model, as the measurement parameter for an experimental measurement would be the THz absorption.

3 Bare quantum wells

Optical or near-infrared light creates optical polarization in semiconductor quantum wells (QWs) between electrons in the conduction band and holes in the valence band, which decays within few picoseconds. These have been studied, e.g., by wave-mixing spectroscopy or resonant Rayleigh scattering [17]. Recently, THz lasers and measurement scenarios made it possible to directly detect and manipulate excitons [7, 8, 17, 18, 63–70]. In this Chapter, we present two experiments with weak optical and strong THz light. The setup is schematically shown in Fig. 3.1 **(a)**. More details about the experiments can be found in Paper I and Paper IV. As described in Chapter 2 and depicted in Fig. 3.1 **(b)**,

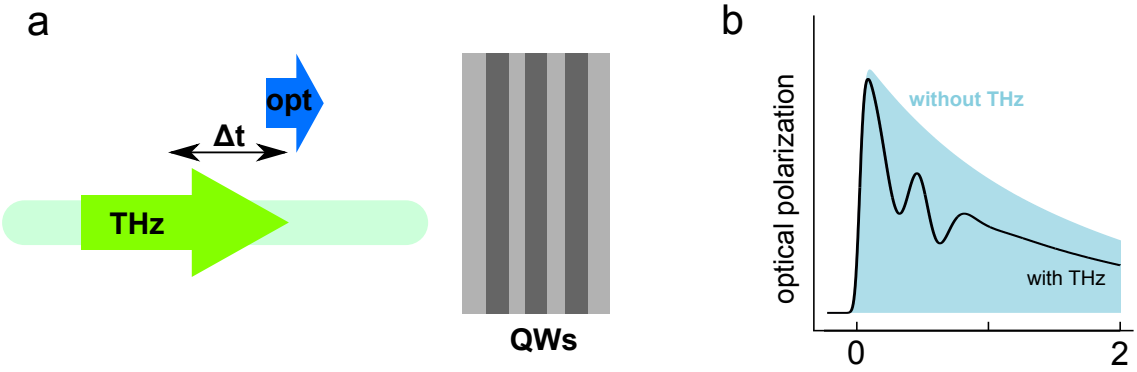

Figure 3.1: **(a)** Setup of weak optical and strong THz excitation spectroscopy: THz and optical arrive at quantum wells with time delay Δt. **(b)** Without THz influence, the optical polarization decays exponentially (shaded area). THz field pushes part of the optical polarization way and back into (optically-) dark polarization (solid).

optical light creates optical polarization while THz light redistributes optical polarization into optically dark polarization. In this Chapter, we describe experiments for which we follow the THz-induced changes in the optical reflection or transmission spectrum. Our microscopic theory reproduces the optical spectra and allows us in addition to monitor the underlying many-body processes.

Section 3.1 describes my first project (Paper I) on weak optical and strong THz excitation spectroscopy on quantum wells. The project started as Benjamin Ewers *et al.* had measured excitonic Rabi splitting in quantum wells using a single-cycle THz pulse. In addition to the Rabi splitting, a bleaching and shifting of the excitonic and Rabi peaks was observed. They asked us to analyze the experimental data to check whether Rabi splitting is a sign of Rabi flopping of excitonic polarization. The fully microscopic theory allowed us to simulate the THz-induced excitation dynamics. In terms of the exciton

basis, we could show that the system was not dominated by Rabi flopping between the $1s$ and $2p$ polarization. The calculation reveals that high excitonic orbitals are invloved and states with energies of up to 4 THz photons: Instead of Rabi flopping inside a two-level system, the exciton was practically ionized by high THz intensities. In addition, we demonstrated the importance of the ponderomotive force for these kind of experiments with strong THz fields.

Still, an open question remained: How much is the ionization of the coherent excitons due to the fact that the THz pulse is spectrally broad and not only focussed on the frequency range of the $1s$–$2p$ transition frequency? A similar experiment has been reported by Wagner *et al.* from the group of the Helmholtz-Zentrum in Dresden-Rossendorf. They used a free-electron laser (FEL) to emit spectrally narrow THz pulses. These quasi-cw pulses can be tuned continuously in the THz frequency range and were used to drive resonantly the $1s$–$2p$ transition frequency from weak THz intensities up to 10 kV/cm. They observed not only Rabi splitting of the $1s$-exciton peak, but also anticrossing behavior of the Rabi peaks when detuning the THz frequency from the $1s$–$2p$ transition frequency. Both effects have been explained within two-level models. To close the gap between these two studies, experiments were performed with the FEL at the Helmholtz-Zentrum Dresden-Rossendorf on a sample with GaAs quantum wells and a larger energetical separation between $1s$-heavy hole and light hole than the ones used in [30]. The results are in publication process in Paper IV. Our fully microscopic theory showed that the observation of anticrossing behavior and Rabi splitting is not sufficient to prove that essentially only two states are involved.

3.1 Exciton ionization

3.1.1 Optical spectrum without terahertz influence

Figure 3.2 shows the 1-transmission (1-T) spectrum without THz influence as calculated from the microscopic theory. The sample DBR13 is made of 30 $Ga_{0.97}In_{0.03}As$ QWs separated by GaAs barriers. The optical spectrum is determined by the s-like excitonic states whose positions are marked as vertical white lines. The $1s$-exciton state has by far the strongest light–matter-coupling strength. From the five higher s-like energy states marked as white lines before the onset of continuum of states, only the $2s$ peak is slightly recognizable in the spectrum: The higher s-like states and the continuum with much lower coupling strength lay energetically too close to each other. They also differ in the peak broadening (not shown here), which determines the decay time of the respective polarization and hence the line width. The energies of the next-higher orbitals (p, d and f) are given for illustrational reason as black vertical lines. They are shifted under the optical spectrum illustrating that they are optically dark and not excited by optical light, as explained in Chapter 2. As the $1s$ state has the dominating light–matter coupling, the optical polarization without THz influence is essentially consisting of the $1s$-exciton polarization. (However, our calculation includes also the higher s-like states.)

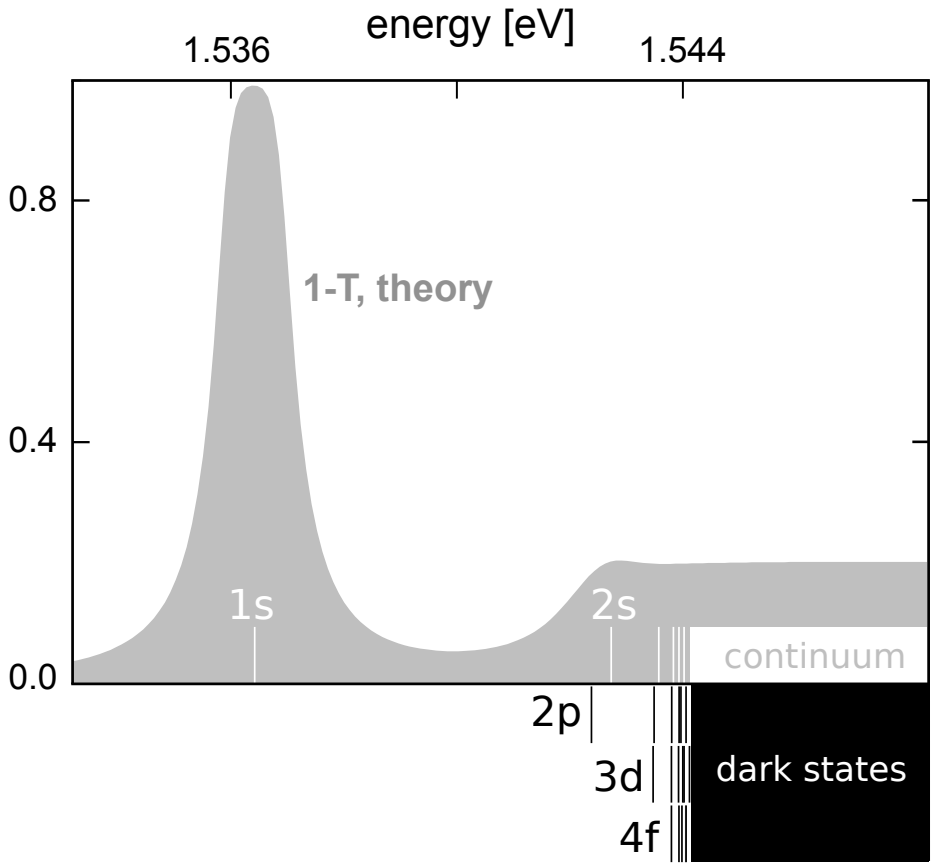

Figure 3.2: 1 - T without THz influence as calculated from the microscopic theory. The energetical positions of the s-like states are shown as white lines inside the spectrum. The first three optically dark orbitals are marked as black lines below the spectrum.

3.1.2 Terahertz pulse

The experimental pulse is an approximately 1-ps long single-cycle THz pulse, produced by a commercially available GaAs-based large-area THz emitter driven by a regenerative Ti:sapphire amplifier system emitting 800-nm, 120-fs pulses. The time trace is shown in Fig. 3.3 **(b)** (shaded area), measured using a ZnTe-crystal [71, 72]. The THz field strength was determined using a calibrated Golay cell outside of the cryostat. The features in the experimental pulse for later times were removed (red line), resulting in a single-cycle pulse in time domain and a broad pulse centered in frequency domain (see red solid lines in Fig. 3.3 **(b)** and **(c)**. We *filtered* the experimental pulse because our analysis was focussed on the effects for delays between -1 and 1 ps. For these delays, the THz features at later times do not contribute as the optical polarization has mostly decayed after 1 ps. The pulse covers the frequency range from lower THz frequencies until higher than the $1s$–$2p$ transition frequency, marked as a vertical line in Fig. 3.3 **(c)**. The theoretical fit for the experimental pulse is plotted in blue. It follows from the THz vector potential

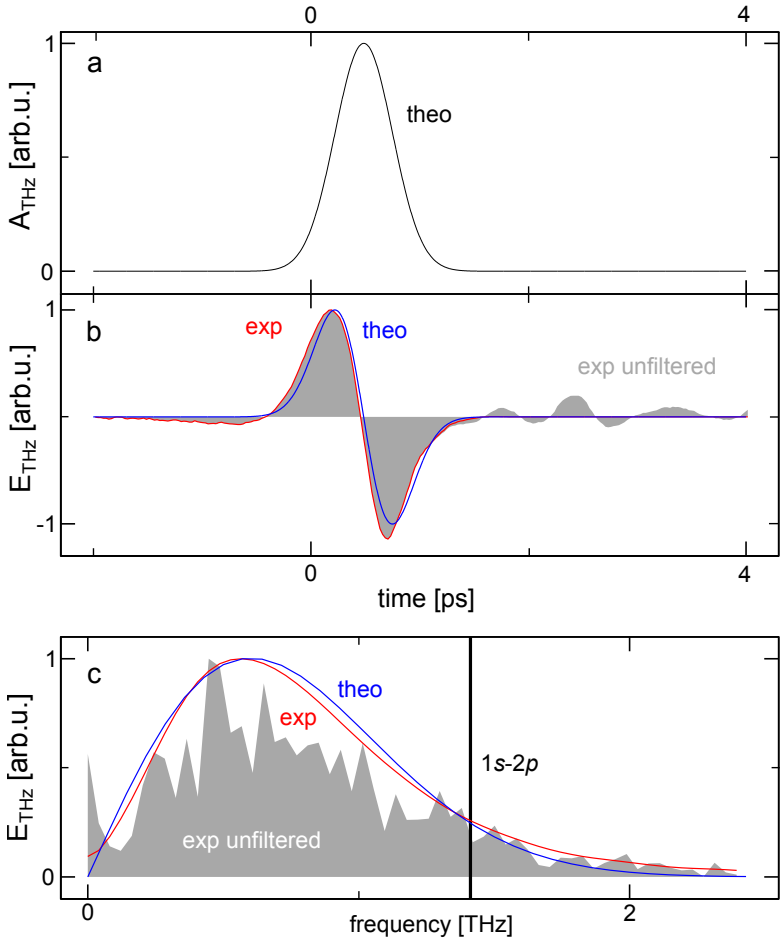

Figure 3.3: Fitting of the experimental single-cycle pulse for experiments with GaAs and germanium. **(a)** Theoretically used THz vector potential $A_{\mathrm{THz}}(t)$. **(b)** Electric field of the THz pulse as measured in the experiment (shaded), filtered experimental field (red solid) and theoretical fitting (blue solid). **(c)** Comparison of the respective spectra: Experimental pulse (red), theoretical pulse (blue) and unfiltered experimental pulse (shaded). The transition frequency for the GaAs $1s-2p$ resonance is marked as horizontal line.

(Fig. 3.3 **(a)**) which enters the theoretical calculations, as described in Section 2. It is related to the electric field via $\mathbf{E}_{\mathrm{THz}} = -\frac{\partial}{\partial t}\mathbf{A}_{\mathrm{Thz}}$.Note that it is not only resonant to the $1s$–$2p$ transition (marked as vertical line), but has also many lower-frequency parts. However, as the $1s$ polarization can only be transferred into $2p$ or higher p-like polarization, we expect in first order still mostly $1s$–$2p$ transitions. Once there is $2p$ polarization existing, the lower THz frequencies will become important and drive also transitions into higher-lying states.

3.1.3 Experimental results

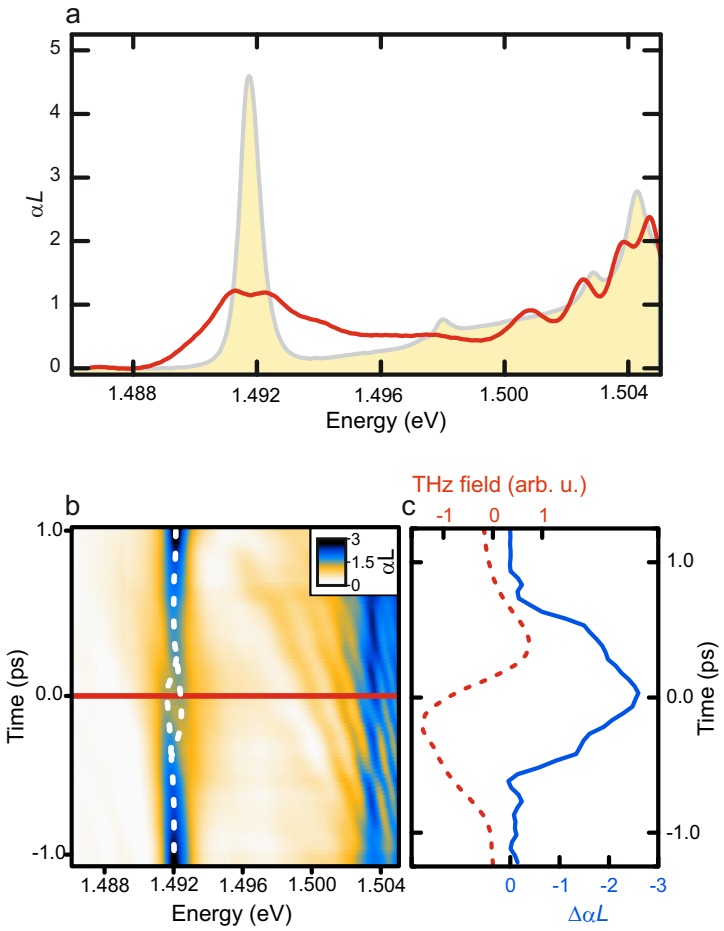

Figure 3.4: (Taken from Paper I) **(a)** Experimental transmission spectrum αL with/without THz (solid/shaded) and zero delay between THz and optical pulse. **(b)** αL as function of delay between optical and THz pulse. The position of the main peak(s) are marked with white dashed line(s), zero delay as red horizontal line. **(c)** Solid line: THz-induced change at the 1s-exciton peak position. Dashed line: THz pulse shape.

Figure 3.4 **(a)** shows the typical experimental αL with and without THz influence (solid line and shaded area). (The experimental transmission αL is linked to the transmission T by $T = \exp(-\alpha \mathrm{L})$.) The shaded area shows the spectrum without THz with a pronounced 1s-exciton peak and smaller peaks at higher energies due to higher-lying states and bands. The solid line shows the spectrum under THz influence: First of all, we observe pronounced Rabi splitting of the 1s-exciton peak. Furthermore, the 1s peak broadens with an additional modulations. More modulations at higher energies in the spectrum are due to high-harmonic generation [19, 33]. In addition to the spectrum under the strongest THz influence (zero time delay) in Fig. 3.4 **(a)**, we present αL for different delays between optical and THz pulse in Fig. 3.4 **(b)**. Like already in Fig. 3.4 **(a)**, clear

Rabi splitting of the 1s-exciton peak around zero delay is observed, accompanied by signatures of higher harmonic around 1.5 eV. The position of the 1s-exciton peak(s) is marked with white dashed line(s). We note the strongest influence of the THz field around zero delay and few changes for delays around −1 and 1 ps. The THz field passes the unexcited semiconductor without changes if it arrives earlier than the optical field (delay of −1 ps). The decay of the polarization also diminishes the THz-induced changes for positive delay. The single-cycle pulse shape of the THz electric field is given in 3.4 **(c)** (red dashed) together with the THz-induced changes in the spectrum (blue). We observe that the THz-induced changes do not follow the single-cycle shape of the electric THz field, but its Gaussian-shaped vector potential (see Fig. 3.3 **(a)**). Similar results were also obtained for the same experimental scheme used on germanium quantum wells (Paper VI, in preparation). This is surprising at first sight as the electric field E_{THz} is the relevant measured quantity in the experiment. However, in the calculations (Eqs. (2.2)), the THz field enters via its vector potential, which explains why the changes follow the intensity profile of the vector potential.

3.1.4 Comparison with theoretical results

A direct comparison of experimental and theoretical results is presented in Fig. 3.5 **(a)**: We plot 1-T for experimental data (left) and theoretical results (right) for THz field intensities of 0 to 12.8 kV/cm (from top to bottom–see caption for details). We note an excellent agreement in the experimental and theoretical spectra, in particular about the bleaching of the 1s-exciton peak and its splitting into two Rabi peaks. In addition, both theory and experiment agree in details like the reversal of the peak heights with growing THz intensity. For high THz intensities, we observe the formation of wing-like structures in addition to the broadening of the 1s-exciton peak.

Figure 3.5 **(b)** shows the relative peak position(s) as compared to the 1s-exciton peak position without THz influence. The peak position without THz is shown as horizontal grey line as a guide to the eye. Additionally, we present in Fig. 3.5 **(c)** the peak height of αL as black circles and the peak splitting (red squares). We can observe three regimes in the THz-induced changes as function of THz intensity, by comparing the changes of peak positions, exciton peak height, and splitting: In the first regime (THz intensity below 2 kV/cm), the peak position is not changing. The THz field is very slightly bleaching the 1s-exciton peak without shifting or splitting the peak. The second regime is found for THz intensities from 2 to 6 kV/cm. It is marked by a splitting of the THz pulse which grows linearly with THz frequency after the field reaches a kind of offset intensity. After reaching the offset intensity, the splitting grows linearly (see squares in Fig. 3.5 **(c)**). Simultaneously, the exciton peak is bleached strongly with growing THz field intensity. In this regime, the behavior seems quite much as expected from a two-level calculation [2], which predicts Rabi splitting for optical fields near the 1s–2p transition frequency. It also predicts the linearly growing Rabi frequency which is given by the splitting width, though not with an offset.

Hence, from this results, one could naively expect that the optical light induces transition between the 1s and 2p components of the polarization which occur with the Rabi

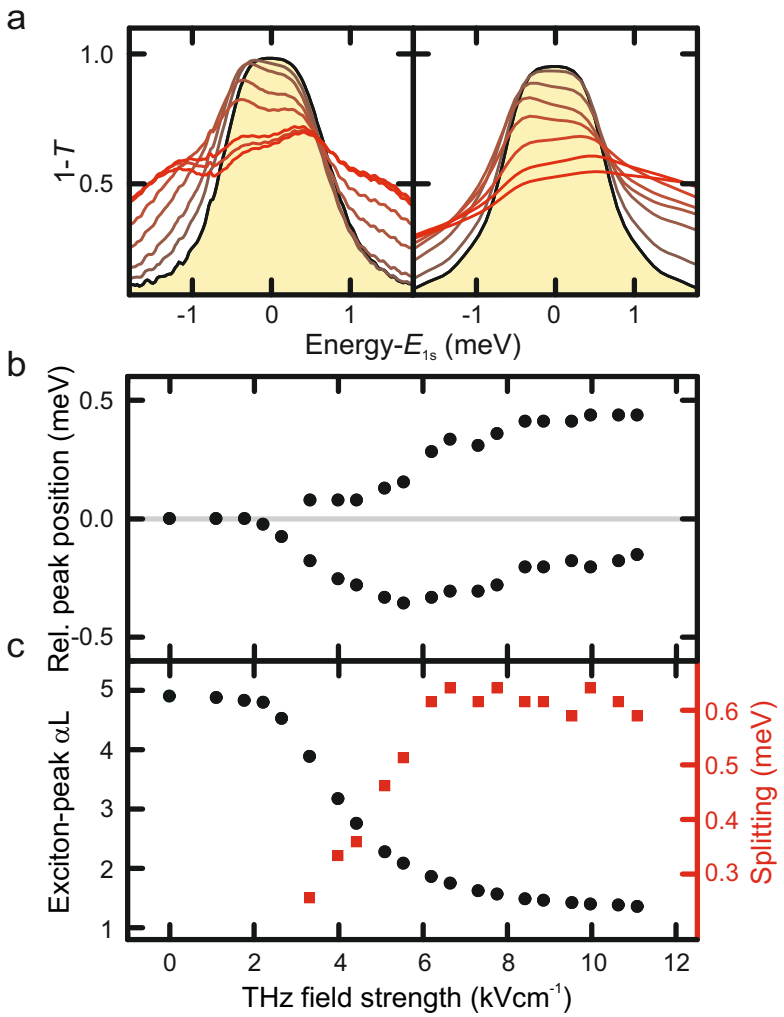

Figure 3.5: (Taken from Paper I) **(a)** 1-T as measured in the experiment (left) and obtained from the theoretical simulation (right) for THz peak intensities of (top to bottom) 0, 1.6, 3.2, 4.8, 6.4, 8.0, 9.6, 11.2, and 12.8 kV/cm. **(b)** Peak position(s) as compared to the position without THz influence as function of THz intensity. **(c)** Exciton peak height in the absorption αL (black circles) and peak splitting (red squares) as function of THz intensity. The background color in **(b)** and **(c)** marks the three different excitation regimes as discussed in the text.

period inversely proportional to the splitting. However, the theoretical analysis revealed that this is not true, as discussed in Section 3.1.5. Finally, the last regime is governed by a saturation behavior: The peak heights are already very low and are only slightly lowered with growing THz intensity. The peak splitting remains constant; instead, the peak positions are undergoing a red shift.

Hence, we see some effects from the THz-induced changes in the optical spectrum which we expected from a two-level model (Rabi splitting that grows with THz intensities

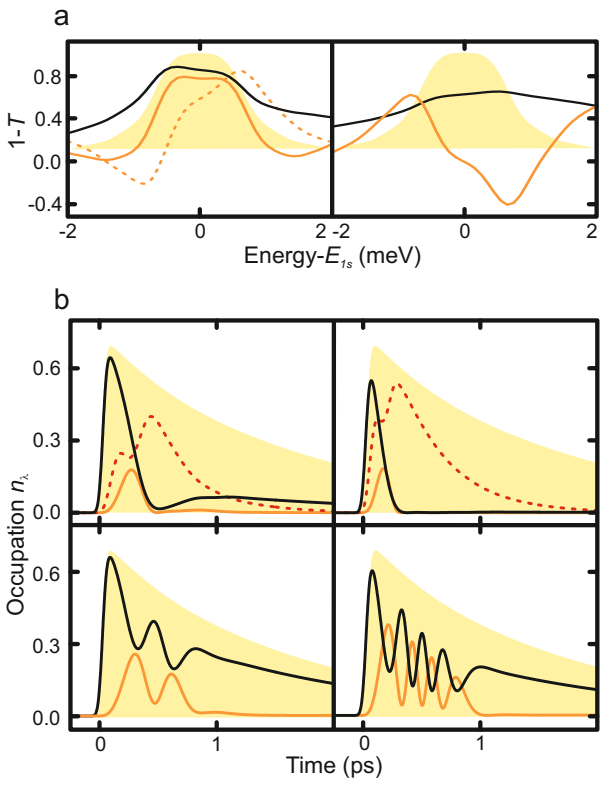

Figure 3.6: (Taken from Paper I) Theoretical data for THz intensity of 4.8 kV/cm **(left)** and 9.6 kV/cm **(right)**. **(a)** 1-T from full theory: black solid; 2LS: orange solid; 2LS for THz intensity of 5.1 kV/cm: orange-dashed; without THz: shaded **(b)** Occupations $|p_\lambda|^2$ for full theory **(top)** and 2LS **(bottom)**. 1s: black solid; 2p: orange solid; dark rest: dashed; 1s without THz: shaded.

and shift due to the AC-Stark shift), but also unexpected features like the formation of wings, the offset intensity or the saturation regime. Therefore, we study in the following Section the occupations dynamics $|p_\lambda(t)|^2$.

3.1.5 Occupation dynamics

The evaluation of the semiconductor Bloch equation in exciton basis (Eq. (2.2)) allows us to follow how the THz field redistributes the different excitonic components of the polarization. We choose two medium THz intensities with already clear Rabi splitting (middle regime in Fig. 3.4) and a high THz intensity (saturation regime in Fig. 3.4) to study whether the Rabi splitting is accompanied by Rabi flopping between the excitonic 1s and 2p state. Figure 3.6 **(a)** shows the transmission spectra with and without THz influence (shaded area and black solid line, respectively) as determined from the full theory. As we already saw, the results from the full theory agree excellently with the experimental spectra which are therefore not replotted here. In addition, we present also the spectra obtained from a two-level system (2LS) analysis, where we restrict the

calculation to only the $1s$ and $2p$ states (orange solid lines).

Looking at the lowest intensity of 4.8 kV/cm (left), one might think that the two-level calculation agrees quite well with the result of the full calculation and thus the experimental values. However, only a slight change of intensity (5.1 kV/cm, orange-dashed line) leads to a completely different spectrum and even the prediction of gain. This shows that the relatively good agreement at 4.8 kV/cm was somehow incidental and that the 2LS is not reliable in the lowest regime with Rabi splitting. For even higher THz intensities, the two-level model also fails completely to reproduce the experimental spectrum (right). Hence, in our experimental situation with a single-cycle THz pulse, the two-level picture seems to be inappropriate.

This becomes even clearer when we follow the dynamics of the occupations $|p_\lambda|^2$ for the two-level model and for the full calculation. Figure 3.6 **(b)** shows the occupations of the $1s$ and $2p$ states in black and orange lines, respectively. The dashed line the sum of higher dark occupations and, as a reference, the shaded are the $1s$ occupation without THz influence. The THz field intensities are 4.8 kV/cm (left) and 9.6 kV/cm (right), like in **(a)** - top are shown the results from the full theory and bottom from the 2LS. For the lower THz intensity, we observe that the THz field induces almost all $1s$ occupation into the $2p$ and higher dark occupations. A part of it is coming back in a revival of the $1s$ occupation. The $2p$ occupation is at its maximum shortly before the $1s$ occupation is at its lowest point, but then also going down. Meanwhile, the higher dark states reach their maximum when $2p$ and $1s$ at their minimum and before the revival of the $1s$. Hence, we see for the lower THz intensity that the $1s$ occupation is transferred into $2p$ and higher dark states, but only a small fraction comes back. This revival of the $1s$ occupation does not happen at the highest THz intensity, when almost all occupation is transferred immediately into dark states ($2p$ or higher dark states).

To understand the missing revival for higher intensities despite the strong coupling between the $1s$ and $2p$ states, we plot in Fig. 3.7 a temporal snapshot of the occupation of the different excitonic states, denoted by their energy and the orbital number. We see that even for the lower THz intensity **(top)**, a huge number of different excitonic states is involved. For the highest THz intensity **(bottom)**, even more states are involved and excitonic states with energies from four-photon-absorption are occupied. The effect is similar to the above-threshold ionization in atomic systems [37]. In the spectrum, we see the occurrence of *ionization wings* around the $1s$-exciton peak for the high THz intensity when the ionization effect is dominant.

3.1.6 Ponderomotive contributions

As a last part of this study, we analyze the importance of the *ponderomotive force*. Sometimes, the ponderomtive current is neglected (see, e.g., [61]), as it is not responsible for transitions but *only* renormalizes the eigenenergies (see, e.g., (2.2)). Steiner *et al.* already showed that one cannot always neglect the ponderomotive contributions [18]. The ponderomotive current $J_{\mathrm{pond}} = \frac{|e|^2}{2\mu} A_{\mathrm{THz}}^2$ describes the motion of carriers in an inhomogeneous field and should be especially important for high THz fields due to the quadratic dependence, hence for field intensities like those in our study.

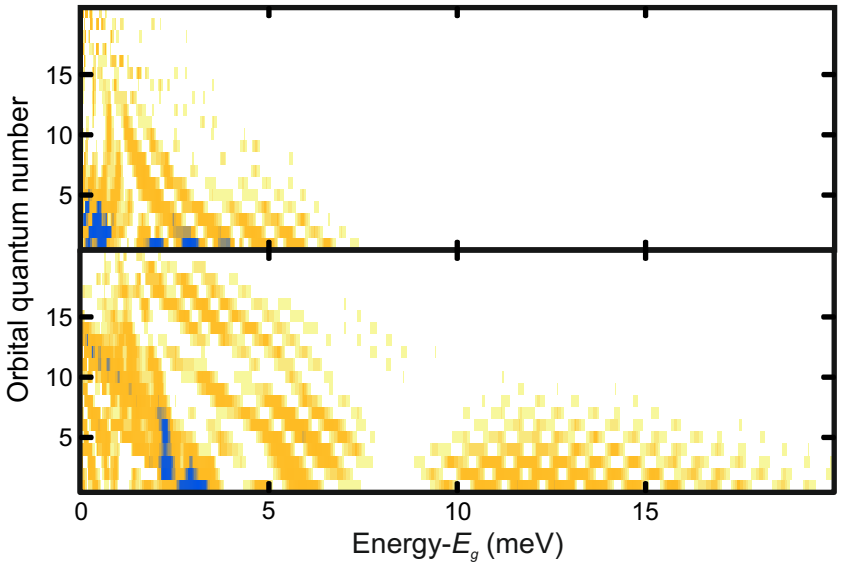

Figure 3.7: (Taken from Paper I) Relative occupations for orbital number and energy and THz intensity of 4.8 kV/cm **(top)** and 9.6 kV/cm **(bottom)** (blue: highest occupations; white: lowest occupations). The snapshots are taken 1.5 ps after the optical excitation.

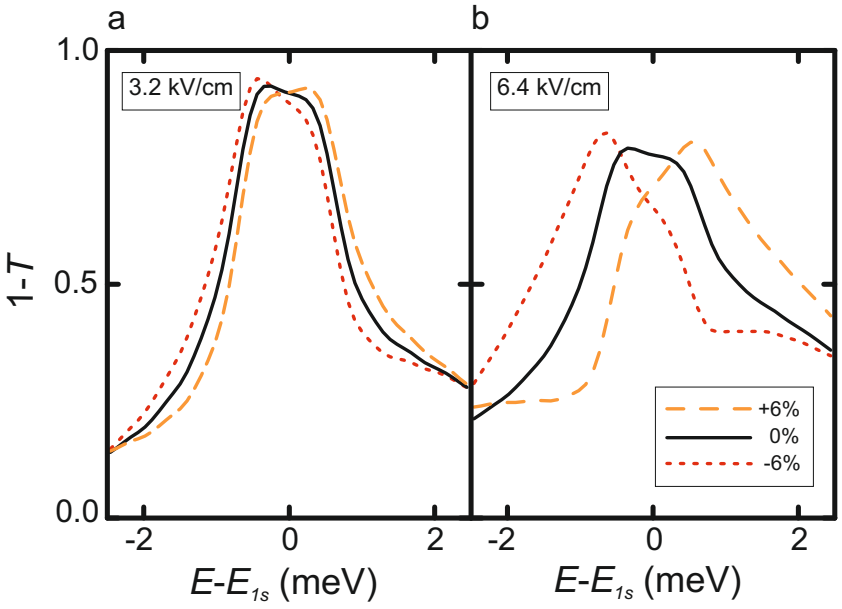

Figure 3.8: (Taken from Paper I) Influence of the ponderomotive current on THz-induced spectral changes for THz intensities of **(a)** 3.2 kV/cm and **(b)** 6.4 kV/cm. The solid lines denote the spectra with the correct treatment of the ponderomotive current, while the results for 6 % smaller (larger) ponderomotive current are plotted as red dotted lines (orange-dashed lines).

This is confirmed by our theoretical investigations, shown in Fig. 3.8: We study the influence of slight changes in the ponderomotive force for a medium and a high THz intensity (3.2 kV/cm and 6.4 kV/cm) by making the ponderomotive force 6 % smaller (red dotted) or larger (orange dashed) as compared to its normal size (solid). For both intensities, the ponderomotive force is important for the optical spectrum: A smaller ponderomotive force leads to a blue shift of the whole spectrum including the Rabi peaks, while a stronger ponderomotive force leads to a red shift. This was to be expected, as the ponderomotive force renormalized the eigenstates, as mentioned before and as seen from the SBE (Eq. (2.2)). For the higher intensity, the shape of the exciton peak changes even completely for a slight change in the ponderomotive current (Fig. 3.8). Hence, a careful treatment of the THz ponderomotive current is very important for the theoretical simulation, especially when using strong THz fields.

3.2 Resonant 1s–2p excitation

In this Section, we analyze the limits of a two-level approximation for resonant THz excitaton of the excitonic $1s$–$2p$ transition. The results were published in Paper IV. The study closes the gap between the work presented in Section 3.1 (Paper I) reporting exciton ionization using a broad THz pulse and a work presented by Wagner *et al.* [30] where a two-level analysis is used for THz spectroscopy on coherent excitons with a spectrally narrow THz pulse. Like in Paper I, we use a fully microscopic theory to analyze the experimental results and study especially the limitations of a two-level approximation (2LA) where we restrict our simulation to the excitonic $1s$ and $2p$ states.

3.2.1 Terahertz pulse

The THz source is a free-electron laser (FEL) at the Helmholtz-Zentrum Dresden–Rossendorf. It allows to change the THz frequency continuously within the range of several THz. The pulse length is about 31 ps, resulting for our time scales in a quasi-cw excitation. The measured experimental data are averaged over several different THz phases as the measurement setup does not allow to control the phase of the THz light. The theoretical spectra are similarly averaged over several THz phases. The sample DBR42 is made of 20 $Ga_{0.06}In_{0.94}As$ QWs [73]. Unlike the sample used in the previous study with the FEL [30], the heavy and light hole are clearly separated.

3.2.2 Experimental results

Figure 3.9 shows the experimental results for three different THz frequencies with photon energies **(a)** above, **(b)** near and **(c)** below the excitonic $1s$–$2p$ transition energy. For each intensity, we present an intensity sweep from the onset of the slight excitonic bleaching until strong Rabi splitting; the intensities in kV/cm are given in the legend. The spectra are vertically shifted for better visibility.

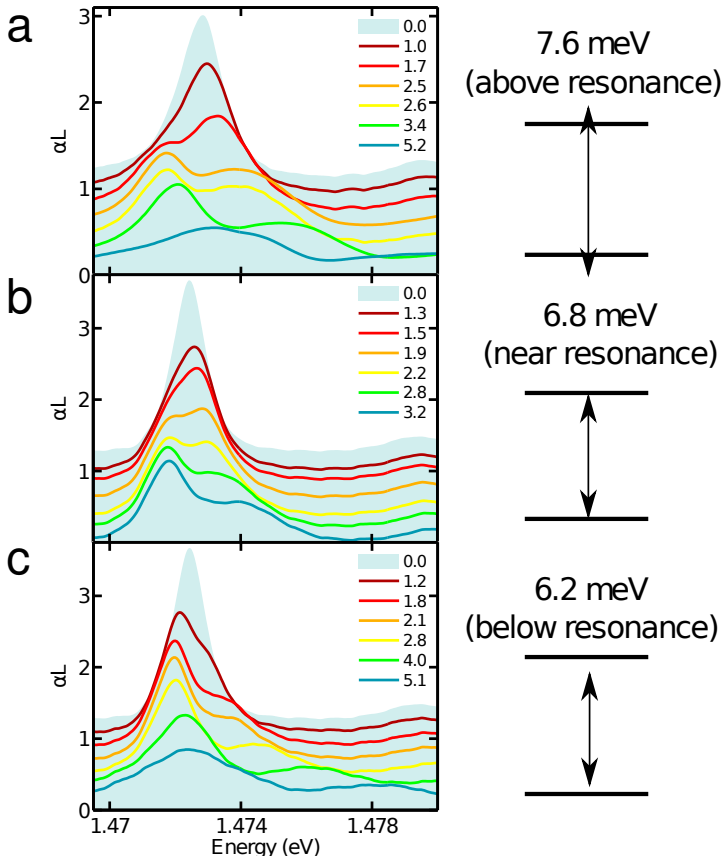

Figure 3.9: THz intensity sweeps for three different detunings of the THz frequency from the excitonic $1s$–$2p$ transition frequency. The intensities in kV/cm are given in the legend. The scheme indicates the THz detuning **(a)** above, **(b)** near and **(c)** below the transition frequency.

The results are in principle similar to those of the broad THz pulse: A slight bleaching is followed by a clear splitting which grows with the THz intensity. However, the third regime of saturation like in the study with the broad THz pulse (Paper I) where the splitting is not growing anymore with higher intensities is not reached. We observe in all cases strong broadening and in Figs. 3.9 **(a)** and **(b)** a peak reversal. Unlike in Paper I, no *ionization wings* occur.

3.2.3 Anticrossing

When analyzing the experimental results, we had a choice of intensity sweeps for five different detunings of the THz photon energy from the $1s$–$2p$ transition energy. Only three representative detunings are shown in Fig. 3.9. For all detunings, the microscopic theory reproduced excellently the experimental results. We benefit from this very good agreement between experimental and theoretical results when studying the behavior of the Rabi peaks for different detunings of the THz photon energy. The results are shown

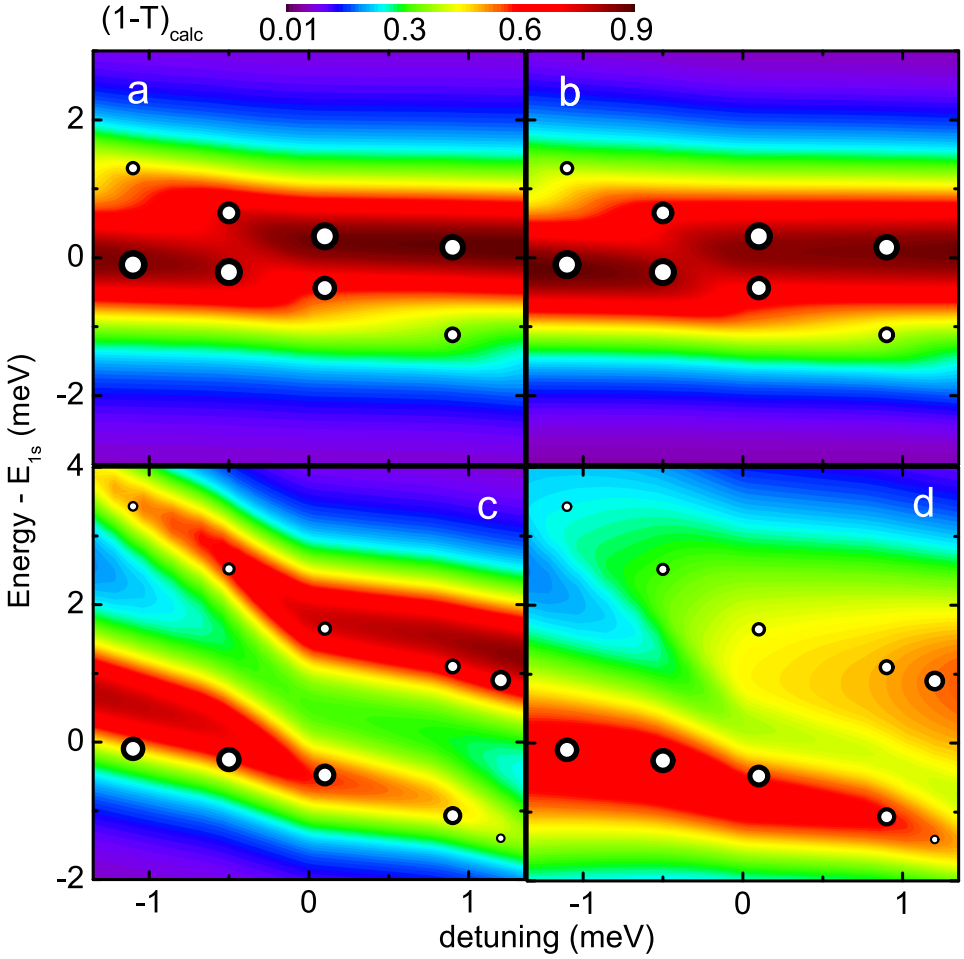

Figure 3.10: (Taken from Paper IV) 1-T for THz intensity of 1.2 kV/cm (**(a)**/**(b)**) and 3.2 kV/cm (**(c)**/**(d)**). The figures **(b)** and **(d)** are extracted from the fully microscopic calculation, **(a)** and **(c)** from the 2LA. The experimental peak positions are marked by white circles whose diameter refer to their peak heights.

in Figure 3.10: We plot 1-T spectra as extracted from the full theory (Figs. **(b)**, **(d)**) and from the two-level approximation (2LA) where we restrict our theory to the 1s and 2p states (Figs. **(a)**, **(c)**). (The two-level approximation is shortened as 2LA inside Paper IV and in the Figures we show here from Paper IV; however, it is the same model as the 2LS in Section 3.1.)

In addition, we mark the peak positions of the experimental results by white circles, whose diameters scale with their peak heights. All figures show clear anticrossing behavior of the two Rabi peaks, as expected from analytical two-level calculations using the rotating-wave approximation [2]. We observe that for the low intensity (Figs. **(a)**, **(b)**), both theoretical models mostly agree with each other and the experimental values. At the higher intensity, the full theory predicts well the exact peak position and the bleach-

ing of the higher-energy Rabi peak for negative detuning. In addition, it also predicts broadening of the Rabi peaks, especially for the higher THz intensity. The broadening is almost absent in the 2LA. Hence, a two-level result seems to be sufficient to describe the transmission spectra at very low THz intensities like in Fig. 3.10 of 1.2 kV/cm, but already for medium THz intensities, the influence of higher order effects is important, as seen from Figs. **(c)** and **(d)** (3.2 kV/cm).

3.2.4 Direct comparison of spectra

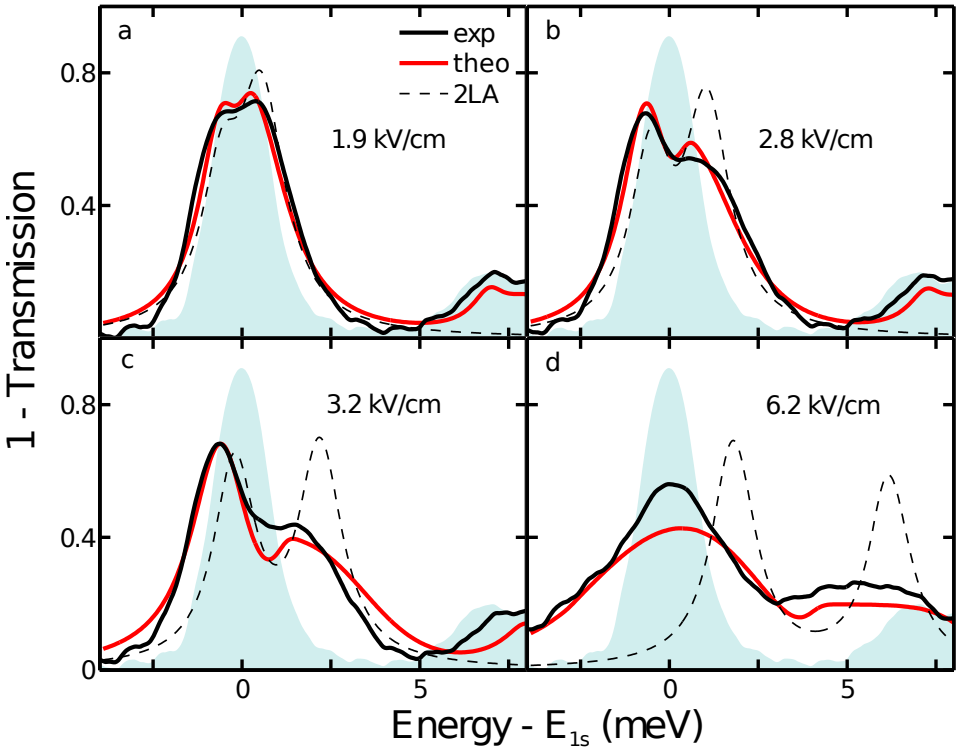

Figure 3.11: (Taken from Paper IV) Direct comparison of the experimental spectra (black) with the results from the full theory (red) and the 2LS (dashed) for different THz intensities. Experimental spectra without THz are shaded. The THz photon energy is 6.8 kV/cm, near the excitonic $1s$–$2p$ transition energy.

Figure 3.11 shows the direct comparison of the experimental 1-transmission (1-T) spectra (black solid) with the results from the full theory (red) and the 2LA (dashed). The THz intensities are **(a)** 1.9 kV/cm, **(b)** 2.8 kV/cm, **(c)** 3.2 kV/cm and **(d)** 6.2 kV/cm. The THz photon energy is 6.8 meV, close to the $1s$–$2p$ transition energy (see Fig. 3.9 **(b)**). We observe a very good agreement between full theory and experimental results, in detail, about the peak heights, position, the broadening of the Rabi peaks and the reversal of the peak heights. In contrast, the results from the 2LA are reasonable for the lowest THz intensity of 1.9 kV/cm (Fig. 3.11 **(a)**). But the coupling to higher states is too

important to let the 2LA describe correctly the peak heights and their reversal until the second-lowest intensity (Fig. 3.11 **(b)**). For the two highest intensities (Figs. 3.11 **(c)** and **(d)**), the 2LA cannot reproduce the spectra. For completeness, a similar comparison of experimental and theoretical values is shown for a THz photon energy of 7.6 meV, above the 1*s*–2*p* transition energy (cf. Fig. 3.9 **(a)**): The direct comparison is plotted in Fig. 3.12. Again, experiment and full theory agree perfectly, while the 2LA is too simpli-

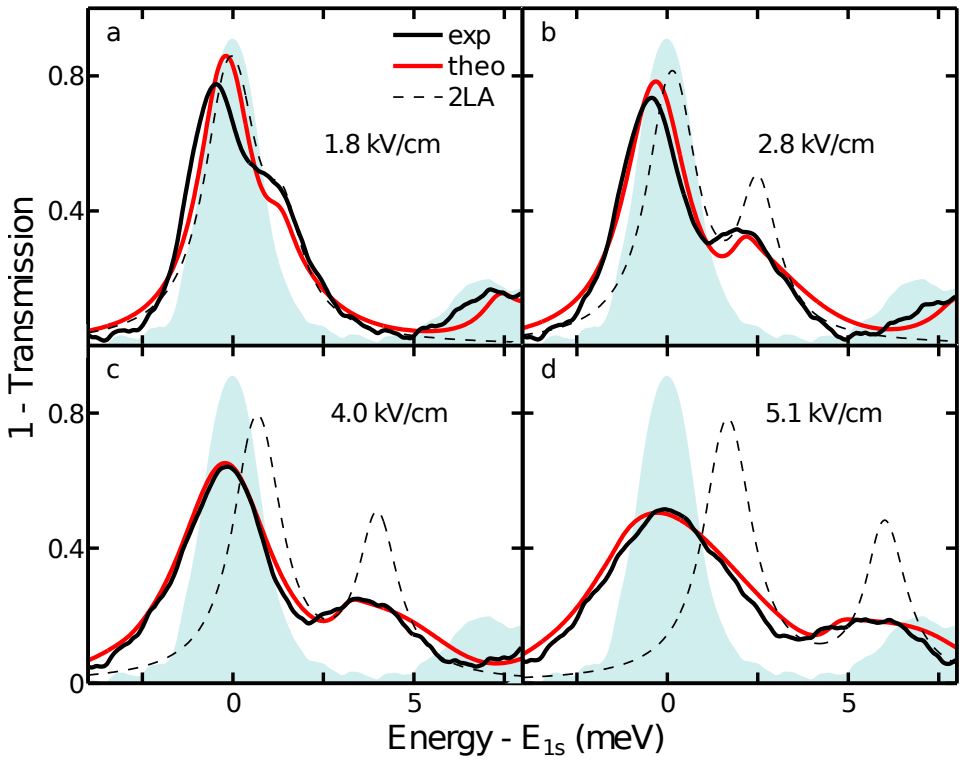

Figure 3.12: (Taken from Paper IV) Direct comparison of the experimental spectra (black) with the results from the full theory (red) and the 2LS (dashed) for different THz intensities. Experimental spectra without THz is shaded. The THz photon energy is 6.2 kV/cm, below the excitonic 1*s*–2*p* transition energy.

fied to describe the spectra. Still, the 2LA gives a rough idea about the peak positions and the peak splitting, as already seen in Fig. 3.10.

3.2.5 Occupation dynamics, resonant

In the last part, we saw by direct comparison of the experimental spectra with those of the full theory and 2LA that the 2LA is not sufficient for reproducing the experimental results. To understand this better, we will look at the occupations dynamics $|p_\lambda(t)|^2$ to follow how the THz field acts on the excitonic components. Figure 3.13 shows the occupations for the same THz photon energy and THz field intensities as in Fig. 3.11.

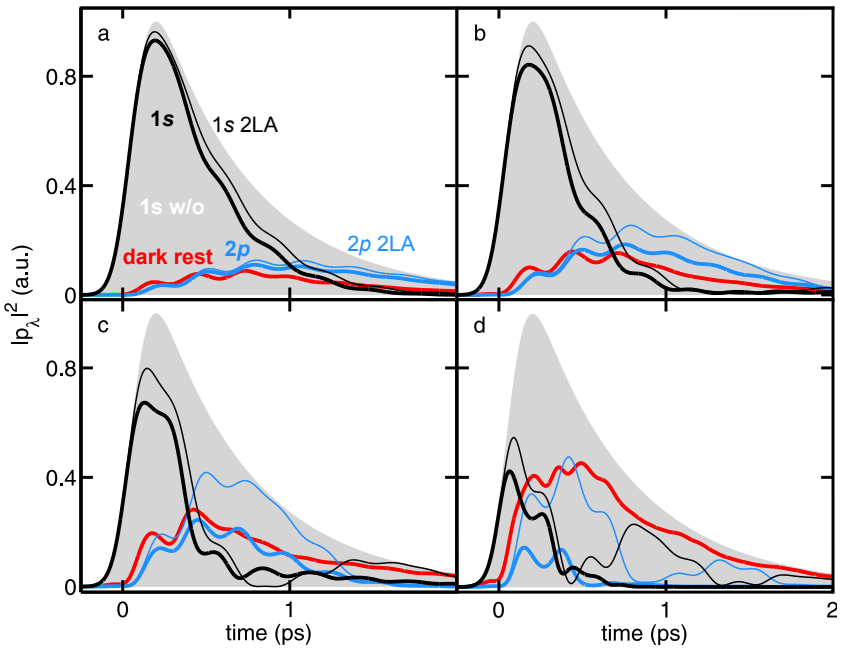

Figure 3.13: Excitonic occupations $|p_\lambda(t)|^2$ for full theory (thick solid) and two-level approximation (thin solid) for spectra from Fig. 3.11. 1s occupation without THz shaded as reference.

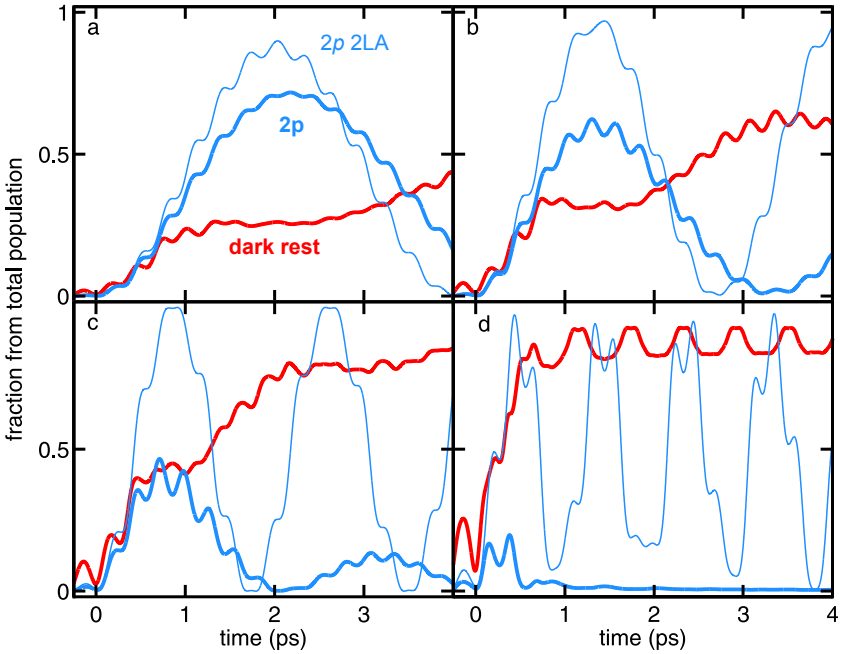

Figure 3.14: Excitonic components $|p_\lambda|^2$ for full theory (thick solid) and two-level analysis (thin solid) as fraction of all temporarily existing polarization for spectra from Fig. 3.11.

The $1s$ occupation is shown in black, the $2p$ occupation in blue and the higher dark states in red. The results from the full theory are thick solid lines, those of the 2LA thin solid lines. As a reference, the $1s$ occupations without THz influence are given as shaded area. First of all, we note that for the lowest THz intensity of 1.9 kV/cm **(a)**, the $1s$ and $2p$ dynamics are almost the same for the full theory and the 2LA, showing Rabi flopping. However, the dark state occupation is already of similar height as the $2p$ occupation. The situation is similar for the second-lowest intensity of 2.8 kV/cm **(b)**, while the difference is clear for the two highest intensities (3.2 and 6.2 kV/cm, **(b)** and **(c)**). Here, all occupations is transferred into the higher dark states after 1.5 ps, while the 2LA keeps on describing $1s$–$2p$ Rabi flopping at all intensities.

However, the occupation dynamics are hard to follow for the later times due to the decay of the polarizations. Therefore, we replot the data for $2p$ and dark rest occupation scaled as a fraction of all temporary existing occupation. The results are shown in Fig. 3.14. The $2p$ results for the 2LA are shown as thin lines. We observe in Figs. 3.14 **(a)**–**(d)** how in both systems the $2p$ fractions undergo periodic maxima and minima. While for the two lowest intensities, the full theory still shows Rabi flopping (Figs. 3.14 **(a)** and **(b)**), the occupation is in the two higher cases almost immediately transferred into higher excitonic states without revival of the $1s$ occupation. Note that even at the lowest intensity, where in both systems the $2p$ occupations seem similar, almost 50 % of the occupations is transferred into higher dark states after 4 ps. The spectra are in this case still similar, as after 4 ps the differences in the $1s$ occupation do not contribute anymore as the occupations are already mostly decayed (see Fig. 3.13 which shows only the first two picoseconds). The small wiggles in the fractions are due to the following behavior of the fractions to the sinusoid quasi-cw THz pulse. Finally, we note in this presentation that the $2p$ fractions all have similar periods for the Rabi oscillations. The Rabi oscillations go down with growing THz intensities, as expected from two-level calculations [2]. This also agrees with the observation that the 2LA gave a good estimate for the Rabi peak splitting (which is linked to the Rabi period).

4 Quantum wells inside a microcavity

In this Chapter, we discuss THz spectroscopy on exciton polarions [35, 36, 74]. These half-light, half-matter states form if quantum wells are grown inside a 1*s*-resonant microcavity. The system is in many ways similar to the one of two harmonic oscillators with the same eigenfrequencies: Coupling them leads to the formation of new eigenstates and eigenfrequencies. In our case, the light-matter coupling couples the light in the cavity with the optical polarization in the QWs. Without detuning between cavity resonance and exciton resonance, two new eigenfrequencies appear symmetric around the original resonances (Fig. 4.1 **(a)**), denoted as lower- and higher-exction polaritons (LEP and HEP). The splitting between LEP and HEP is in our system around 6 meV, which makes that both LEP and HEP resonance are below the 2*p* exciton energy.

The temporal evolution of the new eigenstates is shown schematically in Fig. 4.1 **(b)**: The 1*s* polarization inside a QW is plotted as blue-shaded area, the optical field as yellow-shaded area. In addition to the oscillations, 1*s* polarization and optical field decay within few picoseconds: The optical field decays due to absorption and losses from the microcavity and the 1*s* polarization decays due to scattering and radiative decay. The oscillation period is determined by the coupling strength, which also determines the peak splitting. In the specific system discussed in this Chapter, the peak splitting is around 6 meV, determining an oscillation period of 0.7 ps. In the experiments described in this Chapter, exciton polaritons are studied in both domains: In Section 4.1, we use THz light to study how exciton polaritons couple to light. This is a relevant question as

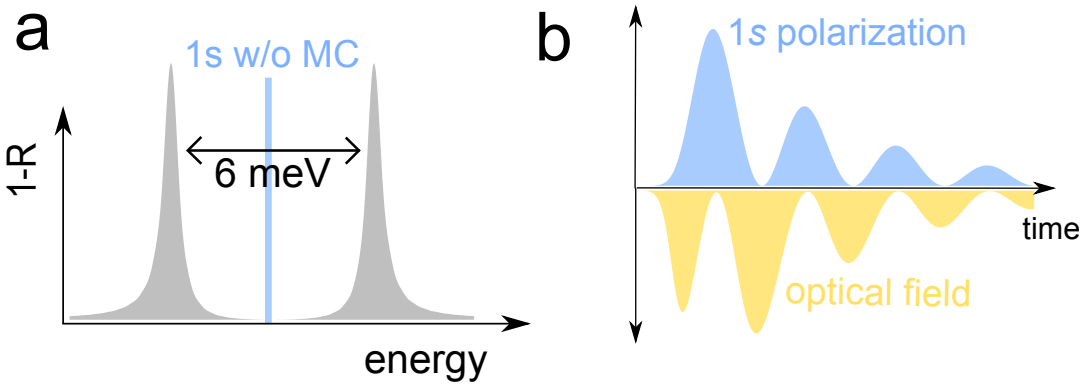

Figure 4.1: **(a)** Schematic of the exciton-polariton spectrum: Two new peaks form around the position of cavity resonance and exciton resonance. In our system, the splitting is around 6 meV. **(b)** Schematic of the time evolution of 1*s* polarization and optical field inside a QW.

they are mixed states made of polarization and optical light. As we saw in Chapters 2 and 3, THz light couples to polarization but not directly to optical light. Therefore, we study which kinds of THz-induced transitions are possible by using spectrally-narrow THz pulses with different frequencies. The experiments were performed in the group of Yun-Shik Lee (Oregon State University) and are published in Paper II. As a result, we found that LEP, HEP and the excitonic $2p$ state form a unique Λ system. This could be seen as a bleaching of LEP or HEP when the THz frequency was resonant to the LEP or HEP transition frequency.

To study this in more detail, we used our microscopic theory and followed how the THz light redistributes the occupations in a numerical study for the parameters of the Λ system. In addition, we compared the THz influence numerically to the same system but without the microcavity. The results are published in Paper III and discussed in Section 4.2. We found that we can see a similar transfer from the $1s$ to the $2p$ state as for the LEP and HEP to the $2p$ state. However, in both system, higher occupations play an important role.

Finally, I will give an outlook on the last study on the same sample and again in cooperation with Yun-Shik Lee's group. Here, we focus on the time-behavior depicted in Fig. 4.1 and use the fact that THz light couples only to polarization but not to optical light. It allows us to measure this *cavity beating* between polarization and field directly by varying the time delay between optical and THz pulse. The results are in preparation for poublication in Paper V.

Setup

The setup of our experiments is depicted in Fig. 4.2. In principle, it is the same as in Chapter 3, where we have a THz pulse and an optical pulse arriving at quantum wells with a variable time delay; the only difference is that the quantum wells are grown

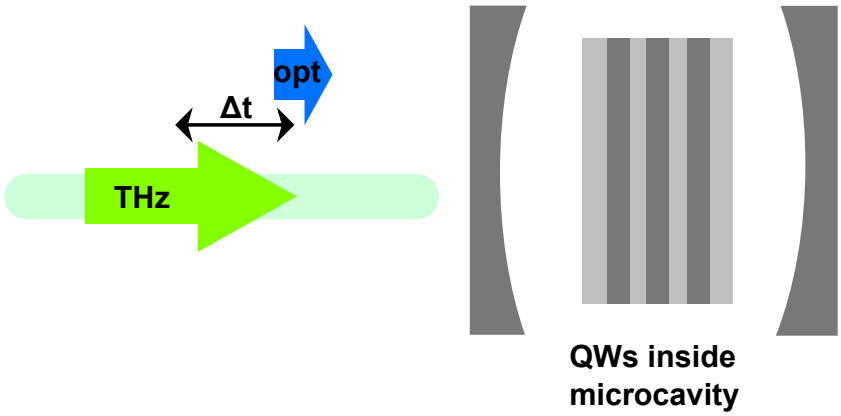

Figure 4.2: The setup is in a simplified way the same as in Chapter 3, apart that the the QWs are inside a $1s$-resonant microcavity. Optical and THz pulse arrive with variable time delay at the sample.

inside a microcavity. (This makes the numerical simulation and measurements more demanding.) The sample NMC66 consists of 10 InGaAs QWs inside a 11 $\lambda/2$ cavity built by 14.5/ 16 Distributed Bragg Reflectors (DBRs) with 99.94 % reflectivity. The sample is wedged which allows us to study different detunings between cavity and exciton resonance. The measurements were performed at 5 K, avoiding scattering of carriers and longitudinal-optical phonons. The THz pulse is a 4 ps long multi-cycle pulse with a maximum intensity of 5 kV/cm. Its spectral width is similar to the peak width of LEP and HEP. The THz pulse made by type-II difference-frequency generation with two linearly-chirped and orthogonally-polarized optical pulses.

4.1 Lambda system

First of all, we address the central question: How will the THz field *see* the exciton polaritons? This is interesting, as exciton polaritons are created by strong coupling from polarization (coupling to THz light) and optical field (not coupling to THz light).

To resolve this, we compare in Fig. 4.3 the influence of two different frequencies: Figure **(a)** shows the experimental result for a THz frequency of 1.1 THz, close to the HEP-to-2p transition frequency and off-resonant from the 1s–2p transition frequency. We observe an

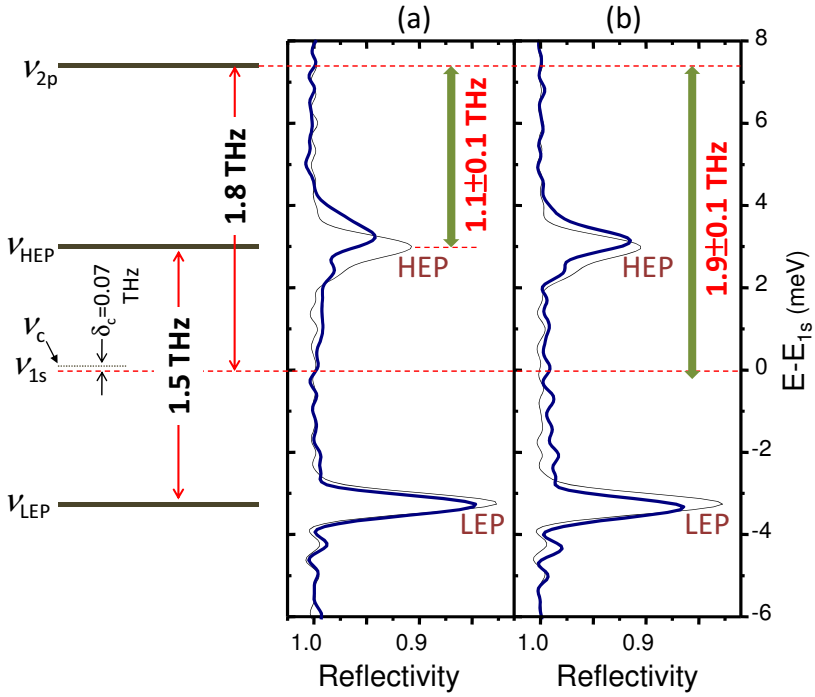

Figure 4.3: (Taken from Paper II) Measured reflectivity spectra with and without THz influence (thin black/thick blue lines) for THz frequency **(a)** close to the HEP-to-2p transition frequency and **(b)** close to the 1s–2p transition frequency.

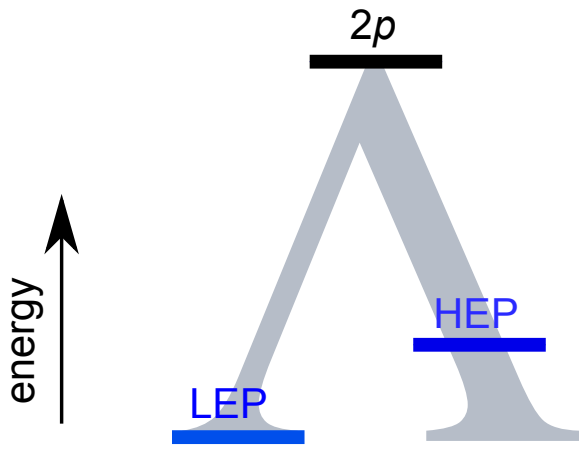

Figure 4.4: LEP, HEP and $2p$ resonances constitute a Λ system: THz transitions are only allowed along the two arms of the Λ, but not from LEP to HEP. The excitonic $1s$ state is replaced by LEP and HEP and not part of the system.

asymmetric bleaching of the HEP resonance, while the LEP resonance remains mostly unchanged. In contrast, tuning the THz frequency near the $1s$–$2p$ transition frequency (Fig. **(b)**) does not induce significant changes in the spectrum. Both experimental results agree with our theoretical simulations (not shown here). We also checked that there are no significant spectral changes when driving the LEP-to-HEP transition (not shown here). This hints that we have found a system which behaves as if we had two s-like resonances instead of one. The s-like property of the resonances is strengthened by the fact that we can drive transitions into p-like states, but not from LEP to HEP, in agreement with excitonic selection rules. This means that LEP, HEP and $2p$ resonance constitute a coherent Λ system, as illustrated in Fig. 4.4: THz transitions are only allowed along the Λ.

In figure 4.5, we study the experiment-theory comparison for THz driving the HEP-to-$2p$ transition **(left)** and LEP-to-$2p$ transition **(right)**. The experimental reflectivity spectra for different delays between optical and THz pulse are given on top **(a)/(b)**, the theoretical simulations down **(c)/(d)**. The THz frequencies are 1.3 THz, near the HEP-to-$2p$ transition frequency (left), and 2.2 THz, near the LEP-to-$2p$ transiton frequency. The detuning between cavity and exciton resonance is -0.56 THz (left) and +0.41 THz (right). The experimental peak amplitudes are smaller than the theoretical one due to disorder effects in the sample [75, 76].

Figures 4.5 **(a)** and **(c)** show contour plots for experimental and theoretical spectra for different delays. We see for both THz frequencies the Λ property as a bleaching of the respective exciton-polariton resonance. The bleaching of HEP and LEP resonance in the contour plots can be seen in more detail in the spectra for time delays of 2, 1, 0, -1 and -2 ps **(b)/(d)**. In both cases, we see a very fast bleaching from -2 ps delay to the strongest modulations around zero delay and a slight recovery until 2 ps. The short onset from -2 ps is due to that for more negative delays, the THz pulse arrives before the optical pulse and passes the sample without interaction. For later delays (2 ps and

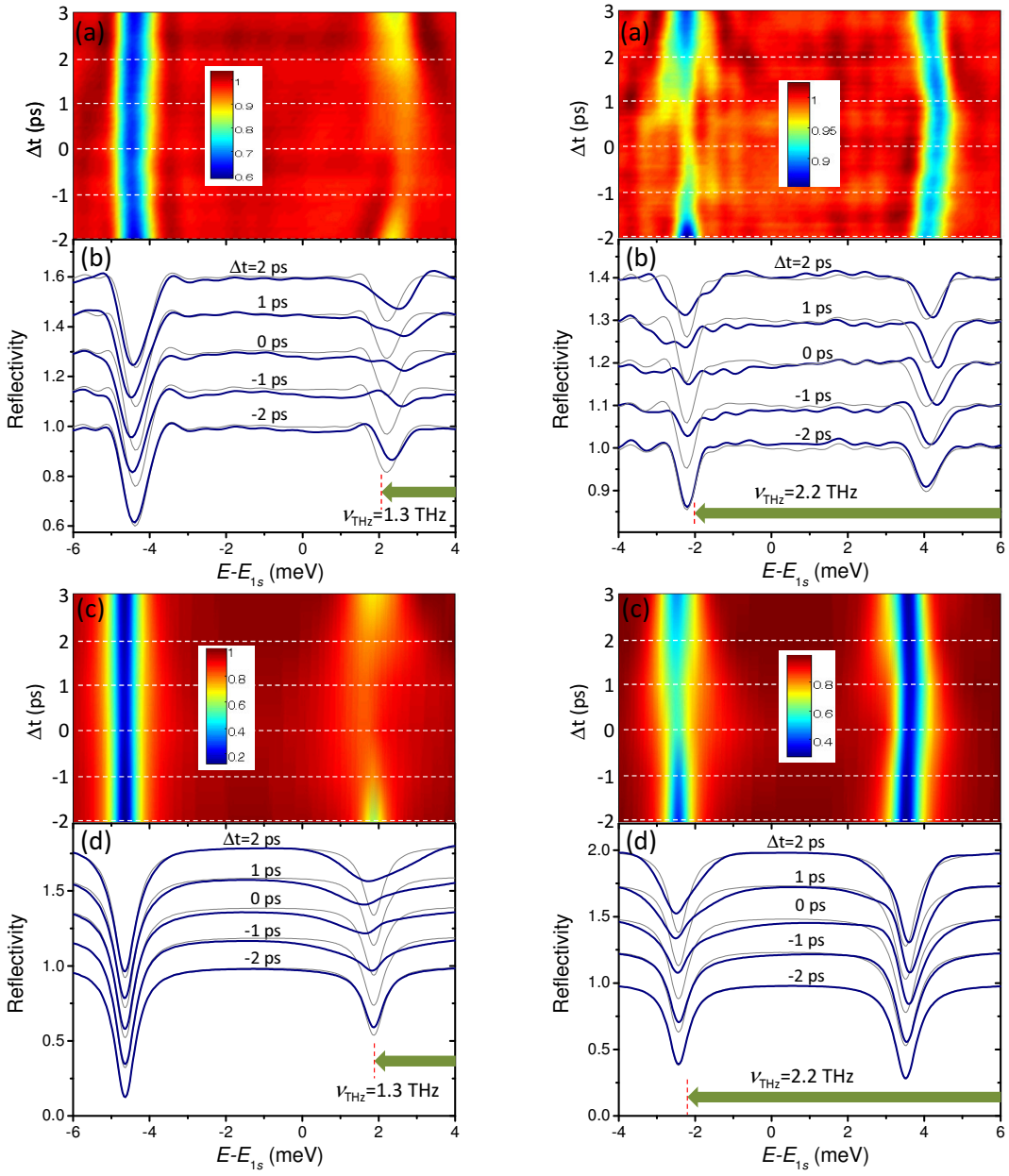

Figure 4.5: (Taken from Paper II) Representative reflectivity data for experiment **(top)** and theory **(bottom)**. **(left)** Reflectivity measured for THz frequency of 1.3 THz and detuning of δ_c = -0.56 THz, so that the THz frequency is close to the HEP-2p resonance. **(right)** Reflectivity measured for THz frequency of 2.2 THz and detuning of δ_c = +0.41 THz, so that the THz frequency is close to the LEP-2p resonance.

later), the exciton polaritons are already partly decayed (see schematic in Fig. 4.1 **(b)**) and thus the THz pulse pushes less polarization into optically-dark states. Hence, we see that the THz field can selectively bleach the LEP and HEP resonance, while it does not induce transitions when being resonant to the $1s$–$2p$ transition. This proves the Λ property depicted in Fig. 4.4.

Figure 4.5 also hints that the LEP is less easily bleached than the HEP. One possible explanation is that THz photons which are resonant to the HEP-to-$2p$ transition have too few photon energy to drive also LEP-to-higher states transitions. Hence, one can bleach the HEP independently from the LEP, but not the other way around. However, further work presented in Section 4.2 hints that the LEP couples in principle less strong to the higher excitonic states, independent also from the detuning. More research is needed to understand these effects.

4.2 Numerical comparison of lambda system with bare quantum wells

In Section 4.1, we saw that the THz pulse could bleach the LEP or HEP when the THz photon energy was resonant to the LEP- or HEP-to-$2p$ transition energy. This appears similar to the bleaching of the $1s$-exciton peak in the system of bare QWs, when the THz frequency was resonant to the $1s$–$2p$ transition frequency in Chapter 3. We compare the Λ system with excitons in bare QWs as a reference. The refractive index profile of both systems is shown in Fig. 4.7: **(a)** is the system with microcavity from Section 4.1, while **(b)** is the same system but without microcavity.

Therefore, we study in this Section how the THz field induces $2p$ occupation $|p_{2p}|^2$

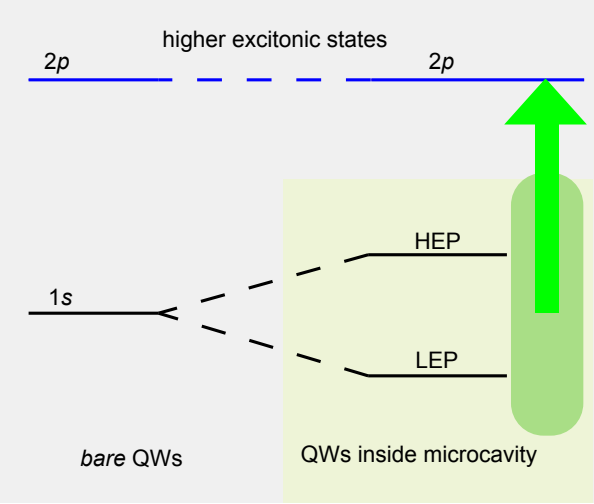

Figure 4.6: Numerical analysis: We study the fraction of $2p$ occupation induced by different THz frequencies for the Λ system from Section 4.1 and for the system of excitons in bare QWs like in Chapter 3.

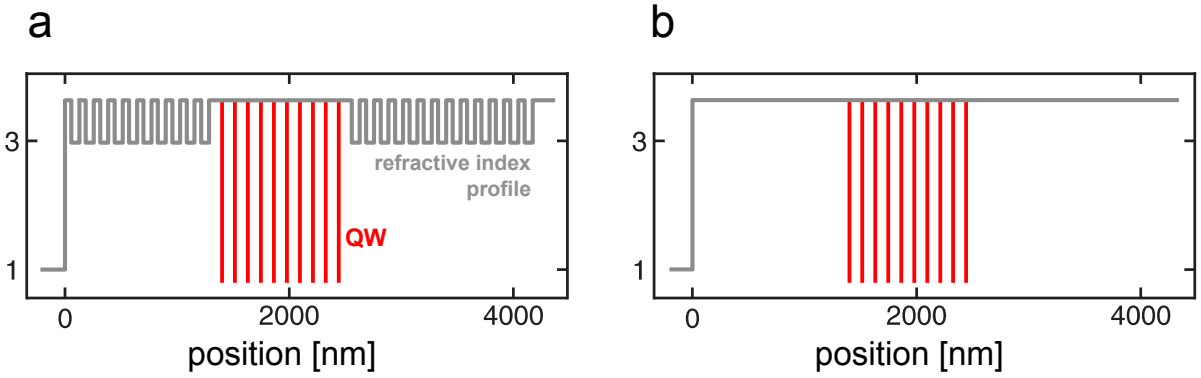

Figure 4.7: Refractive index profile and quantum-well position for microcavity sample from Λ-system study **(a)** and for the sample without microcavity as reference **(b)**

when we sweep the THz frequency (see Fig. 4.6). We take a multi-cycle test pulse as used to simulate the experimental pulse in Section 4.1. The temporal shape of the THz vector potential is given by

$$A_{\mathrm{THz}}(t) = \frac{E_0}{2\pi\nu} e^{-\frac{t^2}{\tau^2}} \left(\cos\left(2\pi\nu\left(t-\Delta t\right)\right) + 0.6\,\cos\left(1.7\pi\nu\left(t-\Delta t\right)\right)\right). \tag{4.1}$$

The THz vector potential A_{THz} is the sum of two Gaussians, which leads in frequency domain to two Gaussians which are close to each other. The pulse intensity is given by E_0 for which we will use the intensities 2, 3 and 4 kV/cm. The delay between optical and THz pulse is $\Delta t = 0.8$ ps. The pulse duration is $\tau = 2.1$ ps. The central THz frequency is denoted by ν. Optical light only induces s-like occupation ($|p_{2p}|^2_{\mathrm{w/oTHz}} \equiv 0$) As a measure of how much occupation is in an excitonic state, we define

$$F_\lambda \equiv \frac{|p_\lambda|^2}{\sum_\beta |p_\beta|^2}, \tag{4.2}$$

which determines the fraction of all existing occupations in excitonic state λ. In Fig. 4.8, we show snapshots of the fractions F_λ for a THz frequency sweep: On top (Fig. **(a)**–**(c)**), we plot the results for the well-understood system of bare quantum wells without microcavity as a reference, down (Fig. **(d)**–**(f)**) the results for the microcavity system. The THz intensities are 2 kV/cm (blue dashed), 3 kV/cm (red solid) and 4 kV/cm (black solid).

First of all, we have a look at the THz-induced changes in the 1s-exciton peak without microcavity, plotted in Fig. 4.8 **(a)**. The 1s–2p transition frequency as determined from the Wannier equation is marked as dashed horizontal line. We note for the lowest THz intensity (blue-dashed line) a dip in the 1s fraction when the THz frequency is resonant with the 1s–2p frequency. This is expected, as the 1s exciton polarization has the strongest coupling to the 2p state. The dip becomes more pronounced for higher THz intensities and shifts to higher energies due to the Stark shift [77], as already seen in the

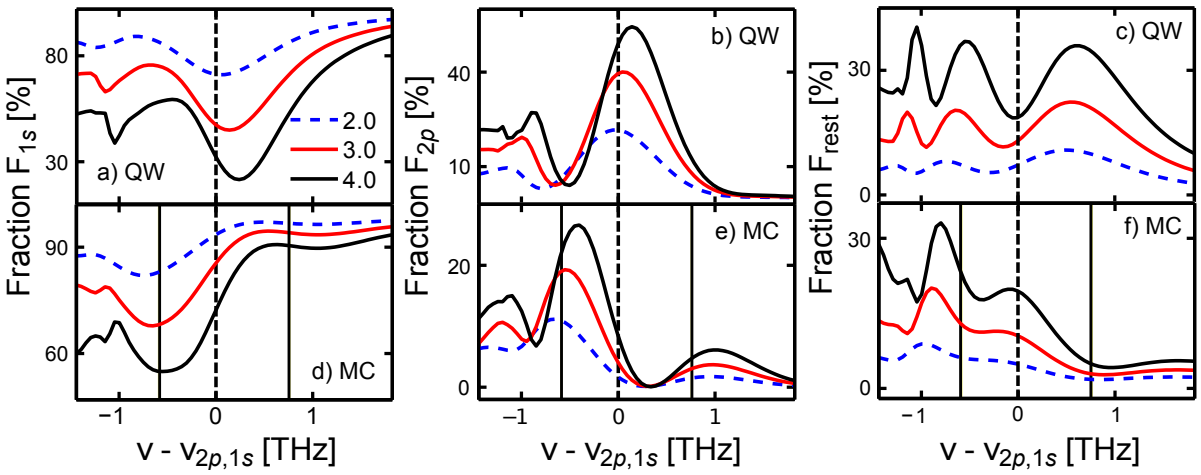

Figure 4.8: (Taken from Paper III) Fractions of excitonic polarization in 1s state (**(a), (d)**), 2p state (**(b), (e)**) and higher dark states (**(c), (e)**) for the system of bare QWs (*QW*, top) and the QWs inside the microcavity (*MC*, bottom).

spectra in Chapter 3. Finally, we observe dips around the half of the 1s–2p transition frequency due to multi-photon absorption.

For the QWs inside the microcavity, the results are shown in Fig. 4.8 **(b)**. Again, the original 1s–2p frequency is marked as dashed vertical line (as in all following figures). In addition, the transition energies expected from the peak position for LEP- and HEP-to-2p transitions are marked as solid vertical lines. Note that even if we do not have a 1s peak in the exciton-polariton spectrum, one can still use the mathematical concept of the exciton basis as described in Chapter 2. For the microcavity system, F_{1s} dips around both expected transition frequencies (LEP- and HEP-to-2p). No feature is shown around the 1s–2p resonance, which underlines that the 1s polarization is splitted into a LEP and HEP part. The dip at HEP-to-2p transition is much deeper than for the LEP-to-2p transition, which fits the fact that in the spectral figure, the LEP is harder to bleach than the LEP (see Section 4.1).

Looking at the figures for F_{2p} (**(b)** and **(e)**), we see clear peaks at the frequencies which show dips in F_{1s}. The same effects as for F_{1s} (Stark shift, multi-photon absorption) are observed as well as the asymmetry for LEP and HEP.

Finally, the fraction of higher optically-dark states is plotted in Figs. **(c)** and **(f)**. The dark states are in both system rarely occupied for the lowest THz intensity (around 10 % for 2 kV/cm THz intensity), but the fraction grows with higher intensity. This is to be expected as we saw in Chapter 3 the importance of dark states growing with increasing THz intensity. In principle, the dark states are more important when the THz frequency is off-resonant from transitions into the 2p state. Interestingly, the dark states play almost no role for high THz frequencies. Numerical simulations (not shown here) hinted that this asymmetry is not changing with the detuning, as one could have guessed from the idea of Hopfield coefficients. Further research will be needed to understand the Λ system concerning the different behavior of the exciton polaritons.

4.3 Cavity beating

As a last topic, I show preliminary results for Paper V which underline the various opportunities of weak optical and strong THz excitation spectroscopy: We use THz spectroscopy to measure cavity beating.

The principle is schemed in Fig. 4.9 **(a)** and **(b)**, where we depict as shaded areas the temporal evolution of optical field and 1*s* polarization inside a quantum well without THz influence: We observe that energy is oscillating between optical field and 1*s* polarization. The oscillation frequency is determined by the coupling strength of the two systems and also manifests in the width of the normal mode splitting. In addition to this *beating* of the energy, both polarization and optical field decay due to scattering inside the material and loss processes of the light from the cavity. To measure the beating, we vary the THz arrival time and use the fact that the THz field couples only to the polarization and not to the optical field: If the THz pulse arrives when the polarization is at maximum (Fig. **(a)**), the 1*s* polarization is bleached (blue solid) as the THz light (grey) pushes 1*s* polarization into optically dark polarization. On the other hand, the THz pulse does not couple to the sample if no polarization is present (Fig. **(b)**). In the experiments, this can be seen as changes in the optical spectrum (schematically shown in Figs. 4.9 **(c)** and **(d)**).

The numerical results were motivated by experimental results from the group of Yun-Shik Lee. First numerical results are plotted in Fig. 4.10 **(a)**, where we show the differ-

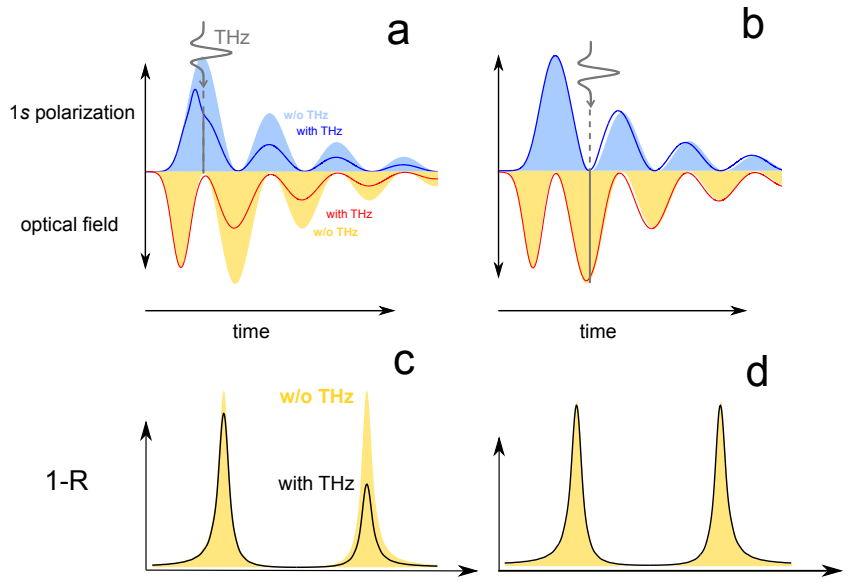

Figure 4.9: Schematics for two different delays influencing the time evolution **(top)** and the spectra **(bottom)**: An arrival of the THz pulse when the polarization is at max **(a)** leads to strong modulations of the spectrum **(c)**, while a THz pulse arriving when no polarization is present **(b)** almost not changes the spectrum **(d)**.

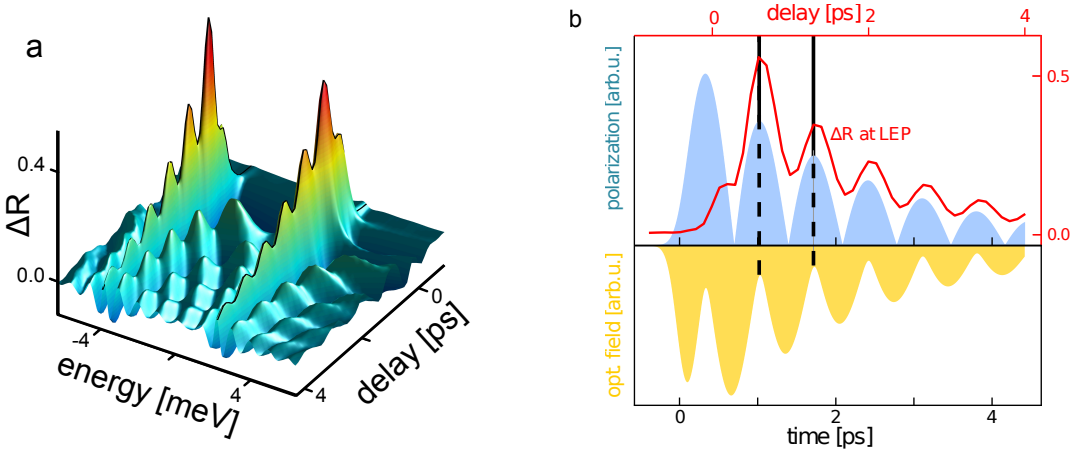

Figure 4.10: **(a)** Theoretical ΔR for different delays between optical and THz pulse. **(b)** Polarization (blue-shaded) and optical field (yellow) without THz influence. Black vertical lines mark two maxima in polarization, which fall together with the minima in optical field. ΔR as function of delay (red axis) at LEP position oscillates with the same frequency.

ential reflectivity $\Delta R = R - R^0$ for different delays between optical and THz pulse. We observe that ΔR is largest around the LEP and HEP positions, where the THz pulse bleaches the spectra the strongest. Furthermore, when sweeping the delay, we see that the changes become smaller for later delays and undergoes additional oscillations. We also see a pattern in between LEP and HEP signatures due to a superposition of oscillations. The oscillations and patterns are also seen in the experimental data (not shown here) with the same oscillation period.

To prove that the oscillations in the ΔR spectra originate from the cavity beating, we plot in Fig. 4.10 **(b)** field (yellow-shaded) and polarization (blue-shaded) without THz together with a cut through the LEP (red solid): We see that the ΔR oscillations have the same period of 0.7 ps as the oscillations in polarization and optical field. This fits also the energetical separation of the normal-mode splitting of 6 meV.

5 Conclusions and outlook

In this Thesis, we have seen several examples of experiments with THz spectroscopy on semiconductor quantum-well nanostructures. In all cases presented, the experimental results have been supported by the analysis with a fully microscopic theory.

The theoretical model we have used for the analysis are the Maxwell-semiconductor Bloch equations. They treat the light–matter interaction self-consistently and enable that basically the same numerical implementation can be used for very different experiments like samples with multiple quantum wells or quantum wells which strongly couple to a microcavity. Following the excitonic occupations in their dynamics makes our theoretical model a powerful tool to study experiments with weak optical and strong THz light.

The first kind of joint experiment–theory studies described is about the interaction of semiconductor quantum wells with weak optical and strong THz light. In all experiments, the THz light manipulates excitonic polarization (so-called *coherent excitons*). A first study with a strong broad-band THz pulse showed clear Rabi splitting. The theoretical simulation has revealed that the single-cycle THz pulse *ionizes* the coherent exciton. Multi-photon absorption with up to four THz-photons has been observed.

A follow-up study with a spectrally narrow THz pulse from a free-electron laser allows us to investigate a multiple-quantum-well system in detail from its transition of an effective two-level system to the multi-level ionization regime. In addition to the first study, anticrossing behavior is observed when changing the THz frequency. The microscopic analysis shows that the Rabi frequency, and thus the splitting width of the Rabi peaks, is already predicted by a two-level model, but that the full theory brings an extra bunch of important information: Indeed, the full theory predicts the exact spectra, the occupation dynamics and, shows that already for low intensities, higher excitonic states are occupied. In addition, the full theory predicts the exact spectra and occupation dynamics and shows that already for low intensities, higher excitonic states are occupied.

These were only few investigations on excitonic polarizations with THz spectroscopy. The same scheme can be also applied to systematically explore other material systems, similarly to the study in preparation with germanium quantum wells (Paper VI). We expect THz spectroscopy to help us gaining a deeper understanding about how coherent and incoherent excitons work precisely, for example, to understand the scattering behavior under the influence of a magnetic field [50]. Controlling the $1s$–$2p$ exciton transition is a possible way to achieve qubits in quantum computing [51]. Finally, understanding excitons in bare quantum wells is crucial to understand even more complicated excitonic systems like those of exciton polaritons, as described in Chapter 4.

The second type of experiments is involving a more complex nanostructure where a multiple-quantum-well system is grown inside a microcavity. Here, the coherent excitons which we studied already in Chapter 3 couple to the eigenmode of the microcavity,

leading to the formation of exciton polaritons. The key of our theoretical analysis was our ability to model the light–matter coupling of coherent excitons self-consistently. Using THz spectroscopy on this strong-coupling system showed that both exciton polaritons build together with the $2p$-exciton state a unique Λ system. Unlike Λ systems known from atomic physics, the states are coherently build, which offer the possibility to control their energetical positions, e.g., by detuning cavity mode and exciton resonance or by designing the cavity. An additional study comparing the three-level system with the $1s$-$2p$ transition in bare quantum wells showed that in fact polarization is transferred into the $2p$ state, but that transitions from the higher exciton polariton are *easier* than from the lower exciton polariton. More research is needed to understand the origin of these differences. At the moment, research is planned on similar systems, e.g., with very large Rabi splitting as in [52]. We believe that this Λ system is stable enough to test phenomena known from atomic Λ systems like Stimulated Raman Adiabatic passage (STIRAP) [53], Electromagnetically Induced Transparency (EIT) [54] or slow light [55]. Investigations in this direction are already in preparation [56].

These were only few examples from the point of view of basic research underlining the importance of theoretical studies on terahertz spectroscopy on semiconductor nanostructures. The theory applied here is not restricted to microcavity or multiple-quantum-well samples, but can be used flexibly for many other kinds of quantum-well nanostructures. The properties of excitonic systems are still under strong research, driven by the ability of growing better samples and better experimental methods like THz measurements.

Bibliography

[1] I. Ferain, C. A. Colinge, and J.-P. Colinge, "Multigate transistors as the future of classical metal-oxide-semiconductor field-effect transistors," Nature **479**, 310 (2011).

[2] H. Haug and S. W. Koch, *Quantum Theory of the Optical and Electronic Properties of Semiconductors* (World Scientific, 2009).

[3] J. H. Davies, *The Physics of Low-dimensional Semiconductors* (Cambridge University Press, 1998).

[4] N. W. Ashcroft and D. N. Mermin, *Solid State Physics* (Thomson Learning, 1976).

[5] R. Huber, F. Tauser, A. Brodschelm, M. Bichler, G. Abstreiter, and A. Leitenstorfer, "How many-particle interactions develop after ultrafast excitation of an electronhole plasma," Nature **414**, 286 (2001).

[6] M. Kira, F. Jahnke, W. Hoyer, and S. W. Koch, "Quantum theory of spontaneous emission and coherent effects in semiconductor microstructures," Progress in Quantum Electronics **23**, 189 (1999).

[7] M. Kira and S. W. Koch, "Many-body correlations and excitonic effects in semiconductor spectroscopy," Progress in Quantum Electronics **30**, 155 (2006).

[8] S. Chatterjee, C. Ell, S. Mosor, G. Khitrova, H. M. Gibbs, W. Hoyer, M. Kira, S. W. Koch, J. P. Prineas, and H. Stolz, "Excitonic photoluminescence in semiconductor quantum wells: Plasma versus excitons," Phys. Rev. Lett. **92**, 067402 (2004).

[9] M. Kira and S. W. Koch, "Exciton-population inversion and terahertz gain in semiconductors excited to resonance," Phys. Rev. Lett. **93**, 076402 (2004).

[10] W. Hoyer, C. Ell, M. Kira, S. W. Koch, S. Chatterjee, S. Mosor, G. Khitrova, H. M. Gibbs, and H. Stolz, "Many-body dynamics and exciton formation studied by time-resolved photoluminescence," Phys. Rev. B **72**, 075324 (2005).

[11] M. Mootz, M. Kira, and S. W. Koch, "Sequential build-up of quantum-optical correlations," J. Opt. Soc. Am. B **29**, A17 (2012).

[12] C. N. Böttge, M. Kira, and S. W. Koch, "Enhancement of the phonon-sideband luminescence in semiconductor microcavities," Phys. Rev. B **85**, 094301 (2012).

[13] A. Chernikov, V. Bornwasser, M. Koch, S. Chatterjee, C. N. Böttge, T. Feldtmann, M. Kira, S. W. Koch, T. Wassner, S. Lautenschläger, et al., "Phonon-assisted luminescence of polar semiconductors: Fröhlich coupling versus deformation-potential scattering," Phys. Rev. B **85**, 035201 (2012).

[14] M. Kira and S. W. Koch, *Semiconductor Quantum Optics* (Cambridge University Press, 2012).

[15] B. E. Cole, J. B. Williams, B. T. King, M. S. Sherwin, and C. R. Stanley, "Coherent manipulation of semiconductor quantum bits with terahertz radiation," Nature **410**, 60 (2001).

[16] S. G. Carter, V. Birkedal, C. S. Wang, L. A. Coldren, A. V. Maslov, D. S. Citrin, and M. S. Sherwin, "Quantum coherence in an optical modulator," Science **310**, 651 (2005).

[17] S. W. Koch, M. Kira, G. Khitrova, and H. M. Gibbs, "Semiconductor excitons in new light," Nature Mater. **5**, 523 (2006).

[18] S. Leinß, T. Kampfrath, K. v.Volkmann, M. Wolf, J. T. Steiner, M. Kira, S. W. Koch, A. Leitenstorfer, and R. Huber, "Terahertz coherent control of optically dark paraexcitons in Cu_2O," Phys. Rev. Lett. **101**, 246401 (2008).

[19] J. R. Danielson, Y.-S. Lee, J. P. Prineas, J. T. Steiner, M. Kira, and S. W. Koch, "Interaction of strong single-cycle terahertz pulses with semiconductor quantum wells," Phys. Rev. Lett. **99**, 237401 (2007).

[20] A. D. Jameson, J. L. Tomaino, Y.-S. Lee, J. P. Prineas, J. T. Steiner, M. Kira, and S. W. Koch, "Transient optical response of quantum well excitons to intense narrowband terahertz pulses," Appl. Phys. Lett. **95**, 201107 (2009).

[21] M. Kira, W. Hoyer, and S. Koch, "Terahertz signatures of the exciton formation dynamics in non-resonantly excited semiconductors," Solid State Commun. **129**, 733 (2004).

[22] D. Golde, M. Wagner, D. Stehr, H. Schneider, M. Helm, A. M. Andrews, T. Roch, G. Strasser, M. Kira, and S. W. Koch, "Fano signatures in the intersubband terahertz response of optically excited semiconductor quantum wells," Phys. Rev. Lett. **102**, 127403 (2009).

[23] F. Blanchard, D. Golde, F. H. Su, L. Razzari, G. Sharma, R. Morandotti, T. Ozaki, M. Reid, M. Kira, S. W. Koch, et al., "Effective mass anisotropy of hot electrons in nonparabolic conduction bands of n-doped InGaAs films using ultrafast terahertz pump-probe techniques," Phys. Rev. Lett. **107**, 107401 (2011).

[24] K. Johnsen and A.-P. Jauho, "Quasienergy spectroscopy of excitons," Phys. Rev. Lett. **83**, 1207 (1999).

[25] D. S. Citrin, "Doubly resonant terahertz sideband generation in quantum wells: Optical signatures of terahertz-dressed subbands," Phys. Rev. B **60**, 13695 (1999).

[26] A. Liu and C.-Z. Ning, "Exciton absorption in semiconductor quantum wells driven by a strong intersubband pump field," J. Opt. Soc. Am. B **17**, 433 (2000).

[27] X. W. Mi, J. C. Cao, and C. Zhang, "Optical absorption in terahertz-driven quantum wells," Journal of Applied Physics **95**, 1191 (2004).

[28] T. Y. Zhang, W. Zhao, X. M. Liu, and C. Zhang, "Nonlinear optical properties of semiconductor quantum wells under intense terahertz radiation," Appl. Phys. Lett. **91**, 041909 (2007).

[29] J.-Y. Yan, R.-B. Liu, and B. fen Zhu, "Exciton absorption in semiconductor superlattices in a strong longitudinal THz field," New Journal of Physics **11**, 083004 (2009).

[30] M. Wagner, H. Schneider, D. Stehr, S. Winnerl, A. M. Andrews, S. Schartner, G. Strasser, and M. Helm, "Observation of the Intraexciton Autler-Townes Effect in GaAs/AlGaAs semiconductor quantum wells," Phys. Rev. Lett. **105**, 167401 (2010).

[31] R. A. Kaindl, M. A. Carnahan, D. Hägele, R. Lövenich, and D. S. Chemla, "Ultrafast terahertz probes of transient conducting and insulating phases in an electronhole gas," Nature **423**, 734 (2003).

[32] J. Černe, J. Kono, M. S. Sherwin, M. Sundaram, A. C. Gossard, and G. E. W. Bauer, "Terahertz dynamics of excitons in GaAs/AlGaAs quantum wells," Phys. Rev. Lett. **77**, 1131 (1996).

[33] J. T. Steiner, M. Kira, and S. W. Koch, "Optical nonlinearities and Rabi flopping of an exciton population in a semiconductor interacting with strong terahertz fields," Phys. Rev. B **77**, 165308 (2008).

[34] I. I. Rabi, "Space quantization in a gyrating magnetic field," Phys. Rev. **51**, 652 (1937).

[35] C. Weisbuch, M. Nishioka, A. Ishikawa, and Y. Arakawa, "Observation of the coupled exciton-photon mode splitting in a semiconductor quantum microcavity," Phys. Rev. Lett. **69**, 3314 (1992).

[36] G. Khitrova, H. M. Gibbs, F. Jahnke, M. Kira, and S. W. Koch, "Nonlinear optics of normal-mode-coupling semiconductor microcavities," Rev. Mod. Phys. **71**, 1591 (1999).

[37] P. B. Corkum, N. H. Burnett, and F. Brunel, "Above-threshold ionization in the long-wavelength limit," Phys. Rev. Lett. **62**, 1259 (1989).

[38] Y.-S. Lee, T. B. Norris, M. Kira, F. Jahnke, S. W. Koch, G. Khitrova, and H. M. Gibbs, "Quantum Correlations and Intraband Coherences in Semiconductor Cavity QED," Phys. Rev. Lett. **83**, 5338 (1999).

[39] J. P. Reithmaier, G. Sek, C. Löffler, A. Hofmann, S. K. L. V. Kuhn, S. Reitzenstein, V. D. Kulakovskii, and A. Reinecke, T. L. Forchel, "Strong coupling in a single quantum dot-semiconductor microcavity system," Nature **432**, 197 (2004).

[40] T. Yoshie, A. Scherer, J. Hendrickson, G. Khitrova, H. M. Gibbs, G. Rupper, C. Ell, O. B. Shchekin, and D. G. Deppe, "Vacuum Rabi splitting with a single quantum dot in a photonic crystal nanocavity," Nature **432**, 200 (2004).

[41] K. Hennessy, A. Badolato, M. Winger, D. Gerace, M. Atature, S. Gulde, S. Falt, E. L. Hu, and A. Imamoglu, "Quantum nature of a strongly coupled single quantum dot-cavity system," Nature **445**, 896 (2007).

[42] G. Günter, A. A. Anappara, J. Hees, A. Sell, G. Biasiol, S. Sorba, L. De Liberato, C. Ciuti, A. Tredicucci, A. Leitenstorfer, and R. Huber, "Sub-cycle switch-on of ultrastrong light-matter interaction," Nature **458**, 178 (2009).

[43] F. T. Y. Yamamoto and H. Cao, *Semiconductor Cavity Quantum Electrodynamics* (Springer, Berlin, Heidelberg, 2000).

[44] H. Deng, G. Weihs, C. Santori, J. Bloch, and Y. Yamamoto, "Condensation of semiconductor microcavity exciton polaritons," **298**, 199 (2002).

[45] J. Kasprzak, M. Richard, S. Kundermann, A. Baas, P. Jeambrun, J. M. J. Keeling, F. M. Marchetti, M. H. Szymanska, R. Andre, J. L. Staehli, et al., "Bose-Einstein condensation of exciton polaritons," Nature **443**, 409 (2006).

[46] R. Balili, V. Hartwell, D. Snoke, L. Pfeiffer, and K. West, "Bose-Einstein Condensation of Microcavity Polaritons in a Trap," **316**, 1007 (2007).

[47] H. Deng, H. Haug, and Y. Yamamoto, "Exciton-polariton Bose-Einstein condensation," Rev. Mod. Phys. **82**, 1489 (2010).

[48] L. Allen and J. H. Eberly, *Optical resonance and two-level atoms* (Dover Publications, 1987).

[49] M. Lindberg and S. W. Koch, "Effective Bloch equations for semiconductors," Phys. Rev. B **38**, 3342 (1988).

[50] W. D. Rice, J. Kono, S. Zybell, S. Winnerl, J. Bhattacharyya, H. Schneider, M. Helm, B. Ewers, A. Chernikov, M. Koch, et al., "Observation of Coulomb-Assisted Dipole-Forbidden Intraexciton Transitions in Semiconductors," ArXiv e-prints (2012), `1203.3994`.

[51] S. Michaelis de Vasconcellos, S. Gordon, M. Bichler, T. Meier, and A. Zrenner, "Coherent control of a single exciton qubit by optoelectronic manipulation," Nature Photon. **4**, 545 (2010).

[52] J. Bloch, T. Freixanet, J. Y. Marzin, V. Thierry-Mieg, and R. Planel, "Giant Rabi splitting in a microcavity containing distributed quantum wells," Appl. Phys. Lett. **73**, 1694 (1998).

[53] K. Bergmann, H. Theuer, and B. W. Shore, "Coherent population transfer among quantum states of atoms and molecules," Rev. Mod. Phys. **70**, 1003 (1998).

[54] M. Fleischhauer, C. H. Keitel, M. O. Scully, C. Su, B. T. Ulrich, and S.-Y. Zhu, "Resonantly enhanced refractive index without absorption via atomic coherence," Phys. Rev. A **46**, 1468 (1992).

[55] L. V. Hau, S. E. Harris, Z. Dutton, and C. H. Behroozi, "Light speed reduction to 17 metres per second in an ultracold atomic gas," Nature **397**, 594 (1999).

[56] A. Bronn, *Terahertz-Induced STIRAP Processes in a Semiconductor Microcavity. Masterarbeit* (Philipps-University Marburg, 2012).

[57] J. D. Berger, O. Lyngnes, H. M. Gibbs, G. Khitrova, T. R. Nelson, E. K. Lindmark, A. V. Kavokin, M. A. Kaliteevski, and V. V. Zapasskii, "Magnetic-field enhancement of the exciton-polariton splitting in a semiconductor quantum-well microcavity: The strong coupling threshold," Phys. Rev. B **54**, 1975 (1996).

[58] J. T. Steiner, *Microscopic Theory of Linear and Nonlinear Terahertz Spectroscopy of Semiconductors. PhD thesis* (Philipps-University Marburg, 2008).

[59] B. R. Mollow, "Power spectrum of light scattered by two-level systems," Phys. Rev. **188**, 1969 (1969).

[60] H. W. Jr. and B. D. Fried, "Quantum mechanical kinetic equations," Annals of Physics **23**, 374 (1963).

[61] A. V. Maslov and D. S. Citrin, "Optical absorption and sideband generation in quantum wells driven by a terahertz electric field," Phys. Rev. B **62**, 16686 (2000).

[62] M. Kira, W. Hoyer, and S. W. Koch, "Microscopic theory of the semiconductor terahertz response," physica status solidi (b) **238**, 443 (2003).

[63] P. C. M. Planken, M. C. Nuss, I. Brener, K. W. Goossen, M. S. C. Luo, S. L. Chuang, and L. Pfeiffer, "Terahertz emission in single quantum wells after coherent optical excitation of light hole and heavy hole excitons," Phys. Rev. Lett. **69**, 3800 (1992).

[64] M. Kira, W. Hoyer, T. Stroucken, and S. W. Koch, "Exciton formation in semiconductors and the influence of a photonic environment," Phys. Rev. Lett. **87**, 176401 (2001).

[65] D. S. Citrin, "Terahertz sideband generation and coherent control in semiconductor microcavities," Phys. Rev. Lett. **82**, 3172 (1999).

[66] D. S. Yee, K. J. Yee, S. C. Hohng, D. S. Kim, T. Meier, and S. W. Koch, "Coherent control of absorption and polarization decay in a GaAs quantum well: Time and spectral domain studies," Phys. Rev. Lett. **84**, 3474 (2000).

[67] R. Ulbricht, E. Hendry, J. Shan, T. F. Heinz, and M. Bonn, "Carrier dynamics in semiconductors studied with time-resolved terahertz spectroscopy," Rev. Mod. Phys. **83**, 543 (2011).

[68] I. Galbraith, R. Chari, S. Pellegrini, P. J. Phillips, C. J. Dent, A. F. G. van der Meer, D. G. Clarke, A. K. Kar, G. S. Buller, C. R. Pidgeon, et al., "Excitonic signatures in the photoluminescence and terahertz absorption of a $GaAsAl_xGa_{1-x}As$ multiple quantum well," Phys. Rev. B **71**, 073302 (2005).

[69] M. Jörger, T. Fleck, C. Klingshirn, and R. von Baltz, "Midinfrared properties of cuprous oxide: High-order lattice vibrations and intraexcitonic transitions of the $1s$ paraexciton," Phys. Rev. B **71**, 235210 (2005).

[70] R. Huber, B. A. Schmid, Y. R. Shen, D. S. Chemla, and R. A. Kaindl, "Stimulated terahertz emission from intraexcitonic transitions in Cu_2O," Phys. Rev. Lett. **96**, 017402 (2006).

[71] Q. Wu and X. Zhang, "Freespace electrooptic sampling of terahertz beams," Appl. Phys. Lett. **67**, 3523 (1995).

[72] P. U. Jepsen, C. Winnewisser, M. Schall, V. Schyja, S. R. Keiding, and H. Helm, "Detection of THz pulses by phase retardation in lithium tantalate," Phys. Rev. E **53**, R3052 (1996).

[73] T. Grunwald, T. Jung, D. Köhler, S. Koch, G. Khitrova, H. Gibbs, R. Hey, and S. Chatterjee, "Measurement of intraexcitonic transition signatures via THz time-domain spectroscopy: A GaAs/(AlGa)As (GaIn)As/GaAs comparison," physica status solidi (c) **6**, 500 (2009).

[74] F. Jahnke, M. Kira, S. W. Koch, G. Khitrova, E. K. Lindmark, T. R. Nelson, Jr., D. V. Wick, J. D. Berger, O. Lyngnes, H. M. Gibbs, et al., "Excitonic nonlinearities of semiconductor microcavities in the nonperturbative regime," Phys. Rev. Lett. **77**, 5257 (1996).

[75] M. Gurioli, F. Bogani, D. S. Wiersma, P. Roussignol, G. Cassabois, G. Khitrova, and H. Gibbs, "Experimental study of disorder in a semiconductor microcavity," Phys. Rev. B **64**, 165309 (2001).

[76] M. Werchner, M. Schäfer, M. Kira, S. W. Koch, J. Sweet, J. D. Olitzky, J. Hendrickson, B. C. Richards, G. Khitrova, H. M. Gibbs, et al., "One dimensional resonant

Fibonacci quasicrystals: noncanonical linear andcanonical nonlinear effects," Opt. Express **17**, 6813 (2009).

[77] K. B. Nordstrom, K. Johnsen, S. J. Allen, A.-P. Jauho, B. Birnir, J. Kono, T. Noda, H. Akiyama, and H. Sakaki, "Excitonic dynamical Franz-Keldysh effect," Phys. Rev. Lett. **81**, 457 (1998).

Paper I

Phys. Rev. B 85, 075307

Ionization of coherent excitons by strong terahertz fields

PHYSICAL REVIEW B **85**, 075307 (2012)

Ionization of coherent excitons by strong terahertz fields

B. Ewers, N. S. Köster, R. Woscholski, M. Koch, and S. Chatterjee
Faculty of Physics and Materials Sciences Center, Philipps-Universität Marburg, Renthof 5, D-35032 Marburg, Germany

G. Khitrova and H. M. Gibbs
College of Optical Sciences, The University of Arizona, 1630 E. University Boulevard, Tucson, Arizona 85719-0094, USA

A. C. Klettke, M. Kira, and S. W. Koch
Faculty of Physics and Materials Sciences Center, Philipps-Universität Marburg, Mainzer Gasse 33, D-35032 Marburg, Germany
(Received 7 December 2011; revised manuscript received 16 January 2012; published 6 February 2012)

The interaction of coherent excitons with intense, single-cycle terahertz (THz) pulses is investigated. A significant bleaching of the 1*s*-exciton resonance develops into a splitting of the absorption peak and the emergence of pronounced wings with increasing THz field strength. A quantum-mechanical many-body analysis attributes the experimental observations to a transition from excitonic Rabi flopping to multi-THz-photon ionization and the population of optically dark exciton states with high quantum numbers.

DOI: 10.1103/PhysRevB.85.075307 PACS number(s): 78.67.De, 42.65.Re, 78.47.D−

I. INTRODUCTION

The observation and analysis of sophisticated coherent effects in atoms[1,2] has often stimulated the search for similar features in solid-state systems. Direct-gap semiconductors exhibit analogous atomic features through the hydrogenlike series of optically induced exciton resonances. These "coherent excitons," also known as the "coherent excitonic polarization," represent a superposition state of electrons in the conduction band and holes in the valence band with the driving light field.[3] Through the many-body interactions in the system, the coherent excitons can be converted into a quasiparticlelike, incoherent exciton population.[4–6]

With the help of additional fields in the range of the terahertz (THz) part of the electromagnetic spectrum, transitions between different excitonic states can be induced and the nature of the many-body configuration can be identified.[7] Experimental studies of optical-pump and THz-probe experiments have been reported and exciton populations, electron-hole plasma signatures, plasmonic features, as well as nonperturbative exciton bleaching and high-harmonic generation have been identified.[8–10] Using the strong THz fields of a free-electron laser, effects such as photoluminescence quenching of magnetoexcitons[11] or the coupling of states in quantum wells[12] have been studied and recently, excitonic Rabi splitting has been demonstrated.[13]

In this paper, we investigate the interaction of coherent excitons with strong single-cycle THz pulses with the goal to identify exciton ionization features: by systematically controlling the THz photon fluency, we monitor the system response all the way from the weakly coupled perturbative regime into the realm of extreme nonlinear THz optics. Our studies can be viewed as the quasiparticle analogy to the above-threshold ionization scenario in atomic systems,[14] thus, significantly expanding on earlier THz experiments in semiconductor systems.[10,13,15]

II. EXPERIMENTAL SETUP

A regenerative Ti:sapphire amplifier system emitting 800-nm, 120-fs pulses at a 1-kHz repetition rate is used as a light source to excite a commercially available GaAs-based large-area THz emitter. It generates the strong, approximately 1-ps-long single-cycle THz pulses covering nearly three octaves of bandwidth (Fig. 1). Using two off-axis parabolic mirrors, the THz field is imaged onto a semiconductor quantum-well (QW) structure containing 30 $Ga_{0.97}In_{0.03}As$ QWs separated by GaAs barriers (DBR13) which is mounted inside a He-flow microscopy cryostat equipped with polymethylpentene (TPX) windows. The THz field coherently manipulates the 1*s* polarization in the sample and another pair of off-axis parabolic mirrors is used to relay the transmitted THz field onto a 0.8-mm-thick ⟨110⟩-cut ZnTe crystal used for standard electro-optical sampling.[16,17] The THz beam path is kept in an encapsulated environment with a constant-flow nitrogen purge eliminating most water vapor. The peak electric field is set by varying the voltage biasing the THz emitter while keeping the spatial, spectral, and temporal field distribution constant. A THz field strength of up to 15 kV/cm in free space is measured by using a calibrated Golay cell and a knife-edge test at the position of the sample without the cryostat window.

A white-light supercontinuum pulse generated in a ⟨0001⟩-cut sapphire crystal is used as a probe. Its light is transmitted through the sample coaxially to the THz pulse by propagating through 2-mm holes drilled through the 2″-diameter off-axis parabolas. The spectrum of the transmitted optical pulse is dispersed using a grating spectrometer with a resolution of 0.014 nm and detected by a liquid-nitrogen-cooled charge-coupled device camera. This configuration is also used to determine the linear absorption of the sample in transmission geometry as the multiple QW stack is antireflection coated for the 1*s*-exciton energy at cryogenic temperatures. The thickness of approximately 100 nm of the coating is significantly smaller than the THz wavelength used in this experiment and is, therefore, transparent for the THz regime.

III. EXPERIMENTAL RESULTS

The central experimental observations are summarized in Figs. 2 and 3. Figure 2(a) displays the absorption spectra αL with (dark red) and without (light gray) the presence of the

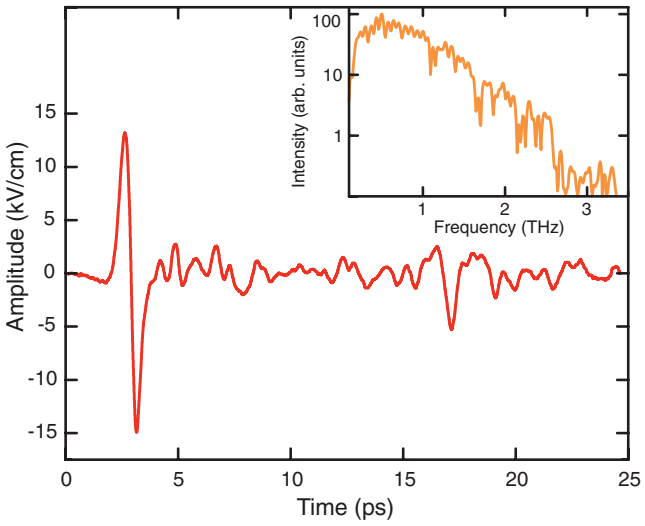

FIG. 1. (Color online) Temporal distribution of the used THz pulses and the corresponding spectrum (inset). The time trace is measured with a standard electro-optical sampling setup based on a 0.8 mm ⟨110⟩-cut ZnTe crystal. The THz field strength of up to 15 kV/cm in free space is measured by using a calibrated Golay cell and a knife-edge test without the cryostat windows.

THz pulse for zero time delay, resulting in the maximum THz-induced changes. We find a pronounced bleaching and splitting of the 1s-exciton resonance as well as the development of wings at energies above and below the two central peaks. The strong modulations of about 10–15 meV above the 1s-exciton resonance are signatures of high-harmonic generation during Rabi flopping of the 1s-2p transition.[10,18]

The time evolution of the measured absorption spectrum αL is given in Fig. 2(b) as the contour plot. Note that the sample is transparent to the THz field when no optical polarization is injected. The THz-induced splitting is observed for times in the range of several hundreds of femtoseconds around time zero indicated by the black horizontal line; the position of the main peak(s) is (are) indicated by the dashed white line(s). The alternating structure around 1.5 eV again results from higher THz harmonics.

Figure 2(c) shows the changes of the absorption $\Delta\alpha L_{\text{peak}}$ as a function of time delay at the peak energy of the 1s-exciton resonance (1.4919 eV) (solid line). The field amplitude of the single-cycle THz pulse is given as a reference (dashed line). We see that the presence of the THz pulse changes $\Delta\alpha L$ by -3 and change occurs only as long as the THz pulse is present.

The measured intensity dependence of the THz-induced spectral changes at zero time delay for a series of THz field strengths is shown in the left-hand side of Fig. 3(a). We clearly see the gradual transition from weak bleaching of the 1s-exciton resonance to a double-peaked spectrum as the THz field strength is increased. For even higher THz intensities, a highly asymmetric spectrum develops featuring pronounced wings on both the low- and high-energy sides of the main peaks.

In Fig. 3(b), the energies of the Rabi-peak resonances are plotted as a function of the THz field strength. We observe the transition from THz-induced exciton bleaching to a pronounced peak splitting which is accompanied by a

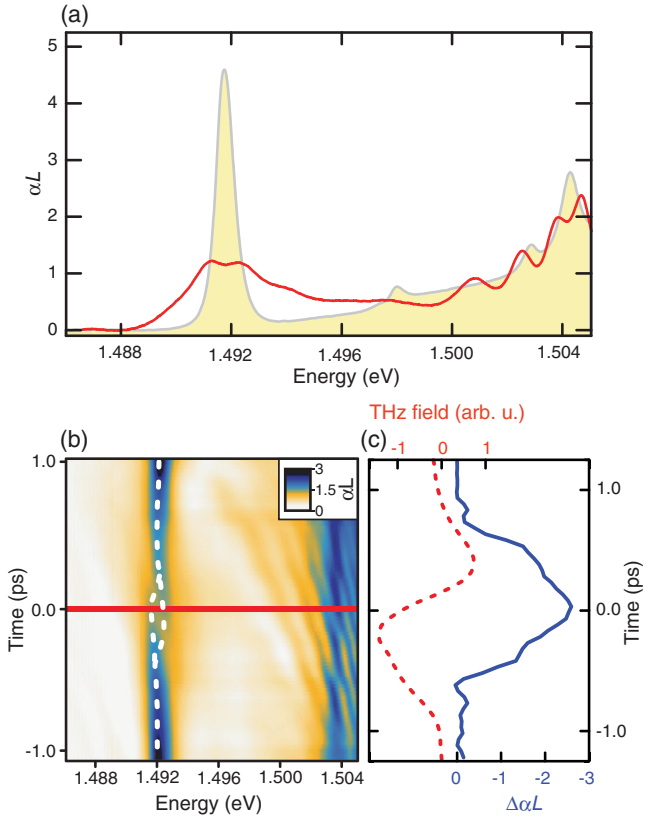

FIG. 2. (Color online) (a) Linear absorption spectrum (red) and absorption under THz radiation at time zero (shaded area). (b) Contour plot of the measured absorption spectrum αL as a function of energy and time delay on a gray scale. The position of the main peak(s) is (are) indicated by the vertical dashed white line(s) acting as a guide(s) to the eye; the red solid line indicates time zero. (c) Peak absorption change $\Delta\alpha L_{\text{peak}}$ at the energy of the 1s-exciton resonance in the linear spectrum (solid line); the THz pulse is given as a reference (dashed line).

slight redshift of the spectrum. The energy separation between the split peaks increases linearly with the THz-field amplitude E_{THz} from ∼2.5 to ∼6.0 kV/cm. For high THz amplitudes, the spectrum becomes very broad and the remaining spectra are blueshifted as the THz field is increased. The same features are identified when considering the peak heights in Fig. 3(c). For weak intensities, the absorption peak changes only moderately. After the split peaks emerge at intermediate intensities, the absorption peak starts to decrease rapidly as excitation is increased. For high excitations, both the absorption peak and the splitting saturate, whereas the spectrum develops extended wings.

IV. THEORY

A detailed understanding of the underlying mechanism is achieved by applying a systematic analysis using a microscopic many-body theory. The approach self-consistently includes the optical and the THz fields as well as the microscopic quasiparticle interactions for the analysis of these effects.[10,18–20] Starting from the standard many-body

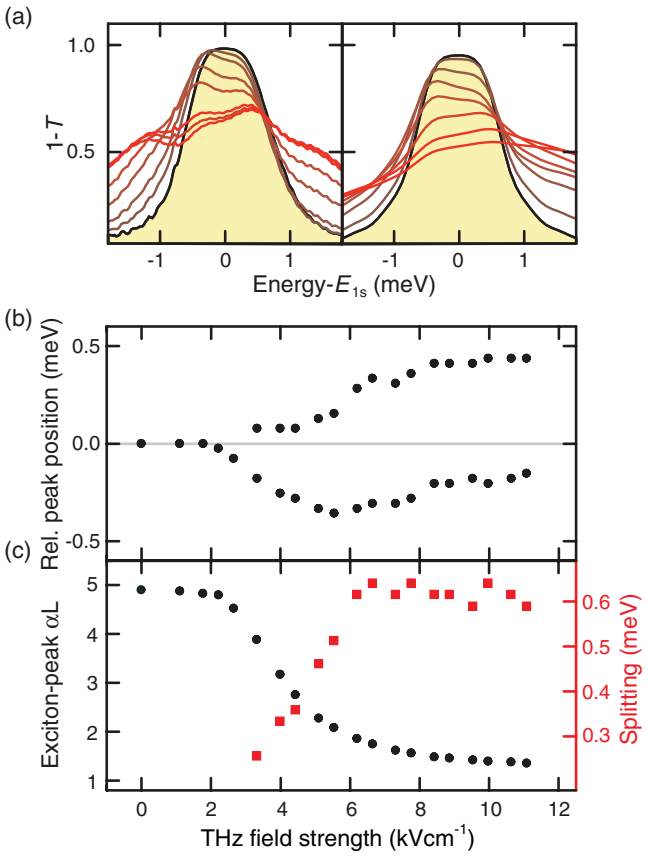

FIG. 3. (Color online) (a) Measured (left) and calculated (right) transmission data $(1-T)$ for various applied THz field strength at time zero: 0, 1.6, 3.2, 4.8, 6.4, 8.0, 9.6, 11.2, and 12.8 kV/cm (from top, gray, to bottom, red). (b) Peak energies relative to the $1s$-exciton resonance in the unperturbed system. (c) Peak absorption (black dots) and splitting of the $1s$-exciton resonance (squares).

Hamiltonian for Coulomb-interacting carriers which couple to light via the minimal substitution Hamiltonian, the dynamic equation for the polarization dynamics is derived using the systematic cluster-expansion approach:[3]

$$i\hbar\frac{\partial}{\partial t}P_{\mathbf{k}} = \left(\epsilon_{\mathbf{k}} - j_{\mathbf{k}}A_{\mathrm{THz}} + \frac{|e|^2}{2\mu}A_{\mathrm{THz}}^2\right)P_{\mathbf{k}} + \sum_{\mathbf{k}'}\Gamma_{\mathbf{k},\mathbf{k}'}P_{\mathbf{k}'} - \left(1 - f_{\mathbf{k}}^e - f_{\mathbf{k}}^h\right)\left(d_{cv}E_{\mathrm{opt}} + \sum_{\mathbf{k}'}V_{\mathbf{k}-\mathbf{k}'}P_{\mathbf{k}'}\right). \quad (1)$$

Here, the first set of parentheses contains the sum of the kinetic carrier energies $\epsilon_{\mathbf{k}}$, the THz current $j_{\mathbf{k}}A_{\mathrm{THz}}$, where A_{THz} is the vector potential of the THz field and $j_{\mathbf{k}}$ is the current-matrix element, as well as the so-called ponderomotive current $\frac{|e|^2}{2\mu}A_{\mathrm{THz}}^2$. The second term, $\sum_{\mathbf{k}'}\Gamma_{\mathbf{k},\mathbf{k}'}P_{\mathbf{k}'}$, describes excitation-induced dephasing due to Coulomb and phonon scattering. The last term is the usual product of the phase-space filling factor $1 - f_{\mathbf{k}}^e - f_{\mathbf{k}}^h$ times the generalized optical Rabi frequency $d_{cv}E_{\mathrm{opt}} + \sum_{\mathbf{k}'}V_{\mathbf{k}-\mathbf{k}'}P_{\mathbf{k}'}$ (Ref. 21) containing the optical field E_{opt} and the dipole-matrix element d_{cv}.

The total electromagnetic field $E(z,t) = E_{\mathrm{opt}}(z,t) + E_{\mathrm{THz}}(z,t)$ for light propagating perpendicular to the QWs and polarized linearly in the x direction is determined from the wave equation

$$\left[\frac{\partial^2}{\partial z^2} - \frac{n^2(z)}{c_0^2}\frac{\partial^2}{\partial t^2}\right]E(z,t) = \mu_0\left(\frac{\partial^2 P_{\mathrm{opt}}(z)}{\partial t^2} + \frac{\partial J(z)}{\partial t}\right), \quad (2)$$

where $P_{\mathrm{opt}} \sim \sum_{\mathbf{k}}P_{\mathbf{k}}$ and J is the sum of THz and ponderomotive currents. The refractive index profile of the system is determined by $n(z)$. The THz contribution satisfies $E_{\mathrm{THz}} = -\frac{\partial}{\partial t}A_{\mathrm{THz}}$.

To monitor the THz-induced transitions between excitonic states, we apply the projection

$$p_\lambda = \sum_{\mathbf{k}}\phi_\lambda^\star(\mathbf{k})\,P_{\mathbf{k}}, \quad (3)$$

where $\phi_\lambda^\star(\mathbf{k})$ is the wave function of the Wannier exciton.[21] The probability to detect the exciton component λ is then defined by $n_\lambda = |p_\lambda|^2$. For QW systems, $\lambda = (n,m)$ is uniquely defined by the principal quantum number n and the orbital quantum number m. The combination $\lambda = (1,0)$ defines the $1s$ state and $\lambda = (2,\pm1)$ identifies the $2p$ state, respectively.

V. ANALYSIS

Results from the full calculation are shown on the right-hand side of Fig. 3(a) for a sequence of THz field strengths. Very good agreement with the experimental data is observed. All the relevant features, such as the increasing bleaching and the growing splitting of the $1s$-exciton resonance with increasing field strength, are clearly observable both in the calculated and the measured data. Furthermore, a slight redshift is obtained for weak THz field strength, which changes into a clear blueshift for stronger fields.

For a more detailed analysis, we present the computed results for the field strengths of 4.8 (left) and 9.6 kV/cm (right) in Fig. 4. These are representative for the medium and high-field excitation situations of the data summarized in Fig. 3. The black solid line indicates the results of the full microscopic calculation and the orange solid line is obtained for a two-level calculation, where only the excitonic $1s$ and $2p$ states are included. As a reference, the shaded area shows the absorption without the THz pump. For the lower THz field strength of 4.8 kV/cm, the two-level calculation [solid orange line in the left panel of Fig. 4(a)] seems to capture the main aspects of the Rabi splitting. However, the relatively good agreement with the full calculation is somewhat incidental as evidenced by the reference calculation for a slightly increased THz field of 5.1 kV/cm. Whereas the full calculation (not shown) is virtually indistinguishable from the 4.8 kV/cm result, the two-level result produces a dramatic change due to its phase sensitivity [cf. Fig. 4(a), as outlined below].

Whereas the failure of the two-level approximation for strong THz fields is not really surprising,[13] its comparison with the full calculation allows us to identify the characteristic high-field signatures. For this purpose, we show in Fig. 4(b) the temporal development of the excitonic occupations n_λ in the different states, using the full model (top frames) and the two-level approximation (bottom frames). Without the THz field (shaded area), the optically induced n_{1s} decays single

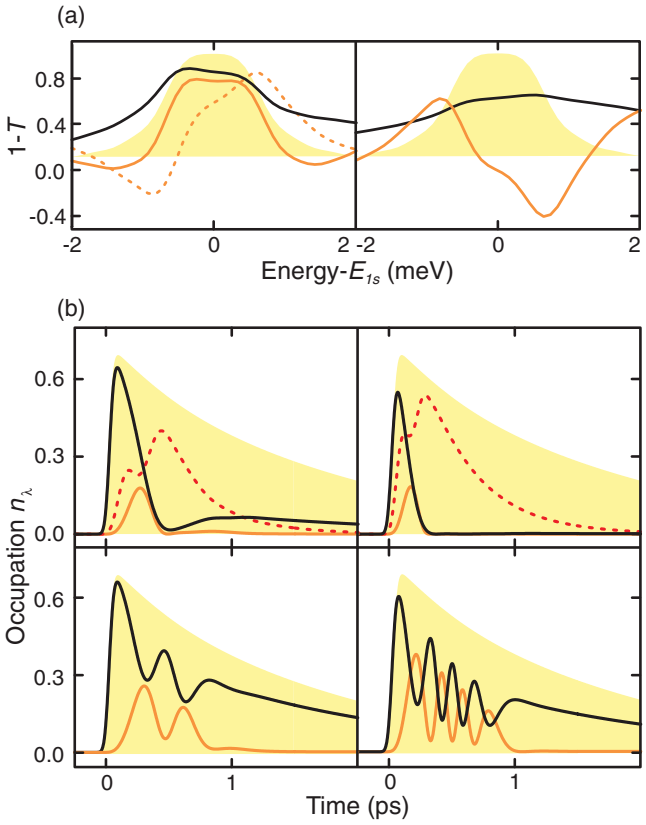

FIG. 4. (Color online) Computed THz-induced effects for 4.8 (left) and 9.6 kV/cm (right) fields. (a) The microscopically computed transmission, plotted as $1 - T$, is shown as a solid black line, and the corresponding result of a two-level analysis is shown as an orange line. The dashed line in the top left panel corresponds to a two-level calculation for a slightly larger THz field of 5.1 kV/cm. The spectra without THz are shown as shaded areas. (b) Time evolution of the $1s$ state (black line), the $2p$ state (orange line), and all other dark states (dashed line) of the polarization are shown as obtained from the full computation (top frames) and the two-level calculation (bottom frames). The shaded area indicates the decaying $1s$ polarization without the THz perturbation.

exponentially. Including the THz field, the $1s$ occupation shows signs of Rabi flopping. For relatively low THz intensities (left), most of the $1s$ excitation is transferred to the $2p$ (orange line) and higher states (dashed line) before some part of it returns back to the $1s$ state (solid line), indicating reversible population transfer. Such a revival of the $1s$ polarization does not occur for strong THz fields (right), because the $1s$ polarization is completely converted into higher states after about 400 fs such that the $1s$ component does not recover. In contrast, the two-level results in the bottom frames of Fig. 4(b) always show pronounced Rabi flopping and reversible population transfer. The rapid oscillations indicate the strong phase sensitivity between the THz-induced $1s$ and $2p$ polarization components which are responsible for the dramatically different results for slightly different THz-field strengths [left frame in Fig. 4(a)].

In order to analyze the results of the strong THz excitation and to identify the roles of the individual exciton states, we investigate the relative occupation probabilities n_λ of the ionized exciton states as a function of the energy and orbital quantum number at the time of 1.5 ps after the THz excitation shown in Fig. 5.

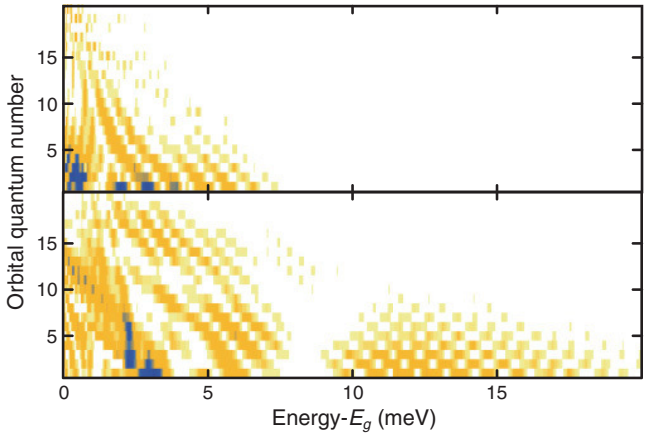

FIG. 5. (Color online) Relative occupation probabilities of the ionized excitonic states as function of energy and orbital quantum number. The computed n_λ are defined as 1.5 ps after 4.8- (top) and 9.6-kV/cm (bottom) excitations analyzed in Fig. 4.

We see that the THz pulse transfers the optically induced $1s$ occupation into states with energies corresponding to more than 4 THz photons and high orbital quantum numbers. This effect can be considered as the THz analogy to the above-threshold ionization of atomic systems[14] mentioned above. The excitation transfer into ionized excitonic states eliminates the phase sensitivity responsible for the failure of the two-level calculations shown in Fig. 4. In the spectrum shown in Fig. 3(a), the ionization effects lead to the appearance of pronounced wings. While significant exciton-ionization effects are observed for both exemplary THz excitations considered here, these become extremely dominant for the strong THz fields shown in the bottom panel.

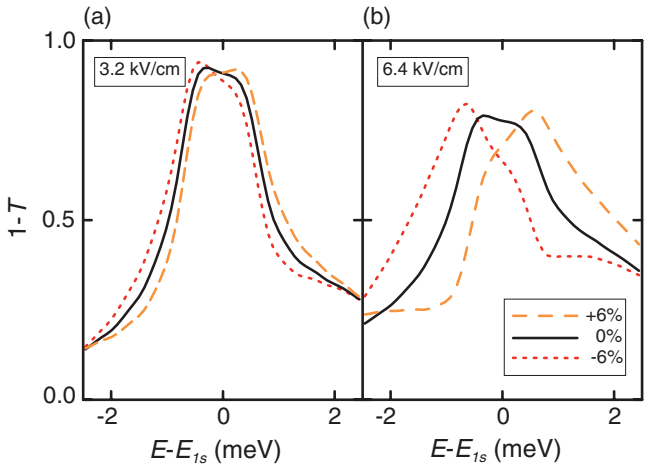

FIG. 6. (Color online) Effect of the THz-induced ponderomotive contribution on the optical transmission. The THz field has the strength of (a) 3.2 and (b) 6.4 kV/cm and the ponderomotive contribution is changed by −6% (dotted line), 0% (solid line), and 6% (dashed line) with respect to the actual value.

To investigate the influence of the ponderomotive current on the peak positions, we systematically vary the original ponderomotive current in Eq. (1) by a factor s. This allows us to either enhance ($s > 1$) or suppress ($s < 1$) the ponderomotive effects in the computations. Figure 6 compares the original ($s = 1$, solid line) transmission spectrum with enhanced ($s = 1.06$, dashed line) and suppressed ($s = 0.94$, dotted line) ponderomotive effects. The left column is computed with a THz field of 3.2 kV/cm that corresponds to the onset of Rabi splitting in Fig. 3. The right column is calculated with 6.4 kV/cm corresponding to the saturation regime, according to Fig. 3.

In both cases, increasing ponderomotive contributions produces a blueshift of the resonances. Whereas this shift is relatively small for THz fields close to the Rabi-splitting threshold, it becomes considerably larger for elevated E_{THz}. This behavior follows from the quadratic A_{THz} dependency of J_{pond}. Due to this blueshift, the ponderomotive contributions produce the asymmetric shift of the low- and high-energy branch of the Rabi peak, observed in Fig. 3(b).

VI. CONCLUSIONS

In summary, we investigated the interaction of strong single-cycle, broadband THz pulses with optically generated coherent excitons in $Ga_{0.97}In_{0.03}As/GaAs$ QWs. By monitoring the optical response for increasing THz-field strengths, we see the gradual transition from bleaching of the $1s$-exciton resonance into Rabi splitting and the development of pronounced wings. The slight absorption redshift for weak THz field strengths turns into a blueshift when stronger fields are applied. Our quantum-mechanical many-body analysis attributes the experimental observations to excitonic Rabi flopping supplemented by multi-THz-photon ionization and the population of optically dark exciton states with high quantum numbers.

ACKNOWLEDGMENTS

S.C. and N.K. acknowledge stimulating discussions with W. W. Rühle.

[1] I. I. Rabi, Phys. Rev. **51**, 652 (1937).
[2] B. R. Mollow, Phys. Rev. **188**, 1969 (1969).
[3] M. Kira and S. Koch, Prog. Quantum Electron. **30**, 155 (2006).
[4] S. Chatterjee, C. Ell, S. Mosor, G. Khitrova, H. M. Gibbs, W. Hoyer, M. Kira, S. W. Koch, J. P. Prineas, and H. Stolz, Phys. Rev. Lett. **92**, 067402 (2004).
[5] M. Kira and S. W. Koch, Phys. Rev. Lett. **93**, 076402 (2004).
[6] W. Hoyer, C. Ell, M. Kira, S. W. Koch, S. Chatterjee, S. Mosor, G. Khitrova, H. M. Gibbs, and H. Stolz, Phys. Rev. B **72**, 075324 (2005).
[7] S. W. Koch, M. Kira, G. Khitrova, and H. M. Gibbs, Nature Mater. (London) **5**, 523 (2006).
[8] R. Huber, F. Tauser, A. Brodschelm, M. Bichler, G. Abstreiter, and A. Leitenstorfer, Nature (London) **414**, 286 (2001).
[9] R. A. Kaindl, M. A. Carnahan, D. Hägele, R. Lövenich, and D. S. Chemla, Nature (London) **423**, 734 (2003).
[10] J. R. Danielson, Y.-S. Lee, J. P. Prineas, J. T. Steiner, M. Kira, and S. W. Koch, Phys. Rev. Lett. **99**, 237401 (2007).
[11] J. Černe, J. Kono, M. S. Sherwin, M. Sundaram, A. C. Gossard, and G. E. W. Bauer, Phys. Rev. Lett. **77**, 1131 (1996).
[12] S. G. Carter, V. Birkedal, C. S. Wang, L. A. Coldren, A. V. Maslov, D. S. Citrin, and M. S. Sherwin, Science **310**, 651 (2005).
[13] M. Wagner, H. Schneider, D. Stehr, S. Winnerl, A. M. Andrews, S. Schartner, G. Strasser, and M. Helm, Phys. Rev. Lett. **105**, 167401 (2010).
[14] P. B. Corkum, N. H. Burnett, and F. Brunel, Phys. Rev. Lett. **62**, 1259 (1989).
[15] H. Hirori, M. Nagai, and K. Tanaka, Phys. Rev. B **81**, 081305(R) (2010).
[16] Q. Wu and X.-C. Zhang, Appl. Phys. Lett. **67**, 3523 (1995).
[17] P. U. Jepsen, C. Winnewisser, M. Schall, V. Schyja, S. R. Keiding, and H. Helm, Phys. Rev. E **53**, R3052 (1996).
[18] J. T. Steiner, M. Kira, and S. W. Koch, Phys. Rev. B **77**, 165308 (2008).
[19] A. D. Jameson, J. L. Tomaino, Y.-S. Lee, J. P. Prineas, J. T. Steiner, M. Kira, and S. W. Koch, Appl. Phys. Lett. **95**, 201107 (2009).
[20] S. Leinß, T. Kampfrath, K. v. Volkmann, M. Wolf, J. T. Steiner, M. Kira, S. W. Koch, A. Leitenstorfer, and R. Huber, Phys. Rev. Lett. **101**, 246401 (2008).
[21] H. Haug and S. W. Koch, *Quantum Theory of the Optical and Electronic Properties of Semiconductors* (World Scientific, Singapore, 2009).

Paper II

Phys. Rev. Lett. 108, 267402

Terahertz Excitation of a Coherent Λ-Type Three-Level System of Exciton-Polariton Modes in a Quantum-Well Microcavity

Terahertz Excitation of a Coherent Λ-Type Three-Level System of Exciton-Polariton Modes in a Quantum-Well Microcavity

J. L. Tomaino,[1] A. D. Jameson,[1] Yun-Shik Lee,[1,*] G. Khitrova,[2] H. M. Gibbs,[2] A. C. Klettke,[3] M. Kira,[3] and S. W. Koch[3]

[1]*Department of Physics, Oregon State University, Corvallis, Oregon 97331, USA*
[2]*Optical Sciences Center, University of Arizona, Tucson, Arizona 85721, USA*
[3]*Department of Physics and Material Sciences Center, Philipps-University, 35032 Marburg, Germany*

(Received 9 December 2011; published 26 June 2012)

Interactions of few-cycle terahertz pulses with the induced optical polarization in a quantum-well microcavity reveal that the lower and higher exciton-polariton modes together with the optically forbidden $2p$-exciton state form a unique Λ-type three-level system. Pronounced nonlinearities are observed via time-resolved strong-terahertz and weak-optical excitation spectroscopy and explained with a fully microscopic theory. The results show that the terahertz pulses strongly couple the exciton-polariton states to the $2p$-exciton state while no resonant transition between the two polariton levels is observed.

DOI: 10.1103/PhysRevLett.108.267402 PACS numbers: 78.67.De, 42.55.Sa, 71.35.Cc, 78.47.jb

An optical microcavity enclosing semiconductor quantum wells (QWs) is an elegant material system to harness light-matter interactions. When the exciton and cavity resonances are nearly resonant, they become strongly coupled giving rise to the so-called exciton-polariton modes [1]. Many fundamental questions concerning quantum optical phenomena in semiconductors-from cavity QED [2–7] to Bose-Einstein condensation of exciton-polaritons [8–11]—have been explored by studying the optical properties of semiconductor microcavities. Yet the excitation dynamics of the optically induced exciton-polariton states is still largely unexplored. For a GaAs-based microcavity, the Rabi splitting and the exciton binding energy both fall in the range of 1–10 meV corresponding to photon energies in the terahertz (THz) part of the electromagnetic spectrum (i.e., 4.14 meV at 1 THz). Hence, one needs high precision THz spectroscopy to directly access these low-energy processes. Strong and short THz pulses allow for the coherent manipulation of the exciton-polariton states, providing a unique perspective of the coupled light-matter system which is inaccessible in purely optical spectroscopy.

In this Letter, we investigate the quantum dynamics of exciton-polariton coherences in a QW microcavity driven by strong few-cycle THz pulses. We generalize the study of intraexcitonic transitions in bare QWs [12–16] to THz spectroscopy in microcavities, including polaritonic effects. Our experimental observations and theoretical analysis show that a resonant THz field couples the optically induced exciton-polariton coherences to the dark $2p$-exciton state while direct dipole transitions between the two polariton modes are forbidden. These results indicate that the lower and higher exciton-polariton (LEP and HEP) states, together with the $2p$-exciton-polarization state, constitute a three-level Λ system, depicted in Fig. 1(a). This polaritonic Λ system is unique and significantly different from the usual atomic Λ system where all levels are matter states while all transitions are provided by light. In our case, only the highest $2p$ state is a pure matter state whereas the LEP and HEP states are mixed light-matter coherences. This scenario offers new coherent control possibilities because one can switch the polaritonic LEP and HEP states with optical fields while applying THz fields to perform simultaneous Λ transitions. Our results indicate that the novel Λ system is robust enough to perform stimulated Raman adiabatic passage (STIRAP) [17] in a semiconductor microcavity by using two-color nonlinear THz spectroscopy.

As schematically shown in Fig. 1(b), we experimentally observe the time-resolved optical reflectivity of the LEP and HEP modes in a QW microcavity in the presence of strong few-cycle THz pulses. We combine strong THz and weak optical excitation using 800-nm, 90-fs pulses from a 1-kHz Ti:sapphire regenerative amplifier. The strong few-cycle THz pulses were produced by type-II difference-frequency generation in a 1-mm ZnTe crystal using two linearly-chirped and orthogonally-polarized optical pulses [16,18]. The THz pulse duration was 4 ps, and the maximum electric-field amplitude reached 5 kV/cm. The frequency of the high-field THz pulses was continuously tunable from 1.0 to 2.5 THz with a bandwidth of

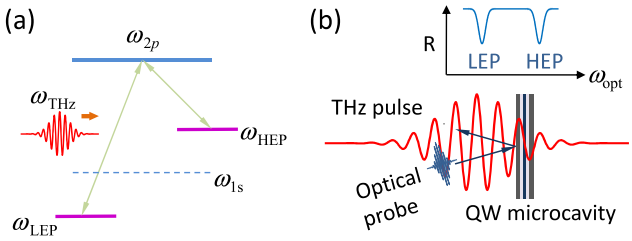

FIG. 1 (color online). (a) LEP, HEP, and exciton $2p$ polarization states form a three-level Λ system. (b) Schematic diagram of the optical reflectivity measurement of a QW microcavity in the presence of an intense THz field.

0.2–0.3 THz. We focused the THz pulses on a QW microcavity sample and measured its optical reflectivity spectra $R(\nu)$ with weak 830-nm, 100-fs optical pulses while varying the relative time delay (Δt) between the THz and optical pulses. The time delay is defined as $\Delta t = t_{\mathrm{THz}} - t_{\mathrm{opt}}$, where a positive time delay means that the THz pulse arrives at the QW later than the optical pulse. The optical pulses were generated with a white-light continuum source and a bandpass filter with an 830-nm central wavelength and a 10-nm bandwidth. The reflectivity spectra of the optical pulses were measured by an imaging spectrometer with a CCD camera (spectral resolution, 0.01 nm). The QW microcavity sample (NMC66) consists of 10 InGaAs QWs in a $11\lambda/2$-microcavity with distributed Bragg reflectors designed for 99.94% reflectivity. The cavity is wedged, which allows us to tune the cavity resonance by scanning the optical beam across the sample. The temperature of the sample was 5 K at which the thermal energy is much smaller than the optical phonon energy and thus carrier-LO-phonon scattering is negligible.

The experimental results are compared with the theoretical analysis performed with a microscopic many-body theory [19,20], including the self-consistent treatment of optical and THz fields. Whereas the full theoretical framework is laid out in the Supplemental Material [21], we can explain most of the experimental features by including the self-consistent coupling between Maxwell's wave equation and the microscopic interband polarization dynamics

$$i\hbar\frac{\partial}{\partial t}P_{\mathbf{k}} = \left(\tilde{\epsilon}_{\mathbf{k}} - j_{\mathbf{k}}A_{\mathrm{THz}} + \frac{|e|^2}{2\mu}A_{\mathrm{THz}}^2\right)P_{\mathbf{k}} + \sum_{\mathbf{k}'}\Gamma_{\mathbf{k},\mathbf{k}'}P_{\mathbf{k}'} - (1 - f_{\mathbf{k}}^e - f_{\mathbf{k}}^h)\Omega_{\mathbf{k}}. \quad (1)$$

Here, $\tilde{\epsilon}_{\mathbf{k}}$ is the kinetic energy of electron-hole pairs and $f_{\mathbf{k}}^{e(h)}$ defines the occupation of electrons (holes) at the carrier momentum $\mathbf{k}$. μ is the reduced effective mass of an electron-hole pair. The optical field generates $P_{\mathbf{k}}$ through the renormalized Rabi frequency $\Omega_{\mathbf{k}}$ while the microscopic Coulomb- and phonon-interaction-induced scattering $\Gamma_{\mathbf{k},\mathbf{k}}$ destroys these coherences. The LEP and the HEP resonances are mixed light-matter states created by the self-consistent coupling between the optically generated $P_{\mathbf{k}}$ and the cavity mode which is fully described by the wave equation. The coherent polarization is further coupled to the vector potential A_{THz} of the THz field. The appearing current-matrix element $j(\mathbf{k})$ has a p-like symmetry coupling the spherically symmetric optical $P_{\mathbf{k}}$ to optically dark exciton states. Interestingly, since the cavity mode is not directly involved in this process, the THz radiation only couples the matter component of the LEP and HEP to the $2p$-exciton state.

Figure 2 shows examples of the THz-induced nonlinear optical effects of the exciton-polariton modes at near-zero cavity-detuning ($\delta_c = \nu_c - \nu_{1s} = 0.07$ THz) and at zero time-delay ($\Delta t = 0.0$ ps) between the optical and THz

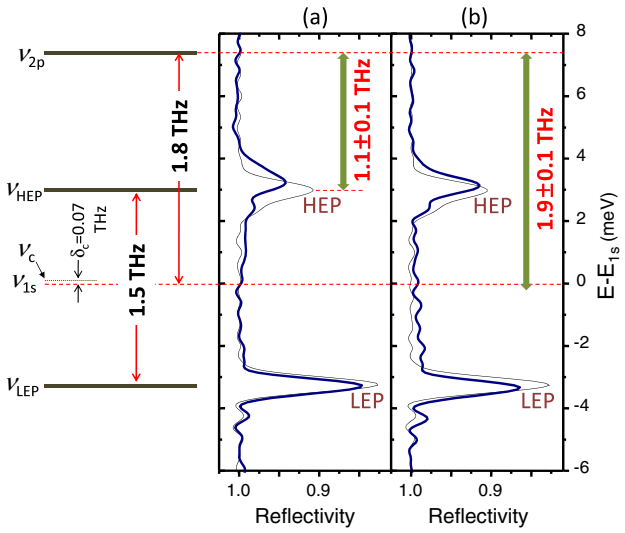

FIG. 2 (color online). Exciton-polariton reflectivity spectra at near-zero cavity detuning ($\delta_c = \nu_c - \nu_{1s} = 0.07$ THz) in the presence of a strong THz pulse, $E_{\mathrm{THz}} = 4$ kV/cm, at $\Delta t = 0.0$ ps (thick solid lines): (a) THz frequency ($\nu_{\mathrm{THz}} = 1.1$ THz) is tuned near to the HEP-to-$2p$ transition ($\nu_{\mathrm{HEP}-2p} = 1.1$ THz) and (b) THz frequency ($\nu_{\mathrm{THz}} = 1.9$ THz) is tuned near to the $1s$-to-$2p$ transition ($\nu_{1s\text{-}2p} = 1.8$ THz). The thin-solid lines indicate the unperturbed exciton-polariton spectra.

pulses. The THz frequency is tuned near to (a) the HEP-to-$2p$ transition ($\nu_{\mathrm{HEP}-2p} = 1.1$ THz) and (b) the $1s$-to-$2p$ transition ($\nu_{1s\text{-}2p} = 1.8$ THz). The peak THz-field amplitudes are 4 kV/cm. We note that the THz-induced nonlinear effects are exceptionally large compared with optically induced nonlinear effects which require at least 10^8–10^9 kV/cm of optical field amplitude to generate the same magnitude of spectral modulation. The unperturbed reflectivity spectra are depicted by the thin gray lines.

The data exhibit several pronounced nonlinear effects showing that the THz-microcavity interaction is resonant with the HEP-to-$2p$ transition because the $\nu_{\mathrm{HEP}\text{-}2p}$ excitation quenches dominantly the HEP resonance [Fig. 2(a)] while $\nu_{1s\text{-}2p}$ creates only moderate changes [Fig. 2(b)] to the measured reflectivity. Furthermore, no resonant transition between the LEP and HEP modes ($E_{\mathrm{HEP}} - E_{\mathrm{LEP}} = 6.2$ meV $= 1.5$ THz) was observed as the THz frequency was tuned in the range of 1.4–1.6 THz, where the spectral modulations are similar to those in Fig. 2(b). When the THz frequency was increased to $\nu_{\mathrm{LEP}-2p} = 2.4$ THz, the reflectivity was changed significantly only at the LEP. These observations clearly show that the LEP, HEP, and $2p$-levels form a three-level Λ system.

In Fig. 2(b), the THz pulse is tuned to be resonant with the $1s$-to-$2p$ transition energy. Here, no major quenching effects are observed, only the energetic difference between the LEP and HEP resonances somewhat increases. Hence, we conclude that the THz field interacts with the QW dominantly via the Λ-like transitions, not via the

$1s$-to-$2p$ transition. Especially, when the THz field is nonresonant with the Λ-like states, the resulting minor modifications stem from the ponderomotive and multiphoton absorption effects induced by the relatively strong THz pulse [16].

To gain more insight, we performed detailed experiment-theory comparisons for the resonant interactions of THz pulses with the exciton-polariton coherences at different cavity detunings. Figures 3 and 4 show the temporal evolution of the exciton-polariton reflectivity when the THz excitation is tuned near to the LEP-to-$2p$ transition at $\delta_c = -0.56$ THz and to the HEP-to-$2p$ transition at $\delta_c = 0.41$ THz, respectively. The principal Λ-like operation is well explained by the theory. Quantitatively, the experimental LEP and HEP peak amplitudes are smaller than the theoretical ones due to the well-known disorder effects in the sample [22,23].

Figures 3(a) and 3(c) show the contour plots of the experimental and theoretical reflectivity, $R(E, \Delta t)$, as a function of photon energy E and time delay Δt between optical and THz pulses, at a negative detuning $\delta_c = -0.56$ THz. The corresponding reflectivity spectra at $\Delta t = -2, -1, 0, 1$, and 2 ps are shown in Figs. 3(b) and 3(d). The results indicate that the THz pulses resonantly drive the HEP-to-$2p$ transition; i.e., in agreement with the expectations for the three-level Λ system, the HEP mode undergoes large amplitude modulations near $\Delta t = 0$ while few changes occur in the LEP mode. Especially, the HEP resonance almost vanishes near $\Delta t = 0$ while the LEP remains almost unchanged. Furthermore, the HEP mode spectrum becomes asymmetric near $\Delta t = 0$; i.e., a broad shoulder appears on the lower-energy side in the experiment and on the higher-energy side in theory—the quantitative differences of spectroscopic signatures between the experiment and theory may arise from the well-known asymmetries in the excitonic resonances induced by disorder and excitation-induced dephasing [23–25]. These peculiar spectral features imply that the HEP polarization is coupled with the exciton $2p$ polarization. The quantum coherence, however, is heavily obscured by fast dephasing. This level of quantum control can be observed up to about $\Delta t = 2$ ps, i.e., in the coherent regime before the dephasing of the polariton coherences.

The coherent control of the LEP branch of the Λ system is studied in Fig. 4 both experimentally [frames (a) and (b)] and theoretically [frames (c) and (d)] by using $\nu_{\mathrm{THz}} = 2.2$ THz and a cavity detuning $\delta_c = +0.41$ THz. As expected for a Λ system response, in this case the THz field predominantly bleaches the LEP. It is also notable that the temporal evolution is not symmetric for the HEP (Fig. 3) and the LEP branches (Fig. 4). For example, the strongest THz-induced modulation occurs between the time delays of 0.0 and 0.5 ps, and the spectral modulation at $\Delta t = 2$ ps is stronger than that at $\Delta t = -2$ ps. The temporal asymmetry results mainly from the coherent transients: at

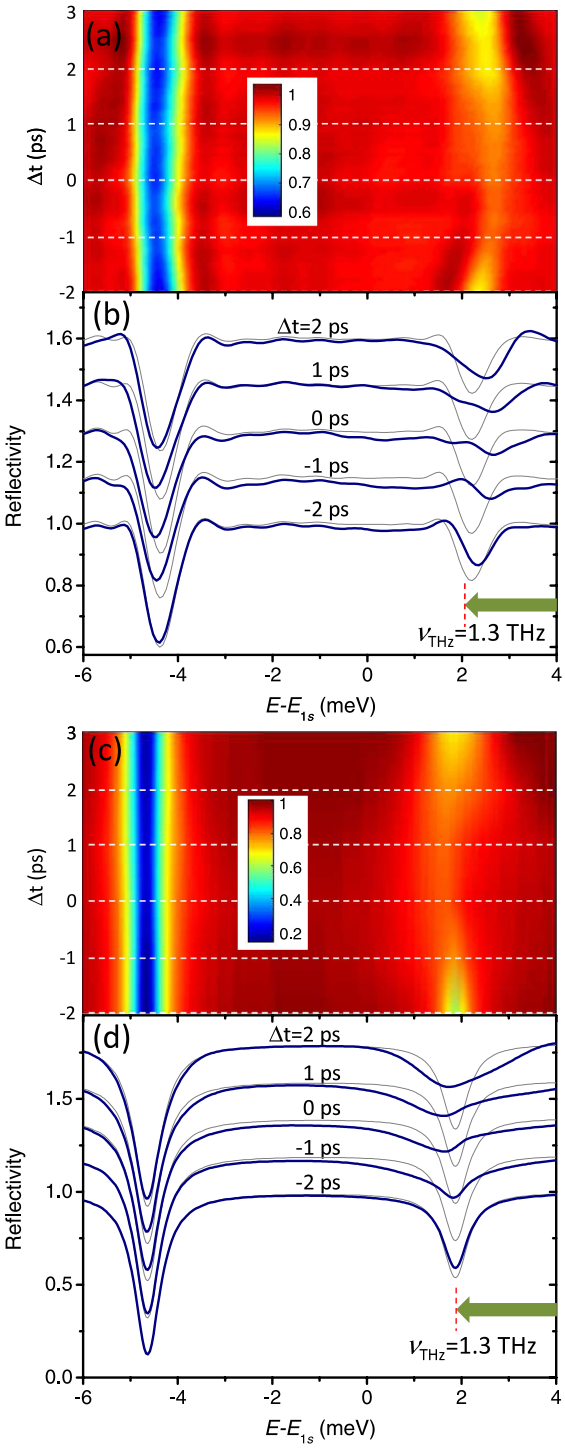

FIG. 3 (color online). Time-resolved exciton-polariton reflectivity spectra at $\delta_c = -0.56$ THz when the THz radiation ($\nu_{\mathrm{THz}} = 1.3$ THz) is tuned near to the HEP-to-$2p$ transition ($\nu_{\mathrm{HEP}-2p} = 1.3$ THz). (a) Experimental and (c) theoretical contour plots of the reflectivity presented with respect to $1s$-exciton energy E_{1s}. The white dashed lines correspond to cross sections at $\Delta t = -2, -1, 0, 1$, and 2.0 ps shown as vertically offset spectra in (b) experiment and (d) theory. The thin lines indicate the unperturbed spectra.

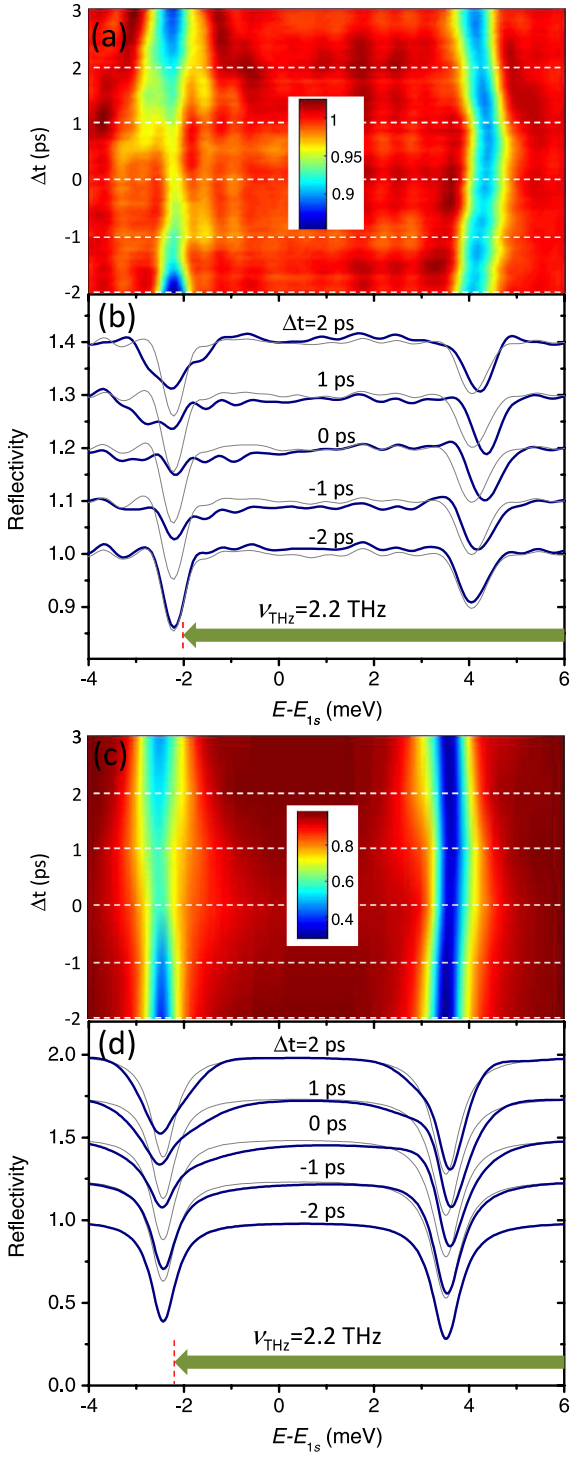

FIG. 4 (color online). Time-resolved exciton-polariton reflectivity spectra at $\delta_c = +0.41$ THz when the THz radiation ($\nu_{\mathrm{THz}} = 2.2$ THz) is tuned near to the LEP-to-$2p$ transition ($\nu_{\mathrm{LEP}-2p} = 2.4$ THz). (a) Experimental and (c) theoretical contour plots of the reflectivity $R(E - E_{1s}, \Delta t)$. The white dashed lines correspond to cross sections at $\Delta t = -2$, -1, 0, 1, and 2.0 ps shown as vertically offset spectra in (b) experiment and (d) theory. The thin lines indicate the unperturbed spectra.

positive time delays up to several picoseconds, the THz pulse perturbs the coherent polariton modes inducing the spectral modulations to the optical reflectivity, while they make no impact on the polariton modes at negative time delays.

In conclusion, our study shows that the THz radiation resonantly drives the exciton-polariton polarizations giving rise to LEP-to-$2p$ or HEP-to-$2p$ transitions. The exceptionally large nonlinear optical effects induced by the THz pulses exhibit peculiar spectral features unique for the light-matter coupled system. Our experiment-theory comparison also confirms that there are no resonant transitions between LEP and HEP levels. Hence, we demonstrate that the LEP, HEP, and $2p$-exciton states form a unique three-level Λ system in an optically excited QW microcavity. The results also indicate the coherent coupling between the exciton-polariton and the exciton $2p$ polarizations that dephase within a few picoseconds. This operational window should be long enough to realize Λ-system applications, such as THz-STIRAP, in a semiconductor microcavity.

The OSU work is supported by the National Science Foundation (DMR-1063632) and the Oregon Nanoscience and Microtechnologies Institute. The Marburg work is supported by the Deutsche Forschungsgemeinschaft. The UofA group acknowledges support from the National Science Foundation under AMOP (PHY-0757707), EPDT (ECCS-0757975) and ERC CIAN (EEC-0812072); AFOSR (FA9550-10-1-0003); and JSOP (W911NF-10-1-0344).

*leeys@physics.oregonstate.edu

[1] G. Khitrova, H. M. Gibbs, F. Jahnke, M. Kira, and S. W. Koch, Rev. Mod. Phys. **71**, 1591 (1999).
[2] Y.-S. Lee, T. B. Norris, M. Kira, F. Jahnke, S. W. Koch, G. Khitrova, and H. M. Gibbs, Phys. Rev. Lett. **83**, 5338 (1999).
[3] J. P. Reithmaier, G. Sęk, A. Löffler, C. Hofmann, S. Kuhn, S. Reitzenstein, L. V. Keldysh, V. D. Kulakovskii, T. L. Reinecke, and A. Forchel, Nature (London) **432**, 197 (2004).
[4] T. Yoshie, A. Scherer, J. Hendrickson, G. Khitrova, H. M. Gibbs, G. Rupper, C. Ell, O. B. Shchekin, and D. G. Deppe, Nature (London) **432**, 200 (2004).
[5] K. Hennessy, A. Badolato, M. Winger, D. Gerace, M. Atatüre, S. Gulde, S. Fält, E. L. Hu, and A. Imamoğlu, Nature (London) **445**, 896 (2007).
[6] G. Günter, A. A. Anappara, J. Hees, A. Sell, G. Biasiol, L. Sorba, S. de Liberato, C. Ciuti, A. Tredicucci, A. Leitenstorfer, and R. Huber, Nature (London) **458**, 178 (2009).
[7] Y. Yamamoto, F. Tassone, and H. Cao, *Semiconductor Cavity Quantum Electrodynamics* (Springer, Berlin, Heidelberg, 2000).
[8] H. Deng, G. Weihs, C. Santori, J. Bloch, and Y. Yamamoto, Science **298**, 199 (2002).
[9] J. Kasprzak, M. Richard, S. Kundermann, A. Baas, P. Jeambrun, J. M. J. Keeling, F. M. Marchetti, M. H. Szymańska, R. André, J. L. Staehli, V. Savona, P. B. Littlewood, B. Deveaud, and L. S. Dang, Nature (London) **443**, 409 (2006).

[10] R. Balili, V. Hartwell, D. Snoke, L. Pfeiffer, and K. West, Science **316**, 1007 (2007).
[11] H. Deng, H. Haug, and Y. Yamamoto, Rev. Mod. Phys. **82**, 1489 (2010).
[12] B. E. Cole, J. B. Williams, B. T. King, M. S. Sherwin, and C. R. Stanley, Nature (London) **410**, 60 (2001).
[13] S. G. Carter, V. Birkedal, C. S. Wang, L. A. Coldren, A. V. Maslov, D. S. Citrin, and M. S. Sherwin, Science **310**, 651 (2005).
[14] S. Leinß, T. Kampfrath, K. v. Volkmann, M. Wolf, J. T. Steiner, M. Kira, S. W. Koch, A. Leitenstorfer, and R. Huber, Phys. Rev. Lett. **101**, 246401 (2008).
[15] J. R. Danielson, Y.-S. Lee, J. P. Prineas, J. T. Steiner, M. Kira, and S. W. Koch, Phys. Rev. Lett. **99**, 237401 (2007).
[16] A. D. Jameson, J. L. Tomaino, Y. Lee, J. P. Prineas, J. T. Steiner, M. Kira, and S. W. Koch, Appl. Phys. Lett. **95**, 201107 (2009).
[17] K. Bergmann, H. Theuer, and B. W. Shore, Rev. Mod. Phys. **70**, 1003 (1998).
[18] J. R. Danielson, A. D. Jameson, J. L. Tomaino, H. Hui, J. D. Wetzel, Y. Lee, and K. L. Vodopyanov, J. Appl. Phys. **104**, 033111 (2008).
[19] M. Kira and S. Koch, Prog. Quantum Electron. **30**, 155 (2006).
[20] J. T. Steiner, M. Kira, and S. W. Koch, Phys. Rev. B **77**, 165308 (2008).
[21] See Supplemental Material at http://link.aps.org/supplemental/10.1103/PhysRevLett.108.267402 for technical details of the methods.
[22] M. Gurioli, F. Bogani, D. S. Wiersma, P. Roussignol, G. Cassabois, G. Khitrova, and H. Gibbs, Phys. Rev. B **64**, 165309 (2001).
[23] M. Werchner, M. Schafer, M. Kira, S. W. Koch, J. Sweet, J. D. Olitzky, J. Hendrickson, B. C. Richards, G. Khitrova, H. M. Gibbs, A. N. Poddubny, E. L. Ivchenko, M. Voronov, and M. Wegener, Opt. Express **17**, 6813 (2009).
[24] F. Jahnke, M. Kira, S. W. Koch, G. Khitrova, E. K. Lindmark, T. R. Nelson, Jr., D. V. Wick, J. D. Berger, O. Lyngnes, H. M. Gibbs, and K. Tai, Phys. Rev. Lett. **77**, 5257 (1996).
[25] R. P. Smith, J. K. Wahlstrand, A. C. Funk, R. P. Mirin, S. T. Cundiff, J. T. Steiner, M. Schafer, M. Kira, and S. W. Koch, Phys. Rev. Lett. **104**, 247401 (2010).

Supplementary Material for Paper II

EPAPS for "Terahertz excitation of a coherent three-level Λ-type exciton-polariton microcavity mode"

J.L. Tomaino, A.D. Jameson, and Yun-Shik Lee*
Department of Physics, Oregon State University, Corvallis, Oregon 97331

G. Khitrova and H.M. Gibbs
Optical Sciences Center, University of Arizona, Tucson, Arizona 85721

A.C. Klettke, M. Kira, and S.W. Koch
Department of Physics and Material Sciences Center, Philipps-University, 35032 Marburg, Germany
(Dated: December 8, 2011)

This documents serves as a supplement to the article "Terahertz excitation of a coherent three-level Λ-type exciton-polariton microcavity mode ". It gives more details concerning the derivation of the microscopic theory applied and the approaches used.

I. INTRODUCTION

Normal mode coupling in semiconductor microcavities occurs when the excitonic resonance of high-quality quantum wells (QWs) is (nearly) degenerate with the cavity eigenmode. Under suitable conditions, the combination of optical and terahertz (THz) excitation of such a system allows for the realization of a coherent three-level Λ-type configuration which exhibits highly nonlinear behaviour. A full microscopic theory is needed to quantitatively analyze the main features of the combined optical and THz excitation kinetics. We formulate here our systematic theory applied to analyze the experiments presented in the main part.

II. HAMILTONIAN

As discussed in Ref.[1], a systematic analysis of optical and THz excitations of semiconductor starts from the system Hamiltonian

$$\hat{H} = \hat{H}_0 + \hat{H}_{\rm lm} + \hat{H}_{\rm C} + \hat{H}_{\rm ph}. \tag{1}$$

We analyze a situation where the Λ system is excited with classical optical and THz pulses such that the quantum-optical effects[2] can be ignored. Consequently, we treat the electromagnetic field classically while the interacting electrons of the QWs are described with a full quantum theory. More specifically, a QW electron with momentum $\hbar\mathbf{k}$ within band λ is described by Fermion creation and annihilation operators $a^\dagger_{\lambda,\mathbf{k}}$ and $a_{\lambda,\mathbf{k}}$, respectively. The resulting non-interacting part becomes

$$\hat{H}_0 = \sum_{\mathbf{k}} \epsilon^\lambda_{\mathbf{k}} a^\dagger_{\lambda,\mathbf{k}} a_{\lambda,\mathbf{k}} \tag{2}$$

where $\epsilon^\lambda_{\mathbf{k}}$ denotes single-particle energies of the electrons in the conduction ($\lambda = c$) and in the valence ($\lambda = v$) band. At the same time, vacancies in the valence band define holes which pair with the electrons in the conduction band to form excitonic resonances, see discussion of Eq. (6) for more details.

The semiclassical light–matter interaction becomes then[1]

$$H_{\rm lm} = -\sum_{\lambda,\mathbf{k}} \left(\mathbf{j}_\lambda(\mathbf{k}) \cdot \mathbf{A} - \frac{|e|^2}{2m_0}\mathbf{A}^2 \right) a^\dagger_{\lambda,\mathbf{k}} a_{\lambda,\mathbf{k}} + \sum_{\lambda\neq\lambda'} \sum_{\mathbf{k}} \frac{|e|}{m_0} \mathbf{p}_{\lambda\lambda'}(\mathbf{k}) \cdot \mathbf{A}\; a^\dagger_{\lambda,\mathbf{k}} a_{\lambda,\mathbf{k}}, \tag{3}$$

where $\mathbf{A}$ is the vector potential evaluated at the position of the QW. We assume here that the light propagates perpendicular to the QW, such that it depends only on the z coordinate. The strength of the light–matter coupling is determined by the momentum matrix element $p_{\lambda\lambda'}(\mathbf{k})$ and the current matrix element

$$\mathbf{j}_\lambda(\mathbf{k}) = -\tfrac{|e|}{\hbar} \nabla_{\mathbf{k}} \epsilon^\lambda_{\mathbf{k}}. \tag{4}$$

As usual, m_0 and $-|e|$ denote free-electron mass and the elementary charge.

The many-body interaction follows from the Coulomb interaction

$$H_{\rm C} = \frac{1}{2} \sum_{\lambda,\lambda'} \sum_{\mathbf{k},\mathbf{k}',\mathbf{q}} V^{\lambda,\lambda'}_{\mathbf{q}} a^\dagger_{\lambda,\mathbf{k}+\mathbf{q}} a^\dagger_{\lambda',\mathbf{k}'-\mathbf{q}} a_{\lambda',\mathbf{k}'} a_{\lambda,\mathbf{k}} \tag{5}$$

with the Coulomb matrix element $V^{\lambda,\lambda'}_{\mathbf{q}}$ for the interaction between electronic states λ, λ'. This term includes both Coulomb repulsion that yields scattering contributions and attraction that produces, e.g., the excitonic states. Finally, $H_{\rm ph}$ contains the carrier–phonon interaction; a more detailed discussion is found e.g. in[1]. In our system, the phonon interaction is effectively leading to a decay of the polarization, which is treated using a diffusive model[1].

III. EQUATION OF MOTION

Deriving the Heisenberg equations of motion with the full Hamiltonian leads to the so-called hierarchy problem, i.e., the N-particle many-body correlations couple

to (N+1)-particle correlations. In our approach, this infinite series of equations is treated by means of a cluster-expansion approach[1] which systematically truncates the hierarchical coupling. As shown in Ref.[3], the dynamics of microscopic polarization follows from the equation of motion

$$\begin{aligned} i\hbar\tfrac{\partial}{\partial t}P_{\mathbf{k}} = &\left(\tilde{\epsilon}_{\mathbf{k}} - \mathbf{j}_{\mathbf{k}}\cdot\mathbf{A}_{\mathrm{THz}} + \tfrac{|e|^2}{2\mu}\mathbf{A}_{\mathrm{THz}}^2\right)P_{\mathbf{k}} \\ &- \left(1 - f_{\mathbf{k}}^{\mathrm{e}} - f_{\mathbf{k}}^{\mathrm{h}}\right)\Omega_{\mathbf{k}} \\ &+ \sum_{\mathbf{k}'}\Gamma_{\mathbf{k},\mathbf{k}'}P_{\mathbf{k}'}, \end{aligned} \tag{6}$$

where $\mathbf{j}_{\mathbf{k}} = \mathbf{j}_{\mathrm{e}}(\mathbf{k}) + \mathbf{j}_{\mathrm{h}}(\mathbf{k})$ is the current-matrix element between electrons and holes and μ is the reduced effective electron–hole mass. The corresponding renormalized kinetic energy of the electron–hole pairs is

$$\tilde{\epsilon}_{\mathbf{k}} = \epsilon_{\mathbf{k}} + E_{\mathrm{G}} - \sum_{\mathbf{k}'}V_{\mathbf{k}-\mathbf{k}'}P_{\mathbf{k}'}\left(f_{\mathbf{k}'}^{\mathrm{e}} + f_{\mathbf{k}'}^{\mathrm{h}}\right) \tag{7}$$

where $\epsilon_{\mathbf{k}} = \epsilon_{\mathbf{k}}^{\mathrm{e}} + \epsilon_{\mathbf{k}}^{\mathrm{h}}$ defines the unrenormalized energy, E_{G} denotes the band gap, and $f_{\mathbf{k}}^{\mathrm{e\,(h)}}$ determine the electron (hole) occupations. The renormalized Rabi energy $\Omega_{\mathbf{k}}$ is given by

$$\Omega_{\mathbf{k}} = d_{cv}E_{\mathrm{opt}} + \sum_{\mathbf{k}'}V_{\mathbf{k}-\mathbf{k}'}P_{\mathbf{k}'}, \tag{8}$$

where d_{cv} is the dipole matrix element. The last term in Eq. (6) denotes the scattering contributions $\sum_{\mathbf{k}'}\Gamma_{\mathbf{k},\mathbf{k}'}P_{\mathbf{k}'}$. Since we study weak optical excitations, $\Omega_{\mathbf{k}}$ induces only linear polarization while changes in carrier densities are negligible because they are nonlinear. At the same time, THz fields act via the first line of Eq. (6) modifying the nature of polarization, without creating densities. Therefore, we can set $f_{\mathbf{k}}^{\mathrm{e}}$ and $f_{\mathbf{k}}^{\mathrm{h}}$ to be constant when analyzing the Λ system.

The optically induced microscopic polarization reradiates light via the macroscopic polarization

$$P = \frac{1}{S}\sum_{\mathbf{k}}\left(d_{cv}\left(\mathbf{k}\right)P_{\mathbf{k}} + \mathrm{c.c.}\right). \tag{9}$$

It appears as a source to the wave equation

$$\left(\tfrac{\partial^2}{\partial z^2} - \tfrac{n^2}{c^2}\tfrac{\partial^2}{\partial t^2}\right)E_{\mathrm{opt}}\left(z,t\right) = -\mu_0\delta\left(z - z_{\mathrm{QW}}\right)\tfrac{\partial^2 P}{\partial t^2}, \tag{10}$$

where μ_0 is the vacuum permittivity, $n = n(z)$ denotes the refractive index profile of the microcavity structure. For thin enough QWs, the polarization appears to be a δ-function source radiating at the z_{QW} position of the QW. We see that Eqs. (6) and (10) are coupled.

We study here a situation where $n(z)$ constructs a cavity around the QWs through distributed Bragg reflectors, to be specified in Sec. IV. Without the QW polarization, Eq. (10) yields a cavity resonance that corresponds to a light mode that is strongly focused inside the cavity. At the same time, the QW polarization has excitonic resonances due to the Coulomb term in Eq. (8). The self-consistent coupling between the wave equation (10) and excitonic 1s resonance in Eq. (6) creates two new polariton modes that are mixed states of light and matter.

The THz part of the electromagnetic field satisfies dynamics analogous to wave equation (10). However, the cavity is designed for optical wavelengths such that THz field propagates essentially freely. As a result, the self-consistent light–matter coupling effects are negligible for the THz field. Therefore, their effects on semiconductor polarization appear as direct driving terms in Eq. (6) through the $\mathbf{j}_{\mathbf{k}}\cdot\mathbf{A}_{\mathrm{THz}}$ contribution.

Close to the bottom of the conduction and valence band, $\epsilon_{\mathbf{k}}^{\lambda}$ are parabolic such that Eq. (4) produces a linear dependence $\mathbf{j}_{\mathbf{k}} \propto \mathbf{k}$. As a result, $\mathbf{j}_{\mathbf{k}}\cdot\mathbf{A}_{\mathrm{THz}}$ is proportional to $\mathbf{k}\cdot\mathbf{e}_{\mathrm{THz}}$ where $\mathbf{e}_{\mathrm{THz}}$ is the direction of the THz field. We apply transversal THz fields that propagate perpendicular to the QW such that $\mathbf{e}_{\mathrm{THz}}$ lies within the plane of the QW. Consequently, $\mathbf{k}\cdot\mathbf{e}_{\mathrm{THz}} = |\mathbf{k}|\cos\theta_{\mathbf{k}}$ depends on the angle $\theta_{\mathbf{k}}$ between the carrier momentum and $\mathbf{e}_{\mathrm{THz}}$. The resulting $\mathbf{j}_{\mathbf{k}}\cdot\mathbf{A}_{\mathrm{THz}}$ contribution drives polarization via a term that has a p-like symmetry, i.e. a $\cos\theta_{\mathbf{k}}$ dependence.

Since the optical excitation can create only rotation-symmetric s-like $P_{\mathbf{k}}$, the THz source breaks this symmetry by converting polarization to p-like states. Since such p-like contributions average to zero in the macroscopic polarization (9), THz hides part of the polarization into optically dark states. This process obviously provides the THz-induced modulations to the optical reflection studied in the main part. At the same time, THz field couples only the excitonic component of the polariton. Therefore, it couples the 1s component of both low-energy and high-energy polariton to 2p-exciton polarization, which forms the Λ system studied.

IV. NUMERICAL IMPLEMENTATION

We solve Eqs. (6) and (10) self consistently by using the fourth-order Runge–Kutta method to solve the polarization dynamics; the wave equation is solved simultaneously with an exact propagation[7]. Microscopic scattering is described using a diffusive model that includes the fundamental features of Coulomb and phonon-induced scattering, as shown in Ref.[1]. The QW microcavity sample (NMC66) is built out 10 GaAs QWs in a $11\lambda/2$ spacer inside 14.5/16 DBR layers (front/back), which produces 99.94% mirror reflectivity. The QWs are positioned at the consecutive cavity-mode maxima to enhance the light–matter coupling.

To describe the experiments in detail, we carefully match the material parameters with the experimental ones. More specifically, we have used effective electron and hole masses $m_{\mathrm{e}} = 0.0665m_0$ and $m_{\mathrm{h}} = 0.235m_0$, respectively. The band gap energy of the system is $E_{\mathrm{G}} = 1.497\,\mathrm{eV}$. The distributed Bragg reflectors are

made out of GaAs and GaAlAs, with refractive indices of $n_{\mathrm{GaAs}} = 3.63$ and $n_{\mathrm{GaAlAs}} = 2.97$, respectively. The 10 QWs are then positioned at the positions matching the experiment. Each of the QWs produces an individual source to Eq. (10).

The strong coupling between cavity resonance and exciton resonance produces a resonant splitting of 6 meV. The corresponding polariton resonances have a width smaller than 1 meV. The reflectivity spectrum is computed from the intensity ratio between incoming and reflected optical field. The numerical analysis not only applies parameters that are typical for GaAs-type systems but it also produces results that explain our experimental findings with a great detail, as shown in the main text.

* leeys@physics.oregonstate.edu

[1] M. Kira and S. W. Koch, Progress in Quantum Electronics **30**, 155 (2006).

[2] M. Kira and S. W. Koch, *Semiconductor Quantum Optics* (Cambridge University Press, 2011).

[3] J.T. Steiner, M. Kira and S. W. Koch, Phys. Rev. B **77**, 165308.

[4] M. Kira, F. Jahnke, W. Hoyer and S. W. Koch, Progress in Quantum Electronics **23**, 189 (1999).

[5] M. Kira, *Lecture notes on excitons in semiconductors*, lecture in physics, Philipps-University Marburg (2004).

[6] H. Haug and S. W. Koch, *Quantum Theory of the Optical and Electronic Properties of Semiconductors* (World Scientific, Singapore, 2004).

[7] F. Jahnke, M. Ruopp, M. Kira and S.W. Koch, Festkörperprobleme/Adv. in Solid State Physics 37, 191 (1997).

Paper III

accepted at phys. stat. solid. (c)

Terahertz excitations of lambda systems in a semiconductor microcavity

physica status solidi, 20 February 2013

Terahertz excitations of lambda systems in a semiconductor microcavity

A.C. Klettke[*,1], M. Kira[1], S.W. Koch[1], J.L. Tomaino[2], A.D. Jameson[2], Y.-S. Lee[2], G. Khitrova[3], H.M. Gibbs[3]

[1] Department of Physics and Material Sciences Center, Philipps-University Marburg, Renthof 5, D-35032 Marburg, Germany
[2] Department of Physics, Oregon State University, Corvallis, Oregon 97331, USA
[3] Optical Sciences Center, University of Arizona, Tucson, Arizona 85721, USA

Received XXXX, revised XXXX, accepted XXXX
Published online XXXX

Key words: microcavity polaritons, terahertz spectroscopy, Lambda-systems

[*] Corresponding author: e-mail Andrea.Klettke@Physik.Uni-Marburg.de, Phone: +49-6421-2824103, Fax: +49-6421-2827076

Recent experiment-theory investigations have demonstrated that the $2p$-exciton state and the polariton resonances of a semiconductor quantum-well (QW) microcavity form a lambda (Λ) system where a terahertz (THz) field can selectively couple to either of the transition-allowed arms. However, semiconductors are open systems because seemingly isolated states are coupled to the continuum of states, either directly or via Coulomb or phonon scattering. A systematic theory is presented to treat these effects in a Λ system and in a two-level system (TLS) described by the $1s$-to-$2p$ exciton transition in a semiconductor QW, without the microcavity. Excitonic occupations of polarization are analyzed as function of THz-field frequency and intensity with (Λ system) and without (TLS) cavity. Even though the existence of Λ and TLS resonances is verified, significant deviations are observed at higher THz intensities, as higher ionized exciton states are generated via multi-THz-photon absorption.

1 Introduction In semiconductors, an optical excitation first induces coherent polarization which can eventually be converted into bound (incoherent) excitons through Coulomb and phonon scattering [1,2]. Excitons are bound electron-hole pairs [3,4] in analogy to the hydrogen atom, but with transition energies scaled down by a factor of 10^3. Therefore, one needs to use terahertz (THz) fields to induce transitions directly between the exciton states [3,5–7]. Also the polarization, induced by optical fields, has excitonic resonances. These features can be excited via THz pulses, as demonstrated experimentally in Refs. [8–10].

When semiconductor quantum wells (QW) are positioned inside a microcavity, the $1s$-exciton resonance splits into a low-energy polariton (LEP) and high-energy polariton (HEP) due to the exciton-cavity coupling [11]. A recent experiment-theory comparison [12] shows that the THz field couples the LEP, the $2p$-exciton state, and the HEP in a Lambda (Λ) configuration, shown schematically in Fig. 1**a**. More specifically, we use a situation where a weak optical pulse is propagated through the microcavity; the center of a strong THz pulse is delayed by Δt with respect to the optical pulse center.

As the optical pulse enters the cavity, it starts to interact with the QWs positioned at the mode maximas of the cavity mode, which generates excitonic polarization that couples to the cavity mode. The cavity–polarization coupling produces the LEP and HEP resonances as indicated in Fig. 1**a**. If one then applies a THz field, one can selectively move either the LEP or HEP coherences to the $2p$ state. This is observed as a vanishing LEP or HEP resonance in the optical probe spectrum. The contour plot in Fig. 1**b** shows an experimental verification [12] that LEP-probe-reflection resonance vanishes when the THz field is present and tuned to be resonant with the energy difference of LEP and $2p$ states. By tuning the THz frequency, one can alternatively bleach the HEP resonance, which verifies that $2p$ and polariton resonances form a Λ system.

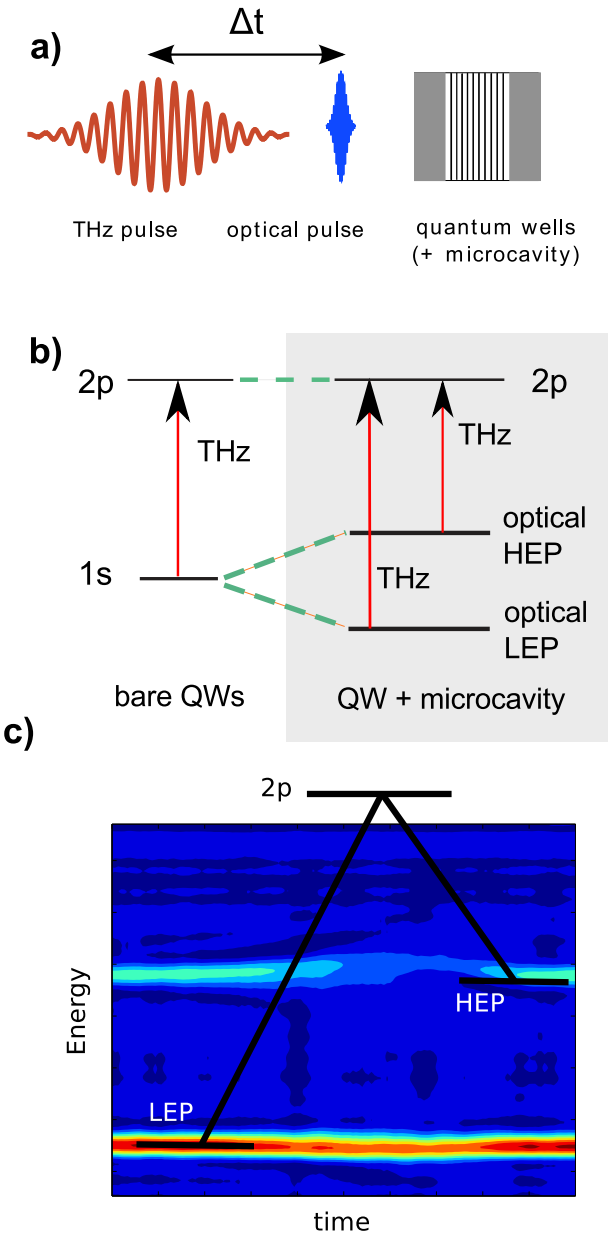

Figure 1 Schematic illustration of Λ system. a) Excitation setup: QWs are positioned inside the cavity, optical pulse excites polarizations, and THz pulse (delayed by Δt induces the intraexcitonic transitions. b) Principal THz transitions. Without cavity, THz pulse converts $1s$ polarization mainly to $2p$ polarization. The cavity splits $1s$ to two polariton modes, HEP and LEP, that both couple to $2p$ polarization via THz transitions. c) Experimental verification of Λ system. Contour plot of measured QW-microcavity reflection. The symbolically illustrated Λ system is realized because only the HEP resonance is depleted.

Former experiment-theory comparisons [8,10,12–15] have repeatedly shown that a systematic many-body theory [1,4] is needed to fully understand the underlying many-body dynamics resulting from the THz exciations. In this paper, we present a systematic theory for THz excitations of either polarization in bare QWs or coherent polaritons in QW-microcavity systems. We choose the material parameters to match 8 nm InGaAs QWs and use the microcavity configuration specified in Ref. [12]. We will then study how many-body aspects modify the THz-generated $1s$-to-$2p$ and Λ transitions as function of the THz field's strength and frequency. We will show that both systems also exhibit transitions beyond the two- or three-level system if sufficiently strong excitations are applied.

2 Theory of THz excitations We start from the general many-body system Hamiltonian [4] and derive the Heisenberg equations of motion for the relevant quantities [1]. As discussed above, the optical excitation, defined by the electric field $E_{\rm opt}(z)$, generates first optical polarization whose dynamics follows from the semiconductor Bloch equations [16]. The THz field is defined by the vector potential $A_{\rm THz}(z)$ and it modifies the polarization dynamics according to:

$$\begin{aligned} i\hbar\frac{\partial}{\partial t}P_{\mathbf{k}} = &\left(\epsilon_{\mathbf{k}} - j_{\mathbf{k}}A_{\rm THz} + \tfrac{e^2}{2\mu}A_{\rm THz}^2\right)P_{\mathbf{k}} \\ &- \left(1 - f_{\mathbf{k}}^{\rm e} - f_{\mathbf{k}}^{\rm h}\right)\sum_{\mathbf{k}'} V_{\mathbf{k}-\mathbf{k}'}P_{\mathbf{k}'} \\ &- \left(1 - f_{\mathbf{k}}^{\rm e} - f_{\mathbf{k}}^{\rm h}\right)d_{\rm cv}\,E_{\rm opt} + \Gamma_{\mathbf{k}}\,, \end{aligned} \tag{1}$$

where $A_{\rm THz}$ and $E_{\rm opt}$ are defined at the QW position. This dynamics contains the Coulomb-renormalized kinetic energy of the electron-hole pairs $\epsilon_{\mathbf{k}}$, the THz field coupling contains the current-matrix element $j_{\mathbf{k}} = -\frac{\hbar|e|}{\mu}\mathbf{k}\cdot\mathbf{e}_{\rm THz}$ and the quadratic ponderomotive contribution $\frac{e^2}{2\mu}A_{\rm THz}^2$ which contain the elementary charge, the reduced mass μ of electron-hole pair [17,18], the carrier momentum $\mathbf{k}$, and the direction of the THz field $\mathbf{e}_{\rm THz}$. The Coulomb coupling among the polarization is given by $V_{\mathbf{k}}$ and it is responsible for the creation of excitonic resonances in the polarization.

The optical excitation generates polarization via the term proportional to the dipole-matrix element $d_{\rm cv}$. Collectively, this induces the macroscopic polarization $P_{\rm opt} = \frac{1}{S}\sum_{\mathbf{k}} d_{\rm cv}^* P_{\mathbf{k}}$ which is scaled by the quantization area S. The emerging electron and hole densities are not directly modified by the THz field but via the THz induced changes to the polarization, c.f. Ref. [17] for further details. The Coulomb and phonon scattering is presented symbolically via $\Gamma_{\mathbf{k}}$; its full microscopic form is presented in Ref. [1].

The microcavity effects are systematically included by solving Eq. (1) together with the wave equation

$$\left[\frac{\partial^2}{\partial z^2} - \frac{n(z)}{c_0^2}\frac{\partial^2}{\partial t^2}\right]E_{\rm opt}(z,t) = \mu_0 g(z)\frac{\partial^2 P_{\rm opt}}{\partial t^2}, \tag{2}$$

where the optical light propagates through the sample along the z-direction. The refractive index profile $n(z)$

defines the microcavity which leads to a formation of a single mode inside the microcavity. The polarization $P_{\mathbf{k}}$ causes the splitting of the resonance, scaled by the vacuum permittivity μ_0 and the QW confinement function $g\,(z)$.

For the THz field, the wave equation has the same structure, but instead of the electric field, we have the vector potential A_{THz} and the polarization is replaced by the THz current. Here, the THz vector potential is not significantly changed by the microcavity, as the DBR spacing is much smaller than the THz period (see Fig. 1**a**).

We solve Eqs. (1)–(2) and the corresponding THz wave equation numerically. More specifically, we assume that the incoming optical field is a 150 fs long Gaussian and is energetically centered at the $1s$ exciton energy. Due to its short duration, the optical pulse overlaps energetically also with the LEP and HEP resonances that are found 3.3 meV below and 2.6 meV above the $1s$ resonance, respectively. The pump pulse is chosen so weak that it dominantly generates only polarization. We fully take into account that $\Gamma_{\mathbf{k}}$ makes the $1s$ component decay roughly four times slower than the other excitonic components, see Ref. [1].

We then apply a THz field that has a temporal shape

$$\mathrm{A}_{\mathrm{THz}} = \frac{E_0}{2\pi\,\nu}\, e^{-\frac{t^2}{\tau^2}} \times \left[\cos\left(2\pi\,\nu\;(t-\Delta t)\right) + 0.6\cos\left(1.7\pi\,\nu\;(t-\Delta t)\right)\right], \tag{3}$$

with a pulse having two central frequencies as in the experiment of [12]. We set the duration of the THz pulse to $\tau = 2.1$ ps and the pump-probe delay to $\Delta t = 0.8$ ps. We scan the central frequency ν of the THz pulse while we use three different values for the peak electric field E_0: 2 kV/cm, 3 kV/cm, and 4kV /cm.

To gain more insight into the generated excitonic dynamics, it is useful to solve the eigen-value problem defined by the homogeneous part of Eq. (1). This yields the generalized Wannier equation [4] and its solutions provide a complete set of right-handed exciton states $\phi^R_\lambda(\mathbf{k})$. This allows us to project the different exciton components from the polarization:

$$p_\lambda = \sum_{\mathbf{k}} \phi^R_\lambda\,(\mathbf{k})\, P_{\mathbf{k}}. \tag{4}$$

Since the exciton states are orthogonal,

$$F_\lambda \equiv \frac{|p_\lambda|^2}{\sum_\beta |p_\beta|^2} \tag{5}$$

defines the fraction of exciton states λ within the polarization. Therefore, it directly reveals how the THz effects redistribute the excitonic components under different conditions.

3 Results We analyze how the exciton fraction F_λ changes as function of THz frequency ν in different situations. For both the TLS and Λ system, we are interested in generating transitions from the ground state ($1s$, LEP, HEP) to the excited $2p$ state. Since all of these ground states contain a $1s$ component, we monitor F_{1s}, F_{2p}, and the rest, $F_{\mathrm{rest}} = \sum_{\lambda\neq 1s,2s} F_\lambda$, to deduce the dynamics in either the TLS or the Λ system. If the THz field excited only the TLS or the Λ system, F_{rest} should not change as the THz pulse is changed.

Figures 2**a**, 2**b**, and 2**c** show F_{1s}, F_{2p}, and F_{rest}, respectively, for the TLS expected for the bare QW case used here. These fractions are defined at the temporal center of the THz pulse for three representative peak THz field strengths: $E_0 = 2$ kV/cm (blue dashed line), 3 kV/cm (red line), and 4 kV/cm (black line).

We observe that the $1s$ fraction dips and the $2p$ fraction grows strongly when the THz frequency matches the $1s$-to-$2p$ transition frequency $\nu_{2p,1s}$, indicated by the dashed vertical line. As the THz field is increased, the peak shifts to higher frequencies due to the AC Stark effect [19]. Besides this nonlinear feature, we notice that additional peaks (dips) appear at discrete positions; these resonances correspond to the absorption of multiple THz photons while the system makes a transition from the $1s$ to the $2p$ state. We also see that the excitation of exciton states beyond the TLS appears because F_{rest} grows to an appreciable fraction as the THz field becomes strong enough. This shows that the THz excitations quickly excite states beyond the intended TLS as the THz intensity is increased. Experimental evidence of these effects is provided in Ref. [10, 20].

The same analysis is repeated for the Λ system in Figs. 2**d**, 2**e**, and 2**f** where the QWs are positioned inside the microcavity. Otherwise the computation and presentation is identical to that in Figs. 2**a**–**c**. For low intensities, F_{1s} dips and F_{2p} peaks when the excitation frequency matches either the HEP-to-$2p$ or the LEP-to-$2p$ transition frequency, indicated by the vertical lines. Especially, we do not observe any special transition for the $1s$-to-$2p$ transition energy (dashed vertical line). These results verify our earlier experimental observation [12] that the principal transitions form a Λ system as in Fig. 1**b**.

As the THz field is increased, we see a slight AC-Stark shift and the onset of multi-photon absorption, in analog to the bare QW analysis. As the major difference to the bare QW case, the multi-photon absorption resonances are shifted because they generate, e.g., the HEP-$2p$ transition. This is another indication that THz transitions involve states of a Λ system.

The behavior of F_{rest} determines when a THz field excites states beyond the Λ system. We see that this happens for elevated THz fields, like for the TLS. The effect is especially strong if the THz field is not resonant with either arm of the Λ system. On can understand this as multi-photon ionization process that can always lift LEP and HEP polarization to ionized exciton states. The same tendency, i.e. the growth of F_{rest} for nonresonant conditions, is observed in the TLS.

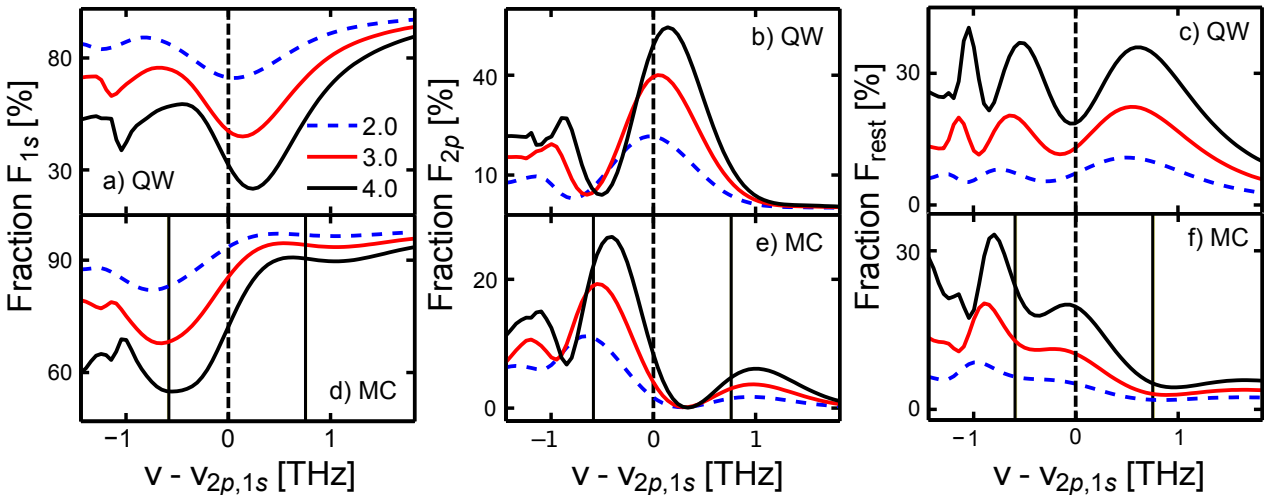

Figure 2 Exciton fractions F_λ in bare QW and microcavity QW THz excitations. The THz frequency ν dependence of bare QW excitations produces a) F_{1s}, b) F_{2p} and c) $F_{\rm rest}$, shown for three representative field strengths 2.0 kV/cm (blue dashed line), 3.0 kV/cm (red line) and 4.0 kV/cm (black line). The dashed vertical line indicates the position of $1s$-to-$2p$ transition frequency $\nu_{2p,1s} = 1.64$ THz. The same analysis is presented for the QW microcavity (MC) by plotting d) F_{1s}, e) F_{2p} and f) $F_{\rm rest}$. The vertical lines define the positions of LEP-to-$2p$ and HEP-tp-$2p$ transitions.

4 Conclusions We have compared the simultaneous excitations of optical and THz light of quantum wells with and without a microcavity. In both cases, the $1s$ (or LEP and HEP) and the $2p$ state are the most important states in the THz-excitation dynamics. By tuning the central frequency of the THz field, we have verified that the THz induces transition between the $1s$ (LEP or HEP) and the $2p$ state for the QW (microcavity-QW) system. Therefore, the principal transitions form a two-level system (TLS) for bare QWs while a cavity introduces a Λ system

Our analysis reveals that an AC Stark shift and multi-photon absorption become clearly visible in these systems. The computation results also confirm that even if the THz field is resonant with the principal transitions in a TLS or a Λ system, these systems become quickly open for elevated THz intensities. In particular, the transitions to other states (beyond the TLS or the Λ system) become important at much lower intensities when the THz is detuned away from the principal transtion energies. In these situations, all states are important and a full microscopic many-body theory is needed to explain the physics involved.

Acknowledgements The work in Marburg is supported by the Deutsche Forschungsgemeinschaft. The OSU work is supported by the National Science Foundation (DMR-1063632).

References

[1] M. Kira and S. W. Koch, Prog. in Quantum Electron. **30**, 155 (2006).
[2] S. Chatterjee et al., Phys. Rev. Lett. **92**, 067402 (2004).
[3] M. Kira et al., Phys. Rev. Lett. **87**, 176401 (2001).
[4] M. Kira and S. W. Koch, Semiconductor Quantum Optics (Cambridge University Press, 2012).
[5] J. Černe et al., Phys. Rev. Lett. **77**, 1131 (1996).
[6] R. A. Kaindl et al., Nature (London) **423**, 734 (2003).
[7] M. Kira, W. Hoyer, and S. W. Koch, Solid State Communications **129**, 733 (2004).
[8] J. R. Danielson et al., Phys. Rev. Lett. **99**, 237401 (2007).
[9] M. Wagner et al., Phys. Rev. Lett. **105**, 167401 (2010).
[10] B. Ewers et al., Phys. Rev. B **85**, 075307 (2012).
[11] C. Weisbuch et al., Phys. Rev. Lett. **69**, 3314 (1992).
[12] J. L. Tomaino et al., Phys. Rev. Lett. **108**, 267402 (2012).
[13] S. Leinß et al., Phys. Rev. Lett. **101**, 246401 (2008).
[14] D. Golde et al., Phys. Rev. Lett. **102**, 127403 (2009).
[15] F. Blanchard et al., Phys. Rev. Lett. **107**, 107401 (2011).
[16] H. Haug and S. W. Koch, Quantum Theory of the Optical and Electronic Properties of Semiconductors, $5^{\rm th}$ edition (World Scientific, Singapore, 2009).
[17] J. T. Steiner, M. Kira, and S. W. Koch, Phys. Rev. B **77**, 165308 (2008).
[18] M. Kira, W. Hoyer, and S. W. Koch, Phys. Status Solidi B **238**, 443 (2003).
[19] K. B. Nordstrom et al., Phys. Rev. Lett. **81**, 457 (1998).
[20] B. Ewers et al., Phys. Status Solidi [in same series].

Paper IV

submitted to Phys. Rev. B

Systematic investigation of THz-induced excitonic Rabi splitting

Systematic investigation of THz-induced excitonic Rabi splitting

M. Teich, M. Wagner, D. Stehr, H. Schneider and M. Helm
Institute of Ion Beam Physics and Materials Research, Helmholtz-Zentrum Dresden-Rossendorf, P.O. Box 510119, 01314 Dresden, Germany

G. Khitrova and H.M. Gibbs*
College of Optical Sciences, The University of Arizona, 1630 East University Boulevard, Tucson, Arizona 85721, USA

A.C. Klettke, S. Chatterjee, M. Kira and S.W. Koch
Faculty of Physics and Material Sciences Center, Philipps University, Renthof 5, 35032 Marburg, Germany
(Dated: January 18, 2013)

Weak near-infrared and strong terahertz excitation are applied to study excitonic Rabi splitting in (GaIn)As/GaAs quantum wells. Pronounced anticrossing behavior of the split peaks is observed for different terahertz intensities and detunings relative to the intraexcitonic heavy-hole 1*s*-2*p*-transition. At intermediate to high electric fields the splitting becomes highly asymmetric and exhibits significant broadening. A fully microscopic theory is needed to explain the experimental results. Comparisons with a two-level model reveal the increasing importance of higher excitonic states at elevated excitation levels.

I. INTRODUCTION

The resonant optical polarization in semiconductor quantum wells (QWs) is often referred to as *coherent excitons* which can be classified using the well-known hydrogen quantum numbers. With the help of additional terahertz (THz) excitation, one can couple the different exciton states, in particular, one can induce transitions between the 1*s* and 2*p* states [1–8]. In this connection, strong resonant quasi-cw THz excitation of the 1*s*-2*p* transition leads to Rabi splitting. Pronounced anticrossing behavior was observed by Wagner *et al.* [9] when detuning the THz frequency from the 1*s*-2*p* transition. These effects were explained within the rotating wave approximation (RWA) which already predicts dressed states.

A number of theoretical investigations have previously been reported on the effect of a strong THz field on e.g. the excitonic absorption [10]. The Autler-Townes splitting and side-band generation for excitonic resonances in QWs were discussed theoretically using the RWA [11, 12]. However, a more extensive framework of a fully microscopic theory has already been developed [6, 8, 13] to fully include non-RWA, ponderomotive, and multi-photon-ionization contributions which are needed to describe extreme nonlinear THz excitation.

In addition, Maslov *et al.* analyzed the quantum confined Stark effect in presence of a THz field oriented in growth direction [14]. More detailed studies concerning the combination of an ac and dc field were computed by Mi *et al.* [15]. The interplay between the dynamic Franz-Keldysh and the ac Stark effect were also discussed by Zhang *et al.* [16]. Yan *et al.* investigated the interplay between ac Stark effect and dynamical localization in a semiconductor superlattice [17]. Rabi-splitting effects were also observed using strong THz single-cycle pulses [18]. In addition to the splitting, also pronounced resonance broadening and induced absorption effects were observed, which could be attributed to the excitation of excitonic states with high quantum numbers and THz-induced exciton ionization.

In this paper, we present a systematic investigation that is intended to fill the gap between the earlier studies

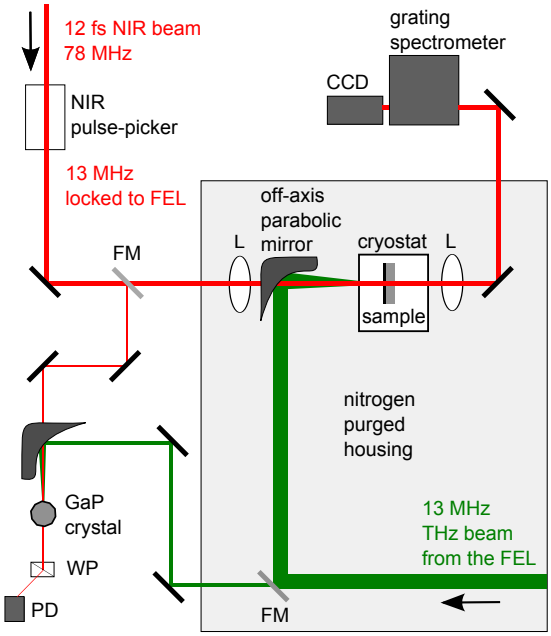

FIG. 1. (Color online) Schematic experimental geometry. FM: flip mirror, L: lens, WP: Wollaston prism, PD: photodiode.

* deceased

and allow us to quantify the limitations of the two-level analysis that includes only the excitonic 1s-2p transition. For this purpose, we use the temporally long (31 ps) THz pulses of a free-electron laser (FEL) that are spectrally sufficiently narrow to enable us to study detuning effects from the 1s-2p transition frequency. Furthermore, we use a sample with larger separation between heavy- and light hole energies than used in Ref. [9]. We record the THz-induced changes in the near infrared (NIR) absorption spectrum for weak (1.2 kV/cm) to high THz fields up to 6 kV/cm. Since a two-level approximation (2LA) is expected to explain only some aspects of the investigation, it is interesting to determine its validity range. As in Ref. [18], we use a microscopic theory [6, 8, 13] for the analysis and we compare the results to a 2LA where we restrict the treatment to the excitonic 1s and 2p states. We quantify when and how a 2LA deviates from the experimental observations, whereas the fully microscopic theory explains the experiments.

II. EXPERIMENTAL SETUP

Figure 1 illustrates the experimental setup which is a two-beam collinear configuration for THz and NIR excitation spectroscopy. The setup allows the simultaneous excitation of the sample with weak broadband NIR and strong narrowband THz light. Apart from the sample used, it is the same setup as in Ref. [19]. Broadband NIR light is generated in a 12-fs Ti:Sapphire laser oscillator with a repetition rate of 78 MHz. The repetition rate is reduced by an acousto-optical pulse picker to the 13 MHz of the free-electron laser (FEL) at the Helmholtz-Zentrum Dresden-Rossendorf. Both beams are synchronized with a timing jitter of 1-2 ps; the delay can be adjusted using a phase shifter. The full width at half maximum (FWHM) of the FEL pulses is about a factor of 100 smaller than its photon energy, i.e., for a photon energy of 6.8 meV (resonant detuning) we measure 0.06 meV FWHM yielding 31 ps FEL pulses. The FEL pulse duration is determined by Fourier transforming the FEL spectrum and confirmed by a cross-correlation measurement in a 300 μm thick GaP crystal using intensity-based electro-optic sampling with a single Si photodiode [20]. The investigated multiple quantum well sample DBR42 contains twenty 8 nm $Ga_{0.06}In_{0.94}As$ QWs separated by 92 nm GaAs barriers grown on a GaAs substrate [21]. Unlike in the sample analyzed in Ref. [9], the light hole is energetically more separated from the heavy hole.

III. RESULTS AND ANALYSIS

An overview of the measured experimental spectra plotted as -log(Transmission) is given in Fig. 2 for a THz photon energy a) above, b) near and c) below the 1s-2p transition energy. The peak field strength in kV/cm is given in the legend. For better visibility, the spectra are

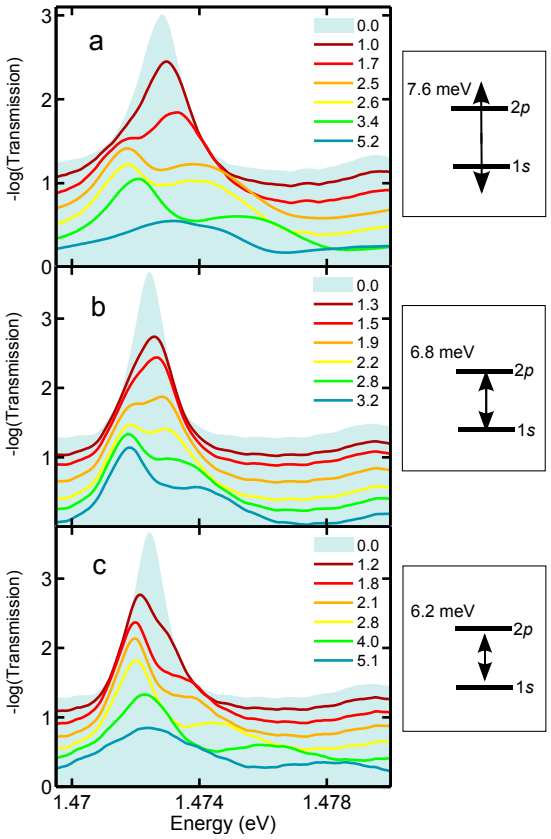

FIG. 2. (Color online) Experimental absorption data (-log(Transmission)) for different THz peak field strengths (in kV/cm) and THz photon energy (a) above (7.6 meV) (b) near (6.8 meV) and (c) below (6.2 meV) 1s-2p resonance.

vertically shifted. In all cases, THz pumping leads to bleaching for low THz intensities, then to Rabi splitting from medium intensities on and, in Fig. 2a and b, to a reversal of the peak heights. For high intensities, both peaks are bleached but the left peak is higher than the right peak.

We use the microscopic theory [6, 8, 13, 18] (semiconductor Bloch equations including THz interaction) to treat the light-matter interaction self-consistently. For the THz interaction, we do not employ the RWA, but fully include the counter-rotating terms. Besides inserting the material parameters appropriate for the sample used in the present study, we additionally evaluate the equations in the limit of the two-level approximation (2LA) where we only include the excitonic 1s and 2p states but keep all other parameters the same as in the full analysis. This allows us to quantify how and when the 2LA analysis deviates from experiments.

Our detailed theory-experiment comparisons show that the fully theory explains all experimentally observed features. As representative examples, we show in Fig. 3 spectra for selected THz field strengths where the THz photon energy is close to the 1s-2p resonance and in Fig. 4 for the case where the THz photon energy is tuned be-

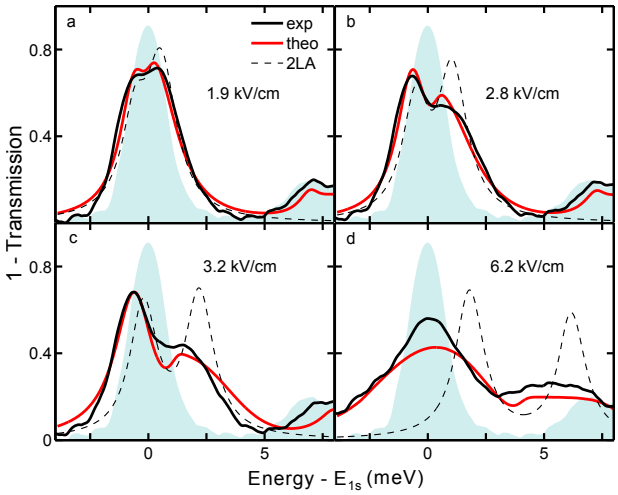

FIG. 3. (Color online) 1-T without THz (shaded area) and with THz photon energy of 6.8 meV, near the 1s-2p resonance, as measured in experiment (black solid), fully microscopic theory (red solid) and the two-level result (dashed) for the THz field strength of (a) 1.9 kV/cm (b) 2.8 kV/cm (c) 3.2 kV/cm (d) 6.2 kV/cm.

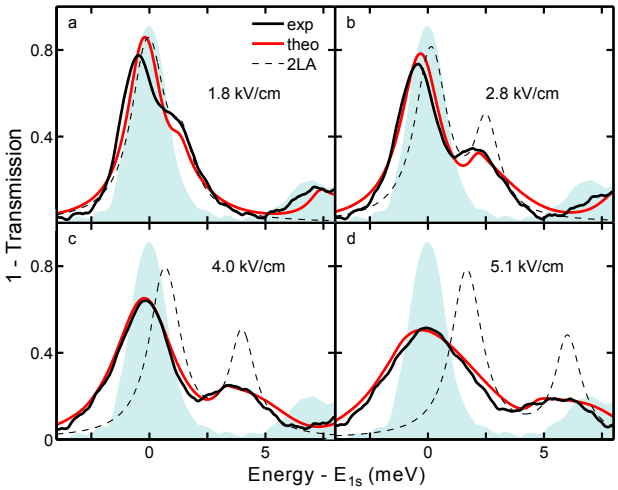

FIG. 4. (Color online) 1-T without THz (shaded area) and with THz photon energy of 6.2 meV , below the 1s-2p resonance, as measured in experiment (black solid), from the fully microscopic theory (red solid) and the two-level result (dashed) for the THz field strength (a) 1.8 kV/cm (b) 2.8 kV/cm (c) 4.0 kV/cm (d) 5.1 kV/cm.

low the resonance energy. Both figures present the direct comparison of the experimental data with THz (black solid) and the microscopic result (red solid). The experimental data without THz are shown as shaded areas, the results from the 2LA are dashed.

The fully microscopic theory nicely reproduces the experimental results, including the peak heights, position and THz-induced broadening. In contrast, the 2LA works only for the lowest THz field (Fig. 3a and 4a). For higher THz field (2.8 kV/cm and higher), the 2LA gets worse about the peak heights and broadening. For example, it overestimates the high-energy Rabi peak height by 55 % for 3.2 kV/cm THz field strength for 6.8 meV THz photon energy. However, it roughly describes the peak splitting correctly and the discrepancy of 2LA and experimental peak positions increases slightly with detuning.

To gain an overview of the dependence of THz field strength and detuning on the Rabi peaks, we present in Fig. 5b and d the results for (1-Transmission) as predicted by the fully microscopic theory for low (1.2 kV/cm) and medium THz field strength (3.2 kV/cm), respectively. The experimental Rabi peaks are depicted as circles inside the contour plot, where the diameter refers to the peak height. We observe that the Rabi splitting increases with the strength of the THz field as expected [22]. The spectra for the 2LA are presented in Figs. 5a and c. For low THz field (1.2 kV/cm, Figs. 5a and b), the 2LA gives similar results as the microscopic theory. However, already for a medium THz field, the microscopic theory predicts asymmetric bleaching and broadening of the Rabi peaks in agreement with the experimental results (Fig. 5d), while the 2LA yields symmetric splitting and bleaching (Fig. 5c). Hence, the observation of anticrossing is not enough to prove the validity of a 2LA. This shows the importance of higher excitonic states for the shapes of the 1s-exciton peak for medium THz fields leading to a complete disagreement of 2LA and experiment for high THz fields as already seen in Figs. 3d and 4d.

The microscopic calculations allow us to follow the redistribution of existing THz polarization also in time do-

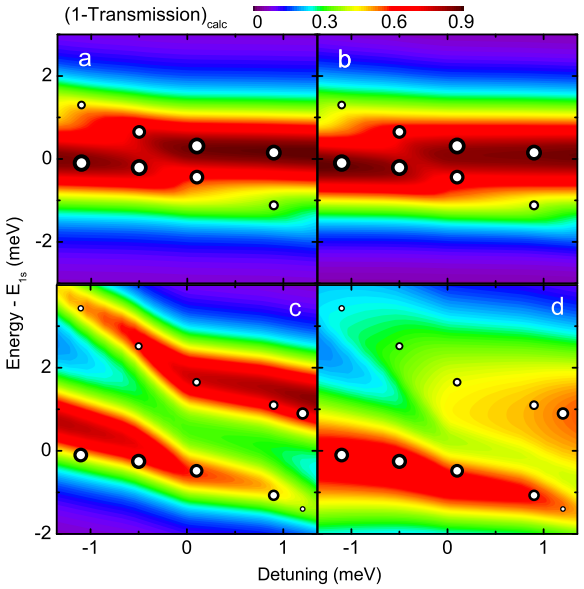

FIG. 5. (Color online) Anticrossing behavior of 1-T extracted from the microscopic calculation. The experimental peak positions (heights) are depicted by the position (diameter) of the open circles. (a)/(c): 2LA (b)/(d) microscopic theory results for a THz field of 1.2 (top) and 3.2 kV/cm (bottom).

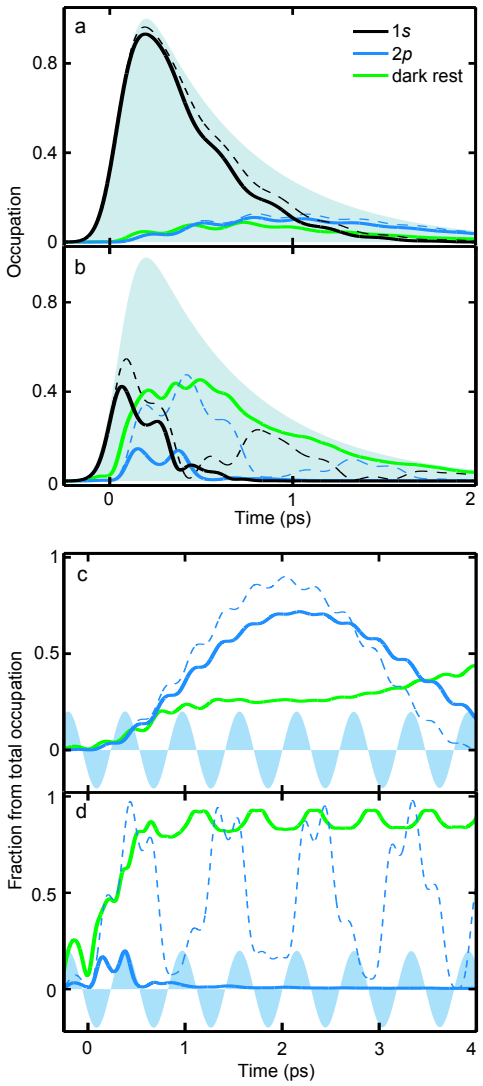

FIG. 6. (Color online) **Top:** Occupations for THz photon energy near the 1s-2p resonance. The THz field strengths are (a) 1.9 kV/cm and (b) 6.2 kV/cm. Shaded area: Sum of all occupations without THz field. Solid/dashed lines: microscopic / 2LA result with THz field. **Bottom:** 2p and the dark rest occupations as fraction of all occupations. Solid (dashed) lines depicts microscopic (2LA) results. Shaded area: THz field oscillations (arb. u.). Note the difference in the time scales for the upper and lower panels.

main. Representatively, we analyze the temporal data for which the spectra were already shown in Figs. 3a and d, for THz excitation near the 1s-2p resonance. In Figs. 6a and b, the 1s occupation $|p_{1s}|^2$ without THz is plotted as shaded area as a reference. The results for the occupations $|p_\lambda|^2$ from the microscopic theory with THz influence are shown in solid lines (1s: black; 2p: blue; other dark states: green). For comparison, we show the 2LA results as dashed lines. For the low THz intensity (1.9 kV/cm, see Fig. 6a), the microscopic theory and the 2LA basically agree. However, the microscopic calculation reveals that we already have an occupation of higher lying exciton states. For high THz field (6.2 kV/cm, see Fig. 6b), we see only one Rabi flop in the microscopic calculation while the 2LA incorrectly predicts multiple Rabi flopping.

To better monitor the THz influence, we replot the data for 2p and the dark states, but scaled as fraction of all temporarily existing occupations. The results are shown in Figs. 6c and d for THz field strengths of c) 1.9 kV/cm and d) 6.2 kV/cm. For illustration, the oscillating THz field is shown by the shaded area. For the low THz field strength (Fig. 6c), the microscopic theory and the 2LA both describe 1s-2p Rabi flopping. The Rabi period decreases with higher THz fields (intermediate fields not shown here) until for the highest THz field, all occupation is immediately transfered into higher dark states (see green line in Fig. 6d) while the 2LA incorrectly predicts continued Rabi flopping. Despite this limitations, however, the 2LA predictions of the Rabi splitting (determined by the Rabi period) are still quite correct.

IV. CONCLUSIONS

We have measured the THz-induced changes in the optical transmission for a THz frequency near the excitonic 1s-2p transition frequency. We have observed bleaching and shifting of the 1s exciton peak and pronounced Rabi splitting. In addition, the Rabi peaks undergo an anticrossing behavior for a detuning of the THz frequency away from the exciton resonance. The fully microscopic theory excellently reproduces all experimental features and follows the transition from Rabi flopping at low THz intensities to exciton ionization at high intensities. We also have quantified how a restriction to only two levels (2LA) deviates from experiments and the fully microscopic theory. The 2LA works reasonably well for low THz fields where the Rabi splitting is weak. For elevated THz fields, only the Rabi-peak positions are rather close to experimental values while the peak heights are not reproduced. This systematic analysis closes the gap between earlier studies showing either dressed state behaviour for low THz fields or THz ionization for strong and spectrally broad THz fields.

ACKNOWLEDGMENTS

We thank P. Michel, W. Seidel and the FELBE team for their dedicated support. The Marburg work is supported by Deutsche Forschungsgemeinschaft. The Tucson group acknowledges support of NSF ERC CIAN and NSF AMOP.

[1] R. A. Kaindl, M. A. Carnahan, D. Hägele, R. Lövenich, and D. S. Chemla, Nature **423**, 734 (2003).

[2] I. Galbraith, R. Chari, S. Pellegrini, P. J. Phillips, C. J. Dent, A. F. G. van der Meer, D. G. Clarke, A. K. Kar, G. S. Buller, C. R. Pidgeon, B. N. Murdin, J. Allam, and G. Strasser, Phys. Rev. B **71**, 073302 (2005).

[3] R. Ulbricht, E. Hendry, J. Shan, T. F. Heinz, and M. Bonn, Reviews of Modern Physics **83**, 543 (2011).

[4] M. Jörger, T. Fleck, C. Klingshirn, and R. von Baltz, Phys. Rev. B **71**, 235210 (2005).

[5] R. Huber, B. A. Schmid, Y. R. Shen, D. S. Chemla, and R. A. Kaindl, Phys. Rev. Lett. **96**, 017402 (2006).

[6] J. R. Danielson, Y.-S. Lee, J. P. Prineas, J. T. Steiner, M. Kira, and S. W. Koch, Phys. Rev. Lett. **99**, 237401 (2007).

[7] M. Kira and S. W. Koch, Phys. Rev. Lett **93**, 076402 (2004).

[8] M. Kira and S. W. Koch, Prog. Quantum Electron. **30**, 155 (2006).

[9] M. Wagner, H. Schneider, D. Stehr, S. Winnerl, A. M. Andrews, S. Schartner, G. Strasser, and M. Helm, Phys. Rev. Lett. **105**, 167401 (2010).

[10] K. Johnsen and A.-P. Jauho, Phys. Rev. Lett. **83**, 1207 (1999).

[11] D. S. Citrin, Phys. Rev. B **60**, 13695 (1999).

[12] A. Liu and C. Z. Ning, J. Opt. Soc. Am. B, **17**, 433 (2000).

[13] J. T. Steiner, M. Kira, and S. W. Koch, Phys. Rev. B **77**, 165308 (2008).

[14] A. V. Maslov and D. S. Citrin, Phys. Rev. B **62**, 16686 (2000).

[15] X. W. Mi, J. C. Cao, and C. Zhang, J. Appl. Phys. **95**, 1191 (2004).

[16] T. Y. Zhang, W. Zhao, and X. M. Liu, Appl. Phys. Lett. **91**, 041909 (2007).

[17] J. Y. Yan, R. B. Liu, and B. F. Zhu, New Journal of Physics **11**, 083004 (2009).

[18] B. Ewers, N. S. Köster, R. Wolscholski, M. Koch, C. Chatterjee, G. Khitrova, H. M. Gibbs, A. C. Klettke, M. Kira, and S. W. Koch, Phys. Rev. B **85**, 075307 (2012).

[19] M. Wagner, M. Teich, M. Helm, and D. Stehr, Appl. Phys. Lett. **100**, 051109 (2012).

[20] G. M. H. Knippels, X. Yan, A. M. MacLeod, W. A. Gillespie, M. Yasumoto, D. Oepts, and A. F. G. Van der Meer, Phys. Rev. Lett. **83**, 1578 (1999).

[21] T. Grunwald, T. Jung, D. Köhler, S. W. Koch, G. Khitrova, H. M. Gibbs, R. Hey, and S. Chatterjee, phys. stat. solid. (c) **6**, 500 (2008).

[22] M. Kira and S. W. Koch, *Semiconductor Quantum Optics* (Cambridge University Press, 2012).

Wissenschaftlicher Werdegang

Name	Andrea C. Klettke
Geburtsdatum	12. August 1984
Geburtsort	Marburg

06/2004	Erlangung der Allgemeinen Hochschulreife an der Elisabethschule Marburg
10/2004 bis 09/2007	Studium der Physik an der Philipps-Universität Marburg
10/2006	Vordiplom in Physik mit Nebenfach Informatik
10/2007 bis 09/2008	Masterarbeit zum Thema "Mean-field theory of a Mott insulator" bei Prof. Dr. Fabian H. L. Essler am Rudolf Peierls Centre for Theoretical Physics, University of Oxford, Großbritannien
seit 02/2009	wissenschaftliche Mitarbeiterin in der Arbeitsgruppe "Theoretische Halbleiterphysik", Philipps-Universität Marburg